001

T-3687 c4 127P

N64 23944

Code 1 cat. 32

NASA CR56279

OTS PRICE

XEROX $ 10.10 ph

MICROFILM $ _____

LIBRARY COPY

AUG 7 1963

LANGLEY RESEARCH CENTER
LIBRARY, NASA
LANGLEY STATION
HAMPTON, VIRGINIA

JET PROPULSION LABORATORY
CALIFORNIA INSTITUTE OF TECHNOLOGY
PASADENA, CALIFORNIA

NATIONAL AERONAUTICS AND SPACE ADMINISTRATION
CONTRACT NO. NAS 7-100

Technical Memorandum No. 33-107

THE BEHAVIOR OF LUNAR SATELLITES AND THE DETERMINATION OF THEIR ORBITS: A PRELIMINARY INVESTIGATION

Edited by C. R. Gates

JET PROPULSION LABORATORY
CALIFORNIA INSTITUTE OF TECHNOLOGY
PASADENA, CALIFORNIA
September 18, 1962

Copyright ©1962
Jet Propulsion Laboratory
California Institute of Technology

CONTENTS

I. Introduction 1

II. Behavior of Lunar Satellites 3

A. Analytical Treatment 3

B. Numerical Study 6

III. Theory of Orbit Determination 57

IV. Accuracy of Radio Measurements 62

V. Orbit Determination 64

A. The Model 64

B. Mathematical Approach 66

C. The Orbits Considered 71

D. The Sampling Procedure 72

E. Results 74

I. INTRODUCTION

by C. R. Gates

In this report, various authors present interim results of a continuing study being carried out at JPL on the behavior and tracking of artificial lunar satellites. The report was prepared primarily for the September 1962 meeting of the Selenodesy Working Group of the Planetology Subcommittee of the NASA Space Sciences Steering Committee. Since it has been extracted from studies which are in process, the report is of a preliminary nature. Many of the technical areas discussed, especially in orbit determination, are evolving, and new or modified ideas should be expected.

In Section II the behavioral problem is discussed. Both analytical and computer treatments are given, and results compared. Only second-order harmonics in the lunar potential are investigated.

In Section III the theoretical aspects of orbit determination for lunar satellites are discussed, including the problem of obtaining values for lunar constants.

In Section IV the accuracy of measurements using radio techniques is discussed.

Finally, Section V gives results on a study of orbit determination, using a much simplified model which should yield useful results. Accuracies for both elements and position are presented for various orbits and data-taking patterns.

The essential conclusions of the study at this stage are as follows:

1. [illegible] reasonably close to the Moon, [illegible] and secular variations in the elements are small; hence there should be no difficulty in choosing an orbit which would possess adequate lifetime.

2. In orbit determination, in one or two orbits in-plane position can be determined to an accuracy of a few tens of meters and out-of-plane position can be determined to an accuracy of a few kilometers, using radio tracking. Several weeks of tracking are needed to obtain all components of position to an accuracy of a few tens of meters. The ultimate attainable accuracy using months or years of data is, at this time, a matter of conjecture. In the opinion of the authors, uncertainties and complexities in the model of the lunar gravitation potential will limit the ultimate accuracy in position to the order of a few meters.

II. BEHAVIOR OF LUNAR SATELLITES

by J. Lorell

A. Analytical Treatment

To describe the behavior of lunar satellites, we will use the standard elements of the orbit[1], a, e, I, ω, Ω and χ, and consider the factors that cause changes in these elements. We will concern ourselves primarily with long-term effects (i.e., over several periods of the satellite) since the amplitude of the short-term variations are, in general, small.

It is a simple matter to write down the average rates of each element induced by the various perturbing forces. These rates are listed in Tables II-2 to II-5 as follows (cf. Ref. 1-3):

Table II-2: Oblateness, J-term

Table II-3: Elliptical equator, L-term

Table II-4: Earth and Sun

Table II-5: Relativity

The effects of other perturbing forces, such as drag, radiation pressure, control thrust engines, and electromagnetic forces are extremely small, except perhaps for specialized vehicles such as the Echo balloon. The relative importance of such forces can be estimated as follows (for a close satellite):[2]

[1]See Nomenclature, Table II-1.

[2]Close satellite refers to satellite with semimajor axis not greater than 2000 km; i.e., within a few hundred km of the lunar surface.

Force	Magnitude of acceleration ft/sec^2
Relativistic effect	10^{-10}
Control jet malalignment	3×10^{-8}
Radiation pressure	1×10^{-7}
Earth	2×10^{-4}
Moon, J-term	1.8×10^{-3}
Moon, surface	6

The relative importance of Earth - Moon perturbations as compared with J and L terms in the Moon's gravity field depends strongly on the distance of the satellite from the Moon. Thus, we can set up the following tabulation for a satellite at 1.1 lunar radii:

Precession rates, deg/day

	J-term	L-term	Earth	Sun
$\dot{\Omega}$	-1.24	+0.25	-0.03	-0.00018
$\dot{\omega}$	2.45	-0.25	+0.05	+0.00030

The above tabulation shows maximum rates for almost equatorial, almost circular orbits.

As the distance from the Moon increases, the rates due to J and L decrease rapidly, while those due to Earth and Sun increase. At about 2.5 lunar radii the rates due to the Earth are comparable to those due to J.

Beyond 5 lunar radii, Earth effects are dominant, the J and L effects being completely negligible for most considerations.

In the case of close satellites, there are two phenomena of interest, the precession rates and the stability. The formulas of Tables II-2 and II-3 tell the story in regard to precession rates. Both the node and the line of apses precess at rates depending strongly on the inclination of the orbit. There is a weaker dependence on eccentricity, and, in the case of L, the rates are periodic functions of the node (measured with respect to Moon - fixed axes).

Long-term behavior can be determined by numerical integration of these equations. Since J exceeds L by a factor of 5, the results in general will show the steady precession due to J on which is superposed the oscillations due to L. Polar orbits and orbits near the critical inclination will behave somewhat differently.

In regard to stability, the behavior is more complex. We refer here to the possibility of the satellite plunging into the surface of the Moon. If we write

$$q = a\,(1 - e)$$

then q represents the distance of closest approach to the center of the Moon. The average rate of change of q is

$$\dot{q} = -a\dot{e}$$

since $\dot{a}$ is zero for all the perturbations of importance. Furthermore, neither J nor L affects e directly. Thus, stability depends only on the effects of Earth and Sun, and on the interaction of these with the forces due to J and L.

Using the expressions for $\dot{e}$ in Table II-4, we get

$$\dot{q} = - \frac{15 n_3^2 a}{8n} e \sqrt{1 - e^2} \sin 2\omega \sin^2 I$$

which for a close satellite is approximately

$$\sim - 4e \sin 2\omega \sin^2 I \text{ km/day}$$

We can draw several inferences from these equations, but will not go into all of them here. Suffice it to remark that for a close orbit with eccentricity of 0.1, the maximum rate of descent to the Moon is 0.4 km/day. Also, the almost circular, almost equatorial orbits are most stable.

B. Numerical Study

The purpose of this study was to check the feasibility of using the JPL n-body program for lunar satellite investigations and to initiate such investigations.

Time and cost limitations restrict the number and variety of orbits that can be evaluated. For example, it takes on the order of one minute of machine time per satellite day to compute a close orbit. Thus, the study was limited to four orbits. Two types of computations were made: (1) fine print-

out for a fraction of a day to study short-period behavior and (2) coarse print-out for up to 60 days to study long-period and secular trends.

In general, the computations agree with the analytic approximations that can be made. However, long-period effects due to the Earth's influence require much longer arcs for proper evaluation--especially in regard to stability studies in which the lifetime of the satellite before it plunges into the lunar surface is in question. To make such studies there is in preparation a computer program to integrate the equations for the rates of the osculating elements. In addition, a restricted-three-body computer program is now available and is being used to compute very long arcs.

1. The Computation

The basic computation program is the precision orbit and trajectory program for the IBM 7090 used for JPL precision trajectory work. For the present purposes, the integration was performed in Moon-centered ecliptic coordinates, using an Encke integration scheme with a basic 120-sec interval.

To gain a feeling for the accuracy and time required for these computations a 2-day arc of a 160-min orbit was computed ten times. A summary of the results is shown in Table II-6.

Though Table II-6 can be used only as a rough indicator, it does suggest certain facts. First, it appears that for the same interval size Encke is slightly better than Cowell, and that perhaps a reasonable accuracy for long arcs will be obtained using 120-sec Encke or 60-sec Cowell. The comparable running times are 3:2 in favor of Encke.

As presently set up, the computation accounts for the following perturbing factors:

Earth's gravity field, including $J_{\oplus}$, $H_{\oplus}$, $D_{\oplus}$ terms

Sun's gravity field

Moon's oblateness, $J_{☾}$

Moon's longitudinal bulge, $L_{☾}$

Venus, Mars, and Jupiter gravity fields

Certain omissions can be noted, such as radiation pressure, atmospheric drag, and relativistic effects--none of which is pertinent to the present problem. In fact, the only significant perturbations for the lunar satellite under consideration herein are Earth, $J_{☾}$, and $L_{☾}$. The Sun's effect is measurable, but two orders of magnitude smaller than the other effects.

Since the computations were made with the existing trajectory program, it was necessary to make some compromise in the computation from that which would have been optimum. For example, the $J_{☾}$ and $L_{☾}$ effects should be exhibited in terms of the effects on the orbital elements referred to the plane of the Moon's equator, thus allowing direct comparison with the theoretical expressions. However, the only coordinate systems available in the computation program are the Earth's equatorial and the ecliptic systems. Since the Moon's equator makes an angle of about 1-1/2 deg with the ecliptic, the latter was chosen.

The computations make use of ephemeris information for position of Sun, Moon, and Earth. Thus, the orbits of these bodies are represented in complete detail, corresponding to calendar date. Conceivably, the lunar

satellite orbit may be affected by such factors as the eccentricity of the Moon's orbit about the Earth or of the Earth's orbit about the Sun. If it is, the effects are in the computations. This means that the satellite behavior is a function of the date of orbiting and that some of the trends shown in the plots may be due to such things as the eccentricity of the Moon's orbit. No attempt was made to isolate such phenomena.

The primary subjects of study were the three effects, Earth, $J_{☾}$, and $L_{☾}$. These effects were evaluated separately by suppressing them, two at a time, and computing with one of the three as the only perturbing force on the satellite orbit. The Sun's effect was also suppressed for these cases.

In any numerical study such as this, only a sampling of the possible types of computations can be performed. It is necessary, then, to note the specialization that has been made, the omissions, and the biases. It would be desirable also to analyze the effect on the results of these shortcomings in the computations. However, the results presented here will not be so analyzed; only the specializations and omissions will be noted.

2. Precession Rates of Close Lunar Satellites

As part of the over-all program of investigating the motion of lunar satellites, the present studies represent a numerical evaluation of the precession rates together with a first look at the stability problem for close-in satellites. Results are presented for four orbits (see Fig. II-1):

a. Low eccentricity, inclined (Fig. II-2 to II-12; elements on Fig. II-2).

b. Highly eccentric, equatorial, direct (Fig. II-13 to II-18; elements on Fig. II-13).

c. Highly eccentric, equatorial, retrograde (Fig. II-13 to II-18; elements on Fig. II-13).

d. Moderately eccentric, critical inclination (Fig. II-19 to II-30; elements on Fig. II-19).

These are a representative group of orbits and should exhibit typical features of lunar satellite motion. Effects of the position and motion of the Moon with respect to Earth and Sun have not been varied, all orbits having been computed for initial epoch January 4, 1960. However, it is felt that the Sun's influence is secondary, since the perturbing force due to the Sun is two orders of magnitude smaller than that due to the Earth. On the other hand, the effect of the Earth is studied over a full period of the Earth-Moon motion, so that the full effect on nonuniformities is included in the computation. The Moon's gravity field is accounted for by assuming a triaxial spheroid with three unequal moments of inertia. This is equivalent to expressing the gravity potential in the form

$$\Phi = \frac{\mu}{r}\left[1 + \frac{J}{3r^2}(1 - 3\sin^2\phi) + \frac{L}{r^2}(\cos^2\phi\cos 2\theta)\right]$$

in which r is the distance to the Moon's center of mass expressed in lunar radii, μ is the gravity constant, ϕ is the latitude, θ is the londitude with respect to the Moon-Earth axis, and J, L are dimensionless coefficients. The current best estimates for J and L are

$$J_{☾} = 3109 \times 10^{-7}$$

$$L_{☾} = 608 \times 10^{-7}$$

Results of the computations are presented graphically as plots of the orbital elements a, e, i, Ω, and ω. Two formats are used, a short-term graph showing the short-period motion of the osculating elements over a period of about three orbits, and a long-term graph showing averaged motion over one or two months.

For the case of Orbit (a), Table II-7 has been assembled, showing the magnitudes of the precession rates as obtained from reading the graphs. The comparison with Table II-8 is colored by the fact that the inclination is referred to the ecliptic rather than the lunar equator--a difference of 1-1/2 deg, which is just enough to displace the J and L components of the rates by the amounts shown. The E component shown in Table II-8 does not include the contribution of long-period terms.

3. Short-Period Effects

Based on the four orbits exhibited in the graphs, it appears that the following conclusions can be drawn:

a. $J_{☾}$ (oblateness), $L_{☾}$ (longitudinal bulge), and E (Earth) are the important factors perturbing the orbital elements.

b. The Sun's effect may be discounted as being of higher order than either of J, L, or E.

c. Contributions to the average rates of the osculating elements due to J and L are closely approximated by the standard formulas.

d. The dominant short-period frequencies are n, the orbital frequency, and 2n, at least as regards J and L. For E, the motion is more complicated.

a. The important perturbing factors are J, L, and E. Figures II-3, II-5, II-7, II-9, and II-11 show the separate contributions of J, L, and E to the variations of a, e, i, Ω, and ω, respectively, for Orbit (a). This being a close orbit, the J and L terms dominate. Notwithstanding, the effect of E is still appreciable and, in fact, its importance for $\dot{\omega}$ exceeds that of L. In general, since J has magnitude about 5 times that of L, the effects on the orbit should be in the approximate ratio 5 to 1. However, for the short-period terms this ratio appears to be only about 2 to 1, i.e., the L effects are relatively more important. Table II-9 summarizes the amplitudes of the short-period terms in a form for quick comparison.

b. Results of the computations showing the effect of the Sun are not shown on the graphs (except for Fig. II-7 and 9) because the effects are nil. To emphasize this point, Table II-9 has been assembled showing the comparison between Earth and Sun effects over an 8-hour (2-2/3 orbit) interval. Rates of the osculating elements are identifiable only in the eighth significant digit of the printout--a figure which most probably is buried in the noise of the computation. The dispersion, shown in the last column of Table II-9, represents the difference between maximum and minimum values over the eight

hours. Camparing with the amplitude of the short-period oscillations due to the Earth, it is apparent that the effect of the Sun is too small to significantly affect the computations.

c. The standard formulas giving the averaged rates (no short-period terms) due to J and L agree with the numerical computations. Differences noted in Tables II-7 and II-8 are accounted for by the fact that the planes of reference are different for the two valuations. For the numerical work, Table II-7, the plane of the ecliptic is the reference plane. Thus, the orbital elements I, Ω, and ω and their rates will differ from the values of Table II-8 which uses the lunar equator as the reference plane. Although the difference between the two planes is only 1-1/2 deg, the effect on the rate computations is still appreciable.

d. The dominant frequencies appear to be the orbital frequency n and the double frequency 2n. Figure II-11 exhibits these oscillations particularly well. The J and L curves are distorted sinusoids with period 1-1/3 hours (the orbital period is 2-2/3 hours). However, successive waves have different patterns, the complete cycle being of period 2-2/3 hours.

On the other hand, the E curve hardly looks like a sinusoid, although it is periodic with period 2-2/3 hours. This points up the fact that the Fourier expansions associated with E are much more complex than those associated with J and L, in the sense that there are many more significant terms.

4. Long-Period Effects

Long-period trends were evaluated by computing 30- to 60-day arcs of orbits and printing the osculating elements at 1/2-day intervals. The

resulting data were smoothed graphically to give the curves presented herein. Unfortunately, there was no short-period averaging prior to sampling; hence when the long-period or secular variations are not large compared to short-period variations (see Fig. II-2 and II-3), the long-period curves are misleading.

a. Stability. Over a long period, the orbit of a lunar satellite subject to the perturbations under discussion may become distorted so much as to cause the satellite to hit the lunar surface. This type of orbit instability is measured by the radius of closest approach, RCA = a(1-e). Graphs of RCA for the four orbits under consideration are shown in Fig. II-4, II-17, II-18, II-21, and II-22.

It is to be noted that in no case is the secular drift appreciable. The largest excursion in RCA occurs in the half-month-period terms for the highly eccentric orbits (Orbits b and c). For these, the oscillation has an amplitude of some 70 km, over which is superimposed a short-period oscillation of 3-km amplitude. The drift of the peaks on the curves is of the order of 6 km in a month, which is getting down into the noise level produced by the short-period oscillations. The trend in orbits a, c, and d is negative; i.e., RCA decreases, while in Orbit (b) it is positive.

Since RCA = a(1 - e), it is evident that the variations in a and e determine those in RCA, and, further, since a varies only very slightly (see Fig. II-2, II-14, and II-20), the primary variation in RCA is due to e, and can be expressed

$$\delta(\mathrm{RCA}) = -a\delta e$$

The analytic formulas for average variation in e show that neither L nor J contributes.

It remains, then, to consider the effect of the Earth and Sun. The computations show that the Sun's effect can be entirely neglected. As far as the Earth's effects are concerned, there remains the possibility of long-term or secular effects. Using the approximation for Earth-induced change in close orbits[3]

$$\dot{q} \doteq -4e \sin 2\omega \sin^2 I \text{ km/day}$$

it is seen that for certain values of ω and I the rate of change of q can be appreciable. However, in the cases studied, $2\omega \sim 0$ deg, so that no effect was observable.

b. Precession rates. The precession rates for Ω and ω can be estimated from the slopes of the appropriate graphs (Fig. II-10, II-12, II-28, and II-30). The rates for Orbits (b) and (c) are indeterminate since these are equatorial orbits. As shown in the following tabulation

Orbit	i deg	$\dot{\omega}$ deg/day	$\dot{\Omega}$ deg/day
(a)	46.7	0.46	-0.44
(d)	64.7	0.11	-0.15

the rates for Orbit (d), which is close to the critical inclination, are much smaller than those for Orbit (a). This result is to be expected, since the

[3]Close orbits refer to those with semimajor axis not greater than about 2000 km.

averaged value for ω contains the factor $(4-5 \sin^2 i)$ in the J term.

c. Restricted 3-body computation. Figures II-31 to II-33 exhibit the behavior of a lunar satellite whose orbit is at the critical inclination as computed using the restricted 3-body computer program. The time interval corresponds to about 2 months, for an orbit with period 2.14 hours. Results appear to be compatible with those obtained from the precision orbit computation.

Table II-1. NOMENCLATURE

a	semimajor axis
c	velocity of light
e	eccentricity
I	inclination
J	coefficient of second-order zonal term
L	coefficient of second-order tesseral terms
n	mean angular rate
n_3	mean angular rate of Moon in its orbit
p	$= a(1 - e^2) =$ semilatus rectum
q	$= a(1 - e) =$ distance to pericenter
μ	gravity constant
χ	$= -n\tau$ when τ is the time of pericenter passage
ω	angle between line of nodes and line of apses
Ω	angle between inertial reference axis and line of nodes
Ω'	angle between axis fixed in Moon and line of nodes

Table II-2. Secular rates due to J-term in gravity field

$$\dot{a} = \dot{e} = \dot{I} = 0$$

$$\dot{\Omega} = -\frac{nJ}{p^2} \cos I$$

$$\dot{\omega} = \frac{nJ}{p^2} \left(2 - \frac{5}{2} \sin^2 I\right)$$

$$\dot{\chi} = \frac{3nJ}{p^2} \sqrt{1 - e^2} \left(\frac{1}{3} - \frac{1}{2} \sin^2 I\right)$$

Table II-3. Long-period rates due to L-term in gravity field

$$\dot{a} = \dot{e} = 0$$

$$\dot{I} = \frac{nL}{p^2} \sin 2\Omega' \sin I$$

$$\dot{\Omega} = \frac{nL}{p^2} \cos 2\Omega' \cos I$$

$$\dot{\omega} = -\frac{nL}{p^2} \cos 2\Omega' \left(1 - \frac{5}{2} \sin^2 I\right)$$

$$\dot{\chi} = \frac{3nL}{2p^2} \sqrt{1 - e^2} \cos 2\Omega' \sin^2 I$$

Table II-4. Long-term rates due to third-body gravity field

$$\dot{a} = 0$$

$$\dot{e} = \frac{15}{8}\frac{n_3^2}{n}\, e\, \sqrt{1 - e^2}\, \sin 2\omega \sin^2 I$$

$$\dot{I} = -\frac{15}{16}\frac{n_3^2}{n}\, \frac{e^2}{\sqrt{1 - e^2}} \sin 2\omega \sin 2I$$

$$\dot{\Omega} = -\frac{3}{4}\frac{n_3^2}{n}\, \frac{\cos I}{\sqrt{1 - e^2}} \left[(1 - e^2)\cos^2 \omega + (1 + 4e^2)\sin^2 \omega\right]$$

$$\dot{\omega} = \frac{3}{4}\frac{n_3^2}{n}\, \sqrt{1 - e^2} \left[1 + \frac{5 \sin^2 \omega\, (e^2 - \sin^2 I)}{2\,(1 - e^2)}\right]$$

$$\dot{\chi} = -\frac{3}{4}\frac{n_3^2}{n}\left\{\frac{7}{3} + e^2 - \sin^2 I\left[(1 - e^2)\cos^2 \omega - 2\,(3 + 2e^2)\sin^2 \omega\right]\right\}$$

Note: These rates have been obtained by averaging both with respect to the satellite period and the perturbing body period.

Table II-5. Rates due to relativistic effects

$$\dot{a} = \dot{e} = 0$$

$$\dot{\omega} = \frac{3\mu n}{c^2 p}$$

$$\dot{\chi} = -\frac{3\mu n}{a^2 c^2\, \sqrt{1 - e^2}}\left(3 - 2\sqrt{1 - e^2}\right)$$

Table II-6. Comparison of accuracy and running time for lunar satellite orbit computations[a]

(Period 160 minutes)

After 2 days (18 orbits)

Integration method	Step size Δt, sec	Closest approach a(1-e)	Furthest distance a(1+e)	Mean anomaly M	Machine running time, sec
Cowell	30	2001.3762	2497.8574	32.069682	300
	60	2001.3763	2497.8580	32.069387	160
	120	2001.3746	2497.8617	32.067497	90
	240	2001.2515	2498.1638	31.820755	60
	480	2260.4022	3169.2815	-77.786689	30
Encke	60	2001.3763	2497.8573	32.068951	200
	120	2001.3757	2497.8583	32.068596	110
	240	2001.3731	2497.8627	32.066921	60
	480	--	--	--	--[b]
	960	--	--	--	--[c]

[a]Compiled with the cooperation of D. B. Holdridge.

[b]Blew after 12 hours, orbit time.

[c]Blew after 0 hours, orbit time.

Table II-7. Numerical precession rates (per day) for Orbit (a), January 6, 1960

	a(km)		e		I	
	(2250) rate	short per amplitude	(0.110) rate	short per amplitude	(46°.7) rate	short per amplitude
J	0	±0.271	0	±0.000127	-0.00075	±0.00125
L	0	±0.158	0	±0.000065	-0.05850	±0.00075
E	0	±0.058	-0.000171	±0.000026	-0.02445	±0.00040
SUM	0		-0.000171		-0.08370	
SUM[a]	-0.040		-0.000194		-0.0742	

	Ω		ω	
	(351°.5) rate	short per amplitude	(181°.0) rate	short per amplitude
J	-0.4239	±0.0040	+0.453	±0.004
L	+0.0600	±0.0010	+0.032	±0.023
E	-0.0120	±0.0005	+0.158	±0.019
SUM	-0.3759		+0.643	
SUM[a]	-0.44		+0.46	

[a] Obtained from coarse printout with all perturbations simultaneously.

Table II-8. Analytic precession rates (per day) for Orbit (a), January 6, 1960

	a(km)	e	I	Ω	ω
J	0	0	0	-0.4223	+0.417
L	0	0	-0.0459	+0.0614	+0.029
E	0	0	0	-0.0226	+0.022
SUM	0	0	-0.0459	-0.3835	+0.468

Table II-9. Comparison of Earth and Sun effects over 8-hour interval, Orbit (a)

	Value	Rates		Short-period amplitude	Dispersion
		⊕	⊙	⊕	⊙
a(km)	2249.85	0	0	580×10^{-4}	5×10^{-4}
e	0.11086	-0.000171	0	2600×10^{-8}	71×10^{-8}
i	46°.731	-0.02445	0	400×10^{-6}	46×10^{-6}
Ω	351°.525	-0.0120	-0.00033	50×10^{-5}	11×10^{-5}
ω	181°.051	+0.158	+0.00075	1900×10^{-5}	33×10^{-5}

REFERENCES

1. Kozai, Yoshihide, "The Motion of a Close Earth Satellite," The Astronomical Journal, Vol. 64 No. 9, November 1959, pp. 367-77.

2. Lorell, J., and Anderson, John, Precession Rates for an Artificial Satellite, Paper to be presented at the XIII th IAF Congress, Varna Bulgaria, September 23-29, 1962.

3. Groves, G. V., "Motion of a Satellite in the Earth's Gravitational Field," Proceedings of the Royal Society of London, Series A, 254, 1960, pp. 48-65.

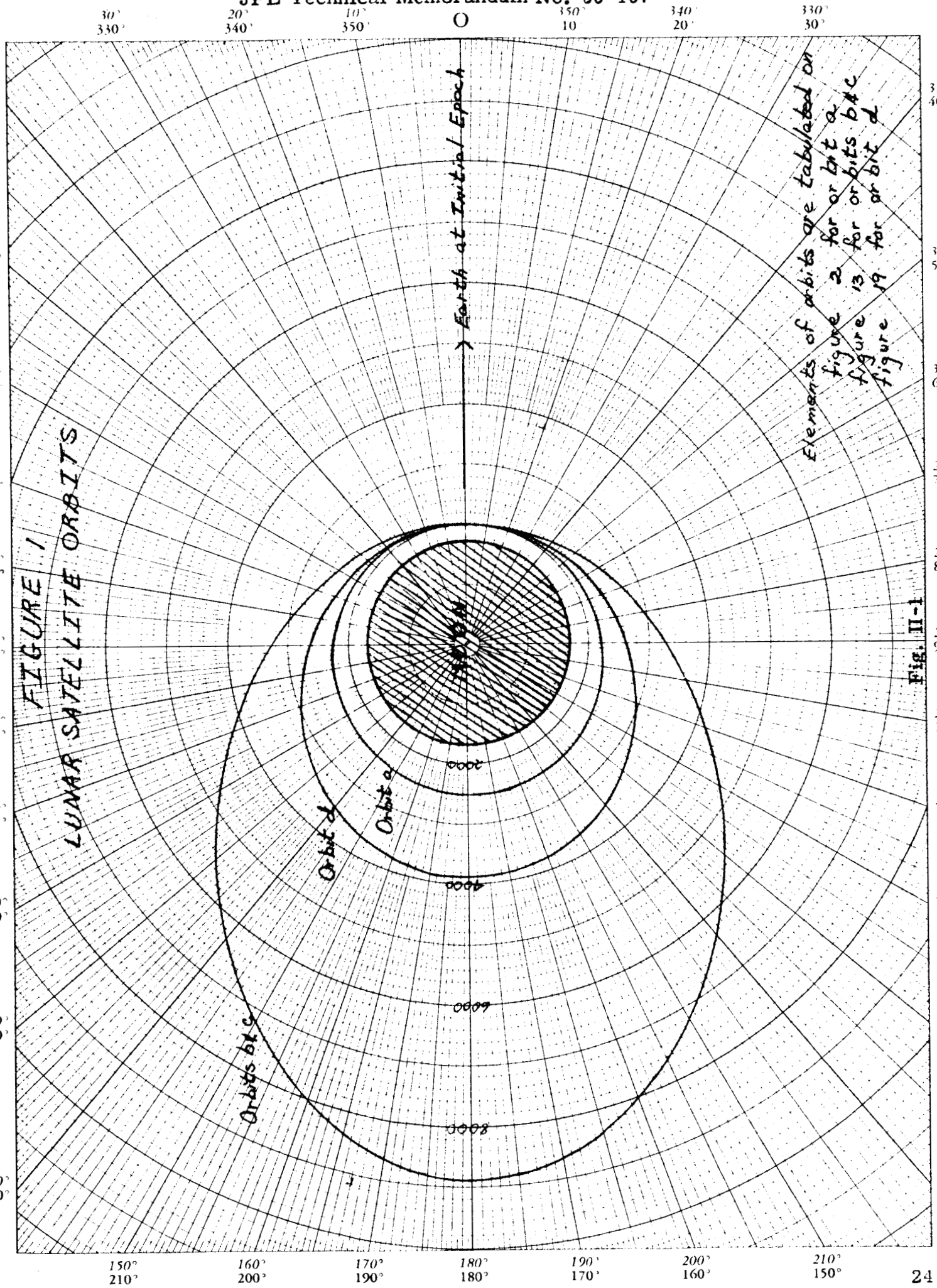

Fig. II-1

PRINTED IN U.S.A. ON CLEARPRINT TECHNICAL PAPER NO. 1015
CLEARPRINT PAPER CO. NO. C324

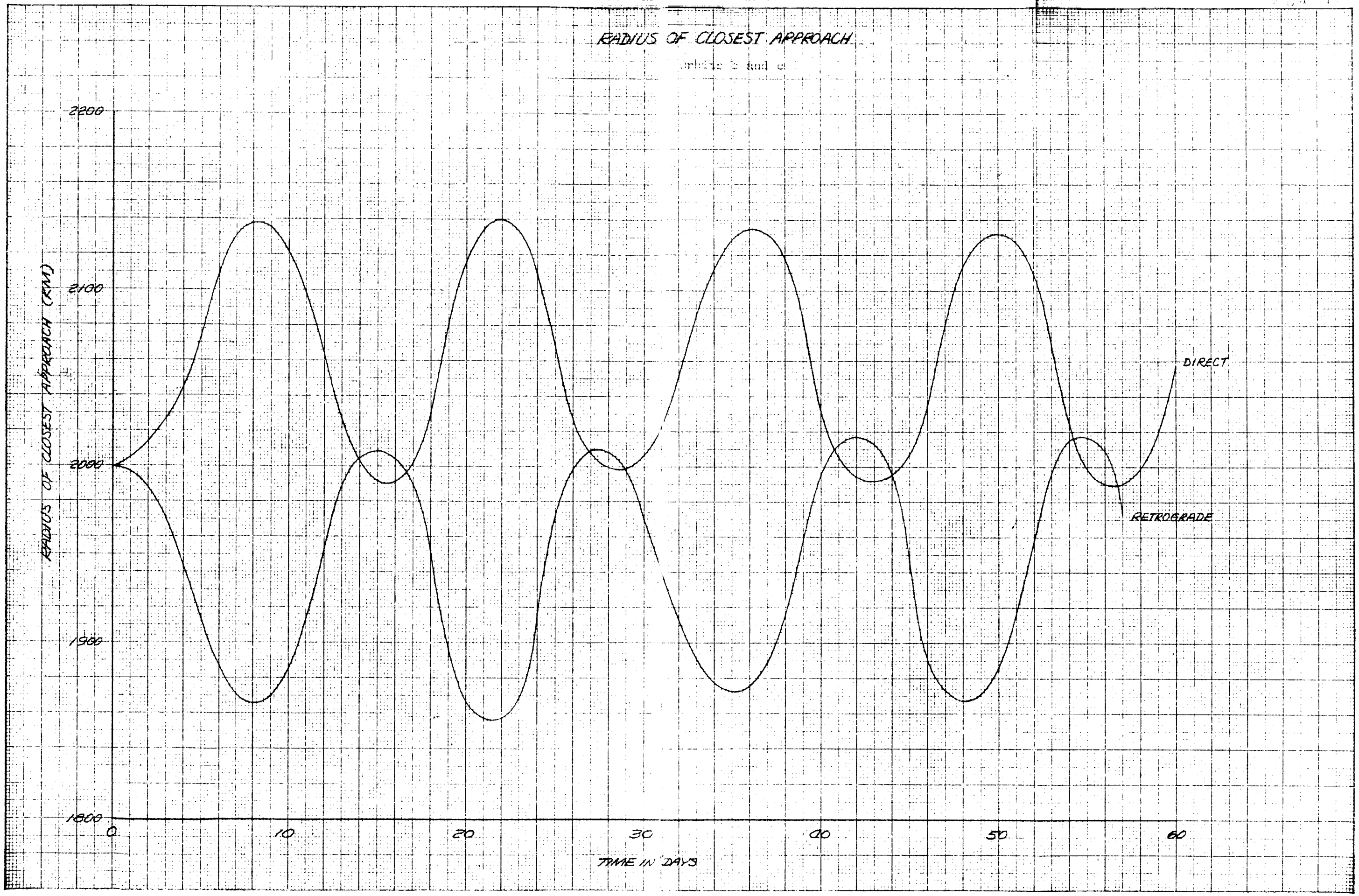

K+E 10 X 10 TO THE CM. 359T-14LG KEUFFEL & ESSER CO. MADE IN U.S.A. ALBANENE ®

Fig. II-18

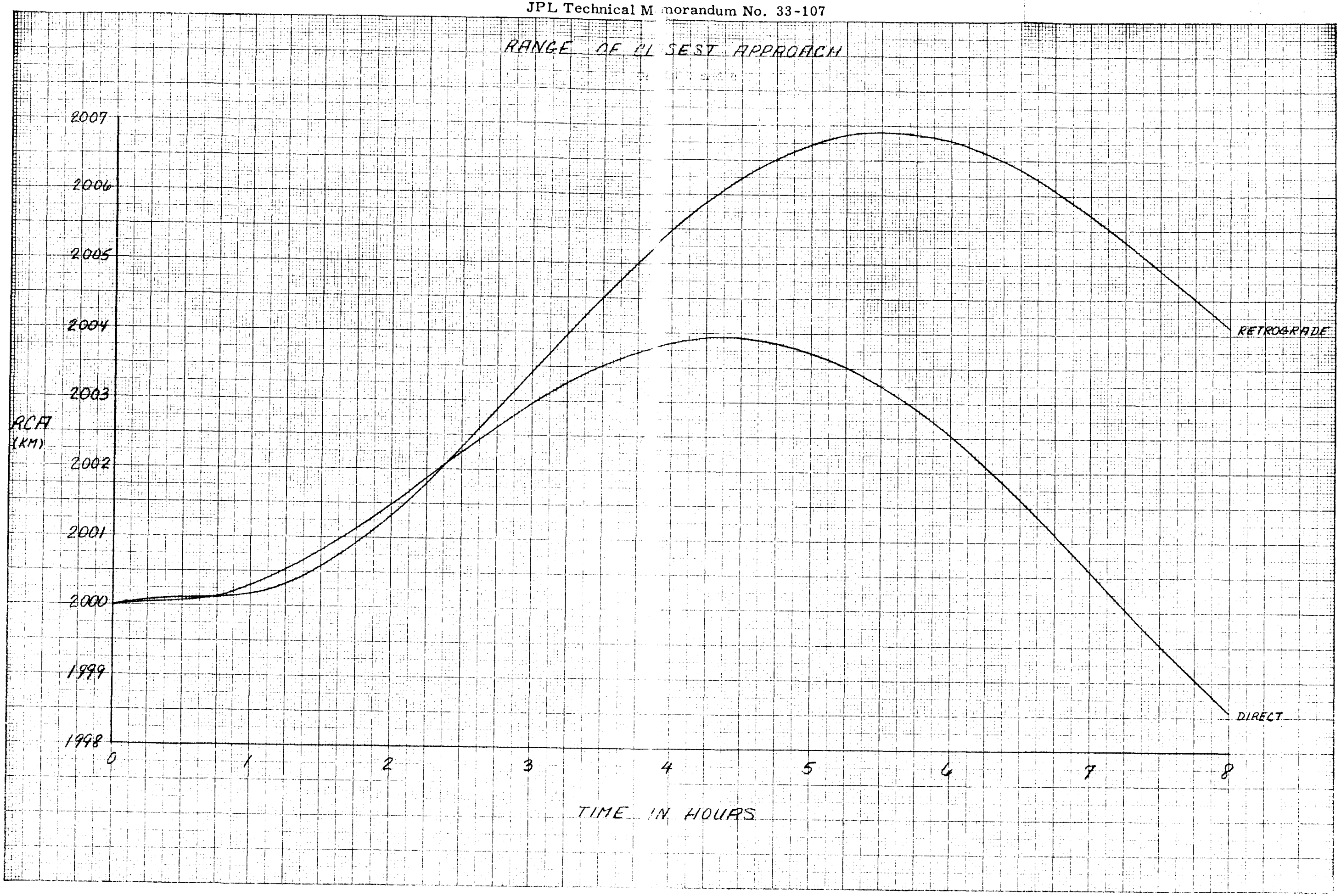
RANGE OF CLOSEST APPROACH
2007
2006
2005
2004
2003
2002
2001
2000
1999
1998
RCA
(KM)
0
1
2
3
4
5
6
7
8
TIME IN HOURS
RETROGRADE
DIRECT

Fig. II-17

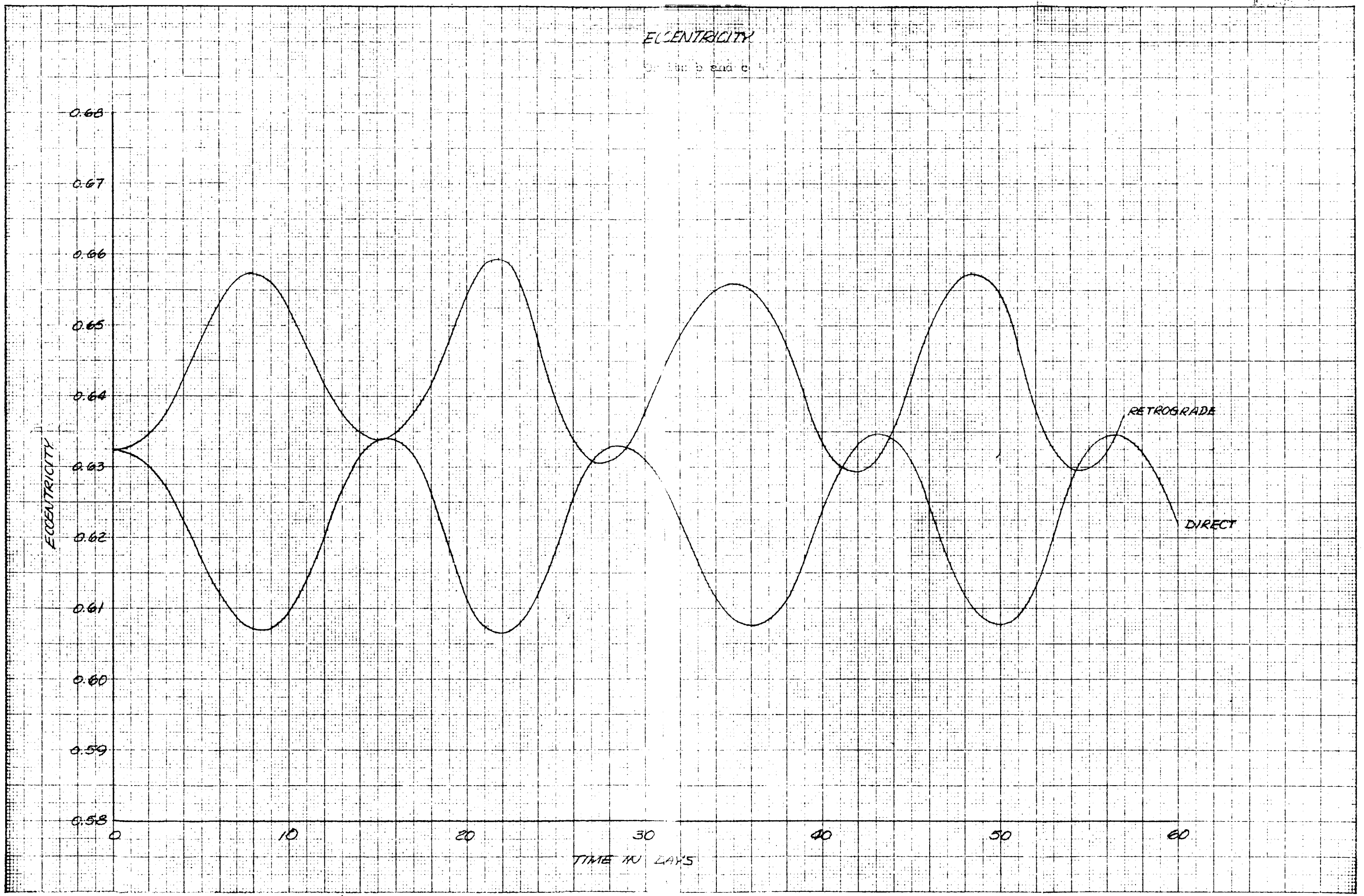
ECCENTRICITY
0.68
0.67
0.66
0.65
0.64
0.63
0.62
0.61
0.60
0.59
0.58
ECCENTRICITY
0
10
20
30
40
50
60
TIME IN DAYS
RETROGRADE
DIRECT

Fig. II-16

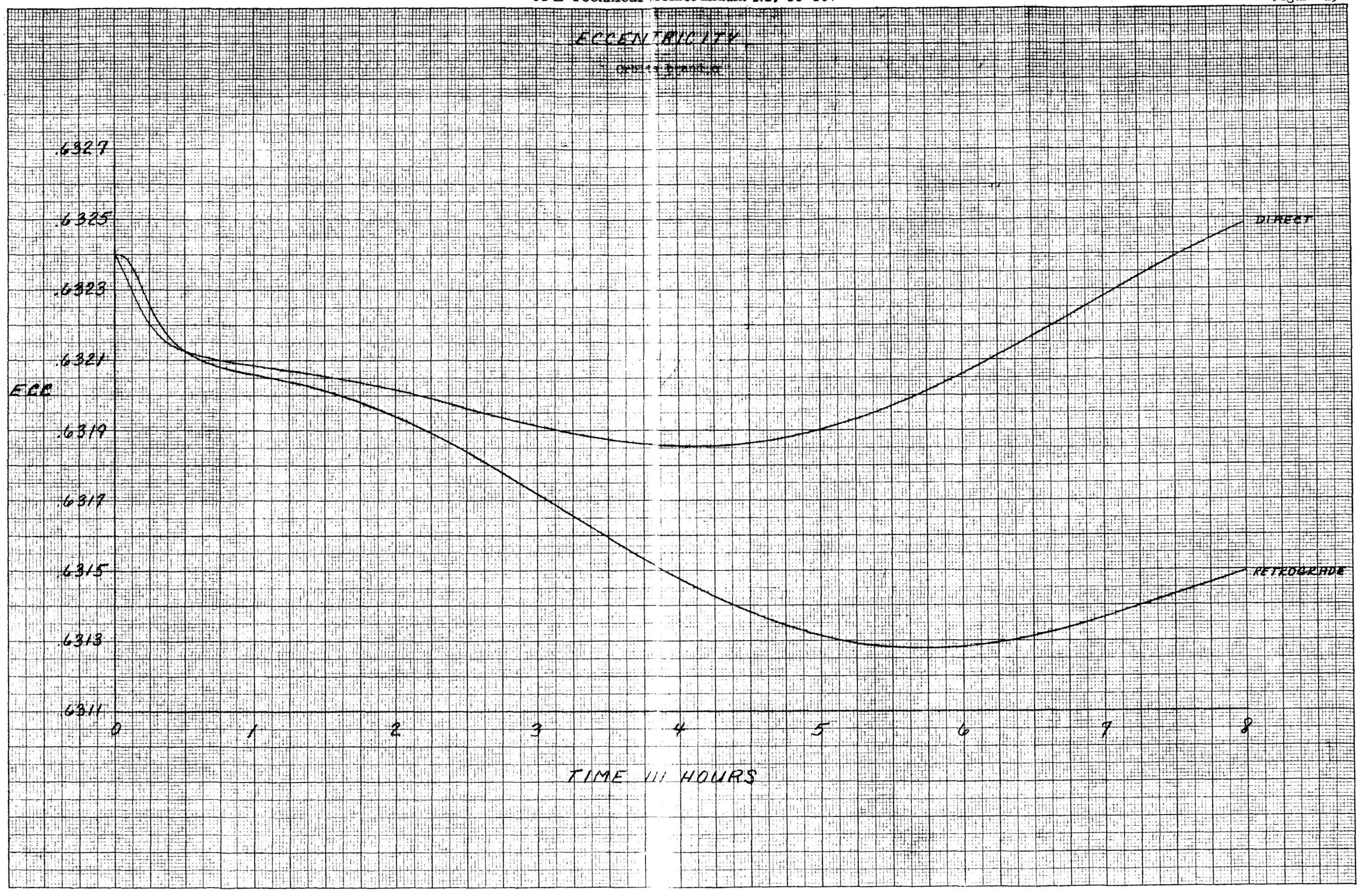
ECCENTRICITY
.6327
.6325
.6323
.6321
ECC
.6319
.6317
.6315
.6313
.6311
0
1
2
3
4
5
6
7
8
TIME IN HOURS
DIRECT
RETROGRADE

Fig. II-15

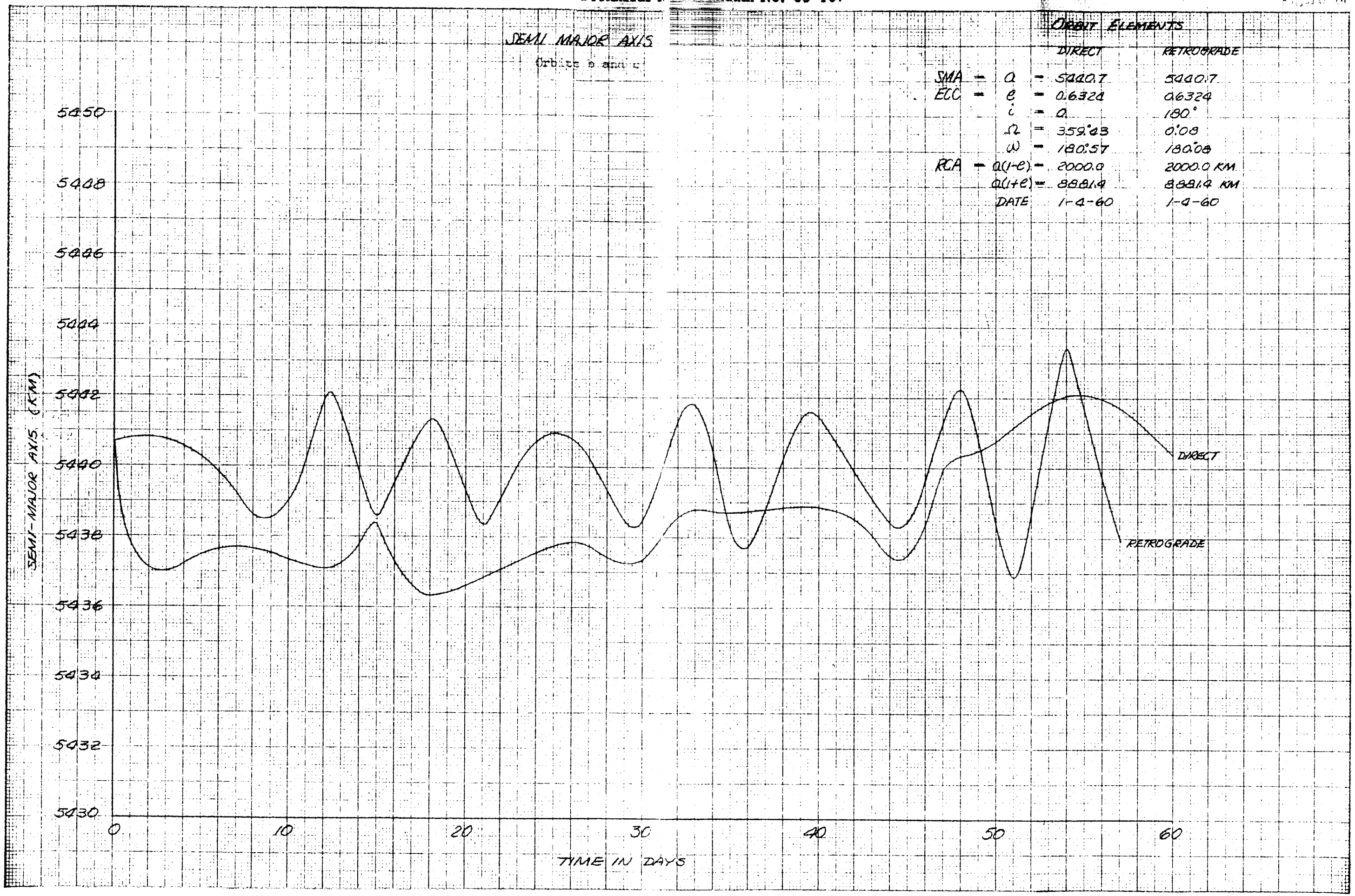
SEMI MAJOR AXIS
Orbits a and c
ORBIT ELEMENTS
DIRECT
RETROGRADE
SMA = a = 5440.7 5440.7
ECC = e = 0.6324 0.6324
i = 0 180°
Ω = 359°.03 0°.08
ω = 180°.57 180°.08
RCA = a(1-e) = 2000.0 2000.0 KM
a(1+e) = 8881.4 8881.4 KM
DATE 1-4-60 1-4-60
5450
5448
5446
5444
5442
5440
5438
5436
5434
5432
5430
SEMI-MAJOR AXIS (KM)
0
10
20
30
40
50
60
TIME IN DAYS
DIRECT
RETROGRADE

Fig. II-14

Figure 1

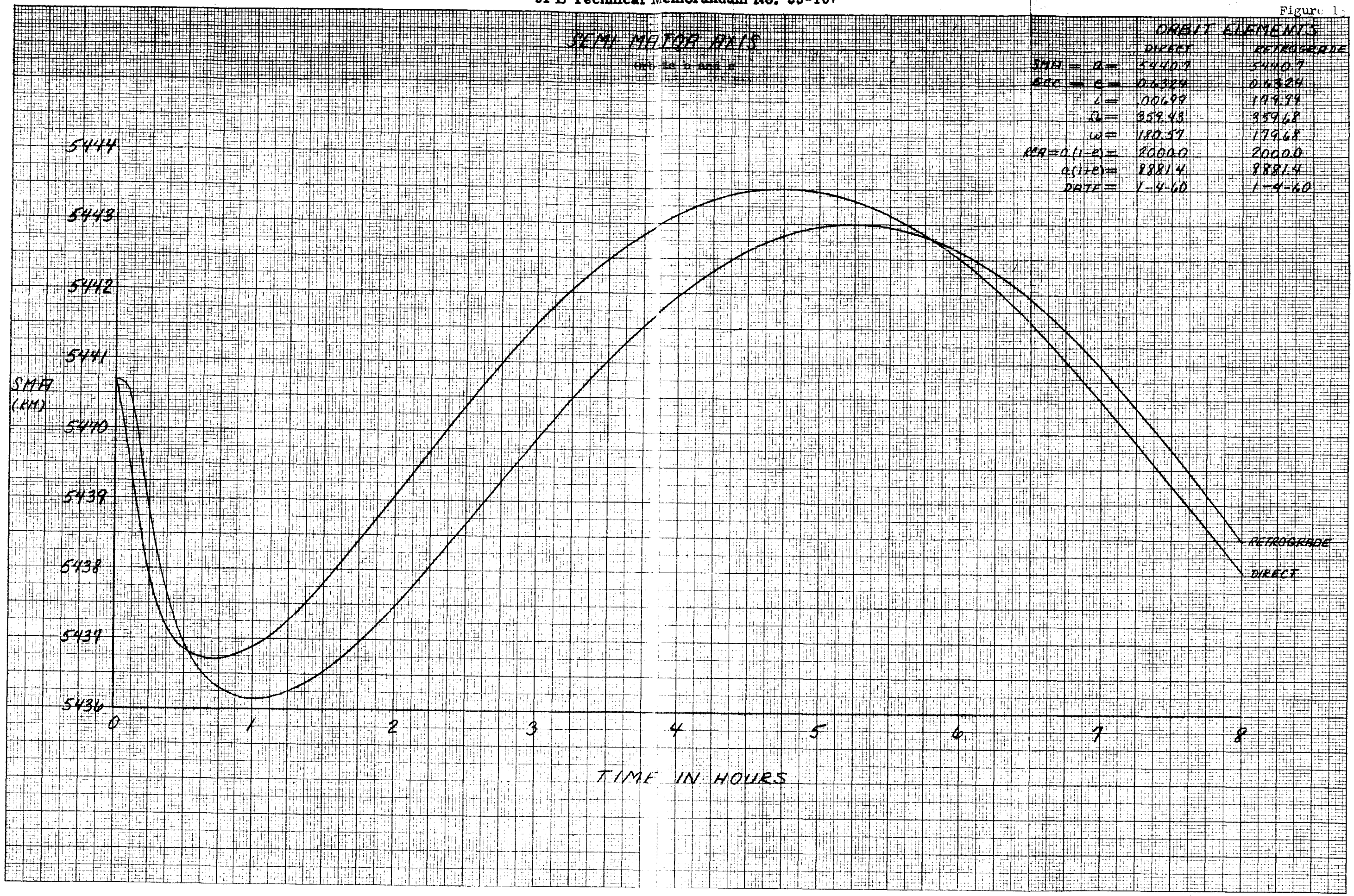

Fig. II-13

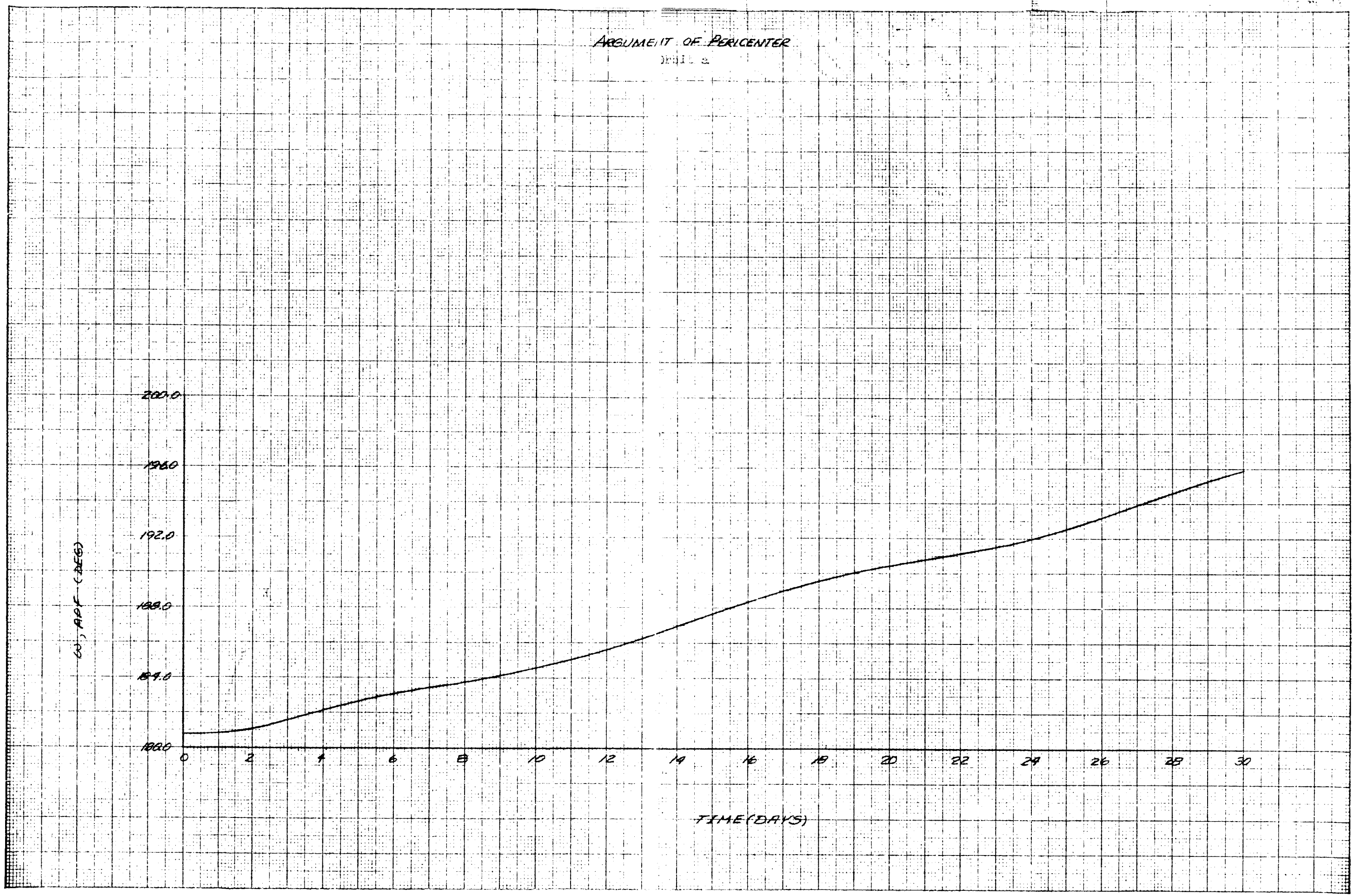
ARGUMENT OF PERICENTER
200.0
196.0
192.0
188.0
184.0
180.0
ω, ARF (DEG)
0
2
4
6
8
10
12
14
16
18
20
22
24
26
28
30
TIME (DAYS)

Fig. II-12

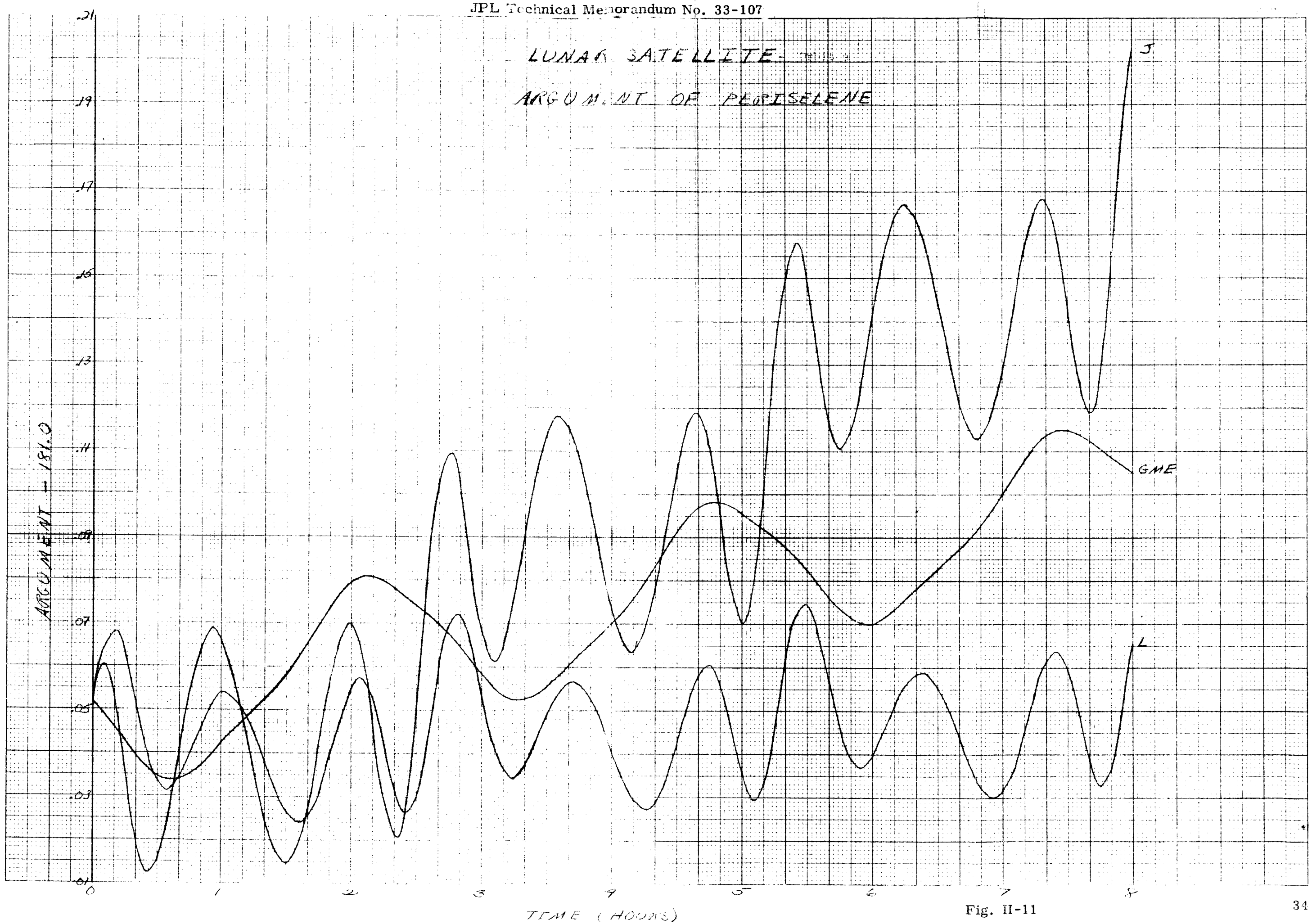
LUNAR SATELLITE
ARGUMENT OF PERISELENE
ARGUMENT - 181.0
.21
.19
.17
.15
.13
.11
.09
.07
.05
.03
.01
0
1
2
3
4
5
6
7
8
TIME (HOURS)
J
GME
L

Fig. II-11

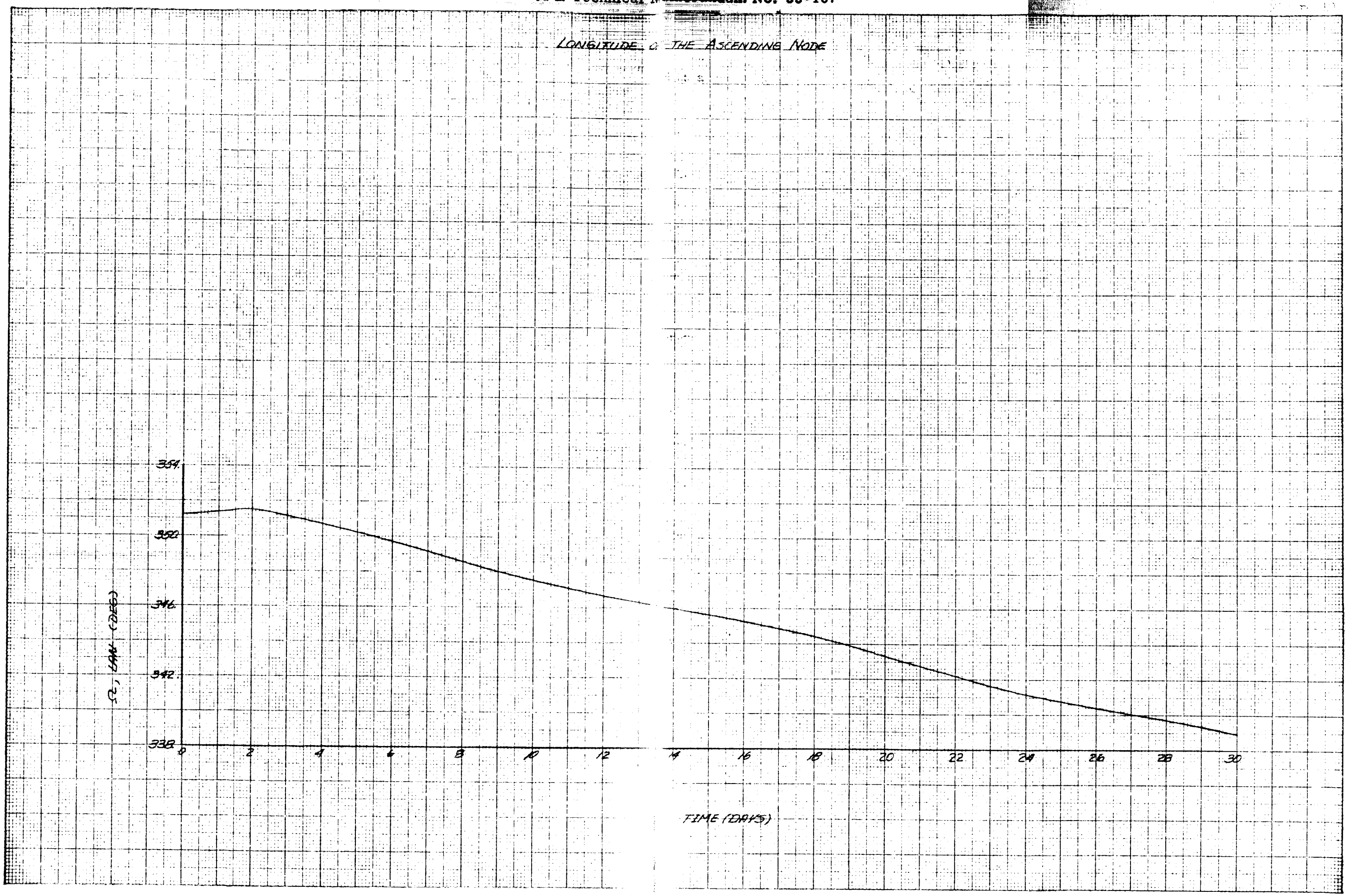
LONGITUDE OF THE ASCENDING NODE
354
350
346
342
338
Ω, LAM (DEG)
0
2
4
6
8
10
12
14
16
18
20
22
24
26
28
30
TIME (DAYS)

Fig. II-10

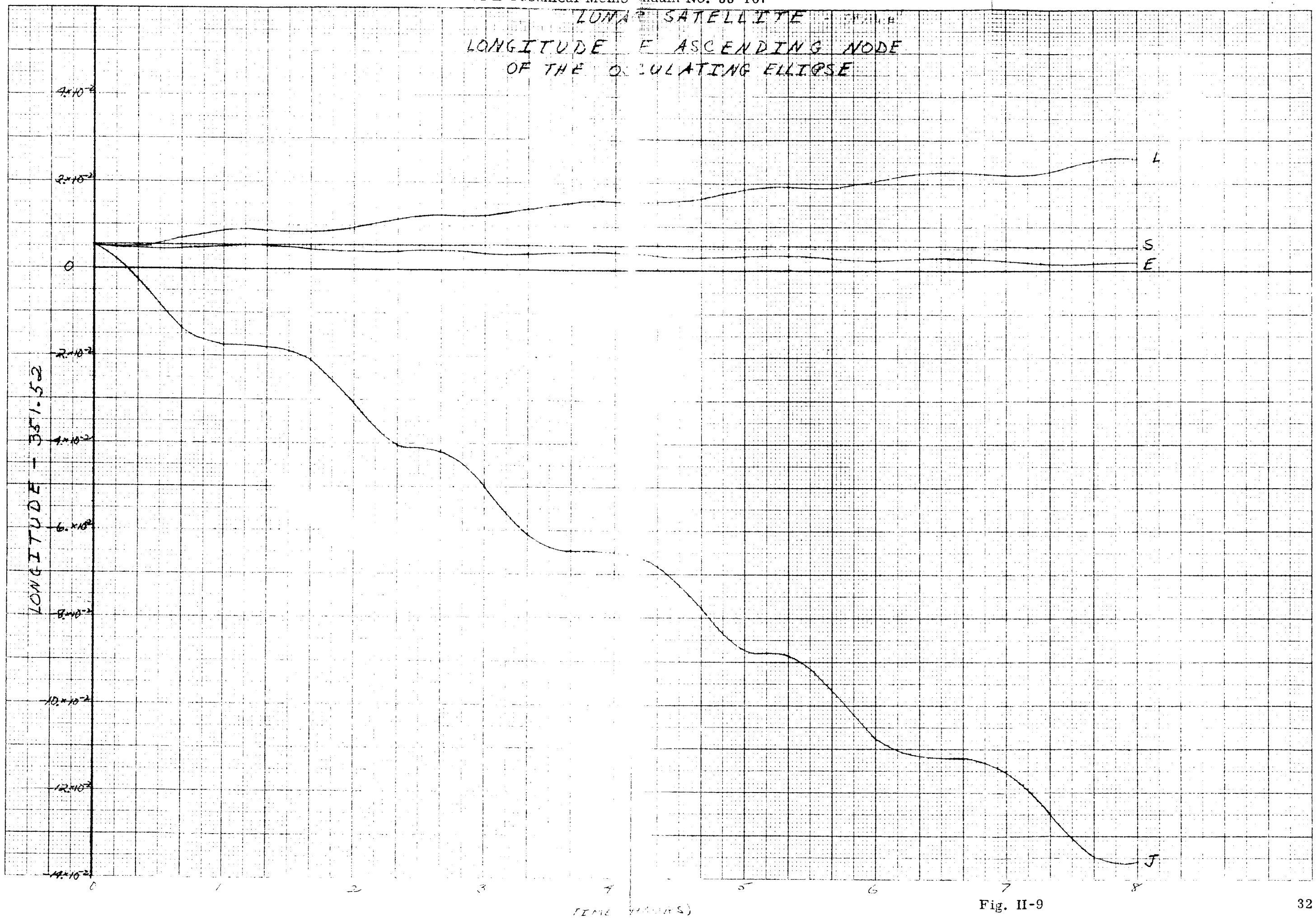
LUNAR SATELLITE
LONGITUDE OF ASCENDING NODE
OF THE OSCULATING ELLIPSE
LONGITUDE - 351.52
4×10⁻²
2×10⁻²
0
-2×10⁻²
-4×10⁻²
-6×10⁻²
-8×10⁻²
-10×10⁻²
-12×10⁻²
-14×10⁻²
0
1
2
3
4
5
6
7
8
L
S
E
J

Fig. II-9

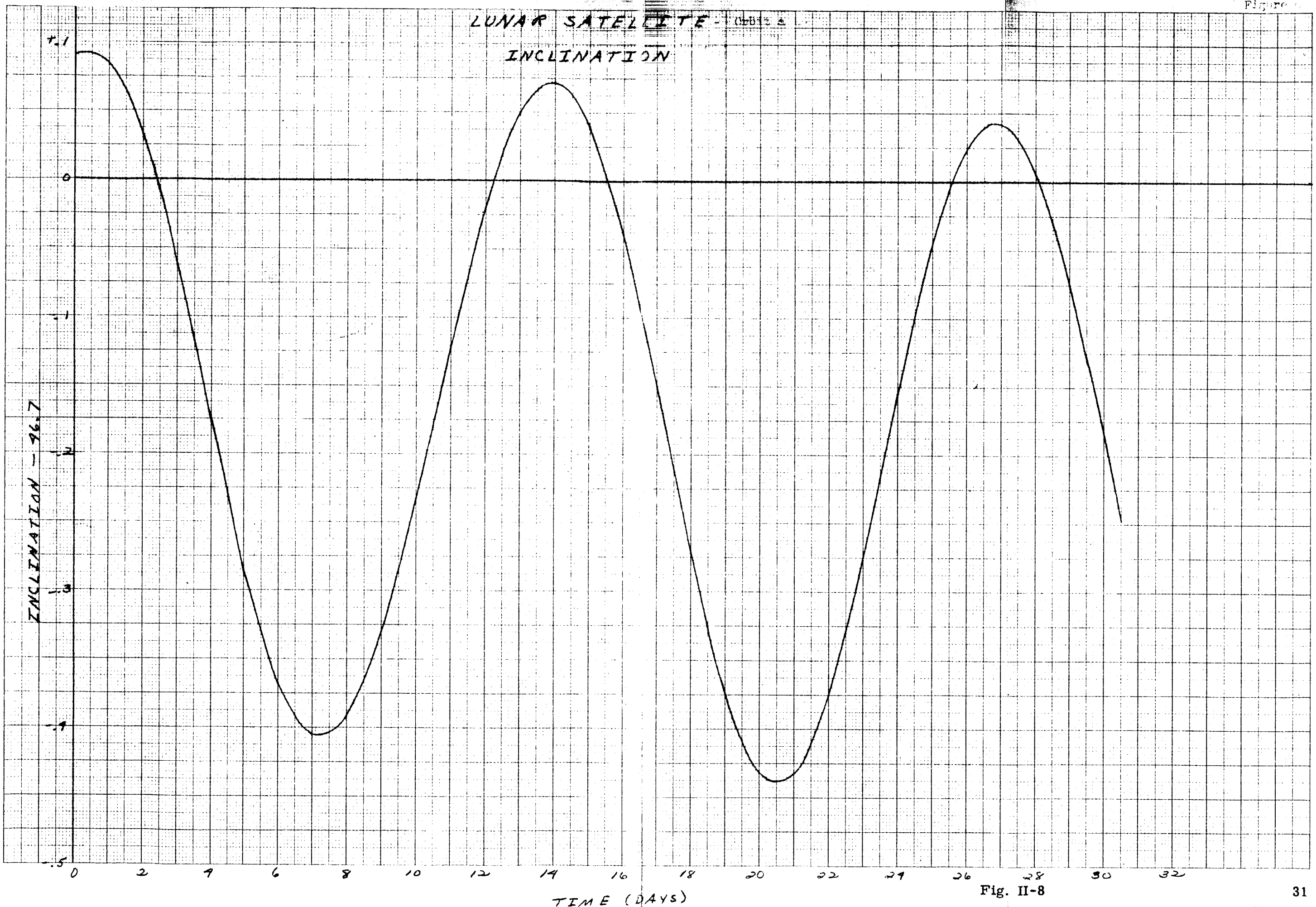

Fig. II-8

PRINTED IN U.S.A. ON CLEARPRINT TECHNICAL PAPER NO. 1015
CLEARPRINT CHARTS
CLEARPRINT PAPER CO. NO. C43 MILLIMETERS, 200 BY 250 DIVISIONS

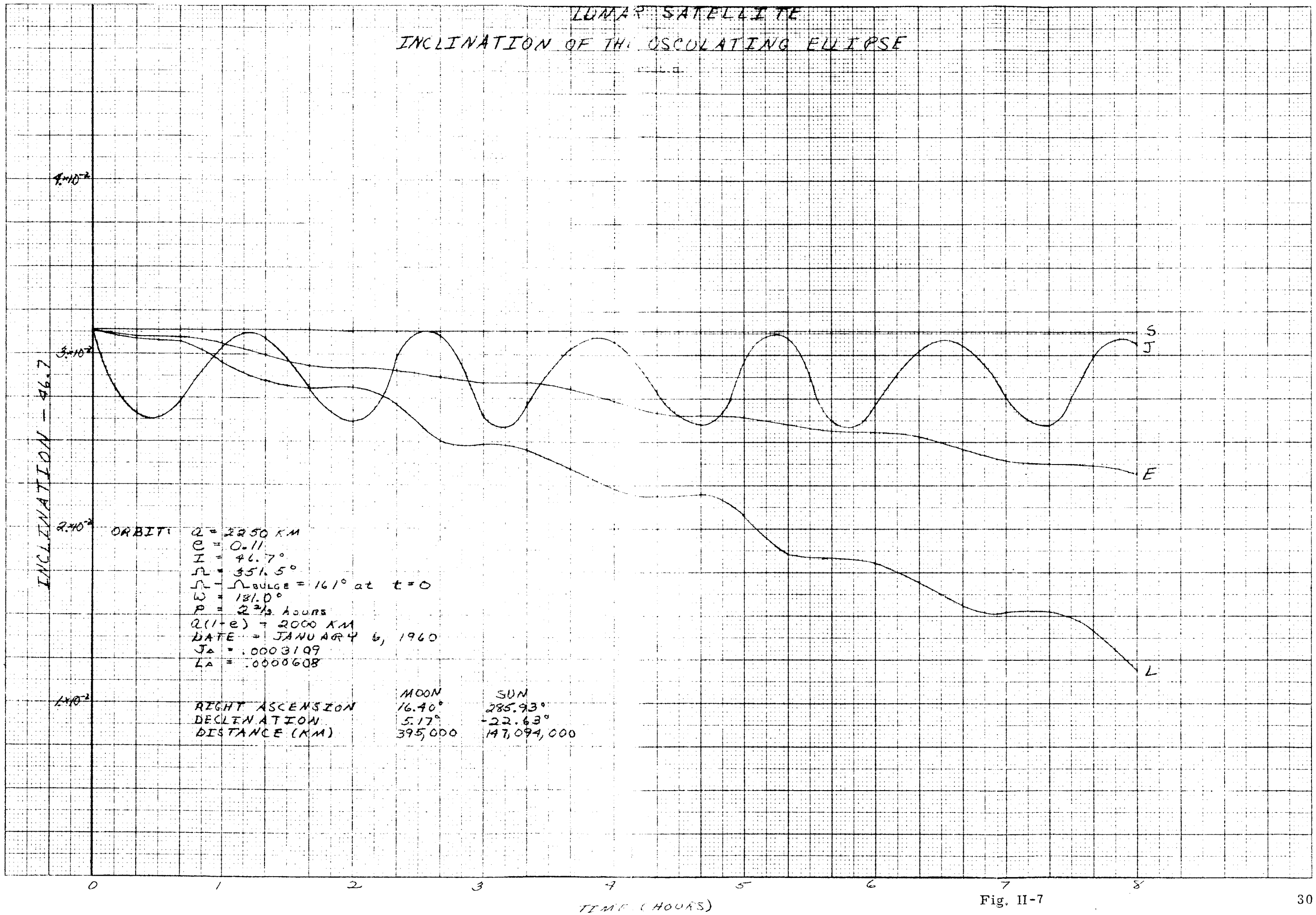
LUNAR SATELLITE
INCLINATION OF THE OSCULATING ELLIPSE
INCLINATION - 46.7
4×10⁻²
3×10⁻²
2×10⁻²
1×10⁻²
S
J
E
L
ORBIT: a = 2250 KM
e = 0.11
I = 46.7°
Ω = 351.5°
Ω - Ω BULGE = 161° at t = 0
ω = 181.0°
P = 2 2/3 HOURS
a(1+e) = 2000 KM
DATE = JANUARY 6, 1960
J2 = .0003109
L2 = .0000608
MOON
SUN
RIGHT ASCENSION 16.40° 285.93°
DECLINATION 5.17° -22.63°
DISTANCE (KM) 395,000 147,094,000
0
1
2
3
4
5
6
7
8
TIME (HOURS)

Fig. II-7

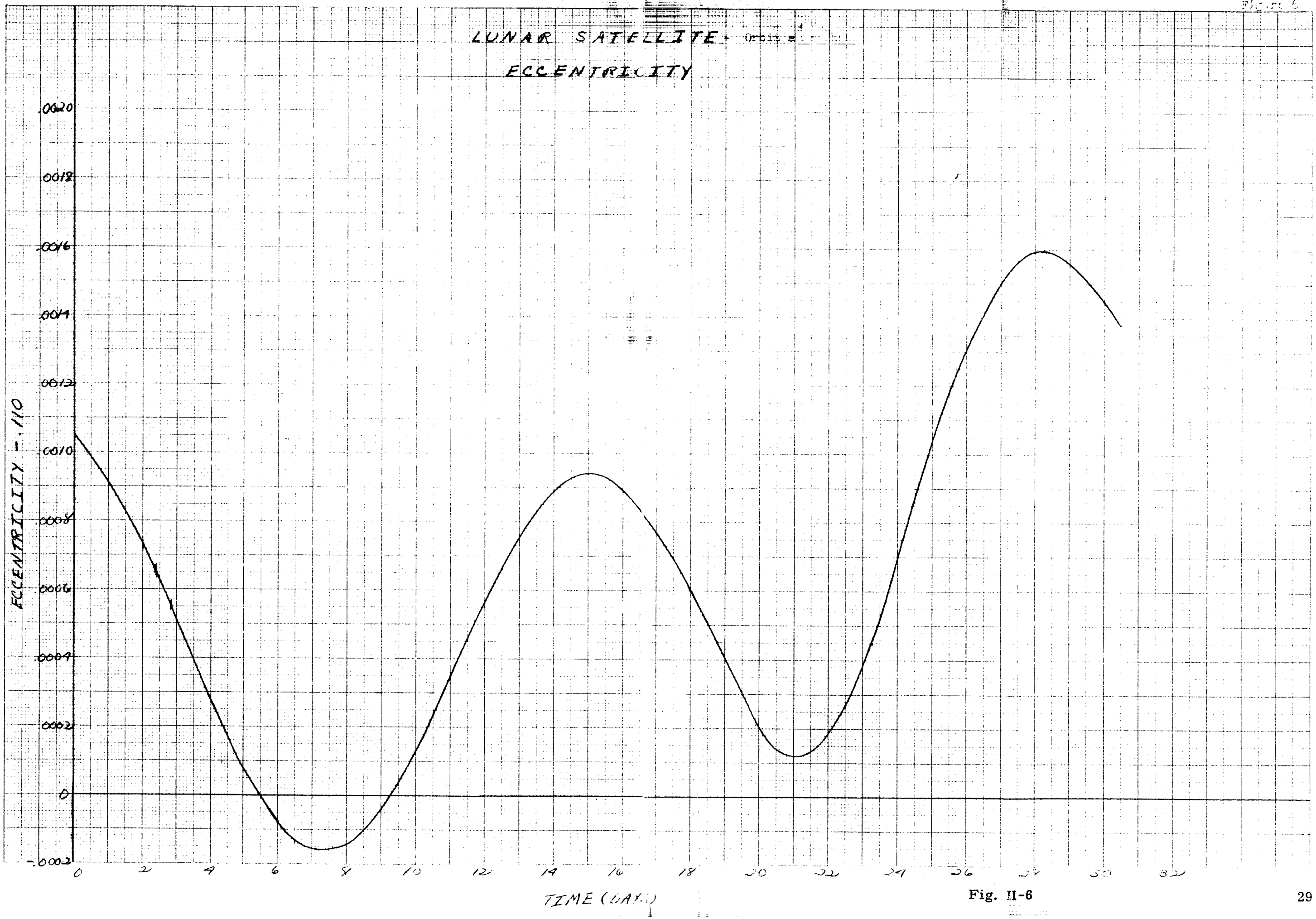
LUNAR SATELLITE
ECCENTRICITY
ECCENTRICITY - .110
.0020
.0018
.0016
.0014
.0012
.0010
.0008
.0006
.0004
.0002
0
-.0002
0
2
4
6
8
10
12
14
16
18
20
22
24
26
28
30
32
TIME (DAYS)

Fig. II-6

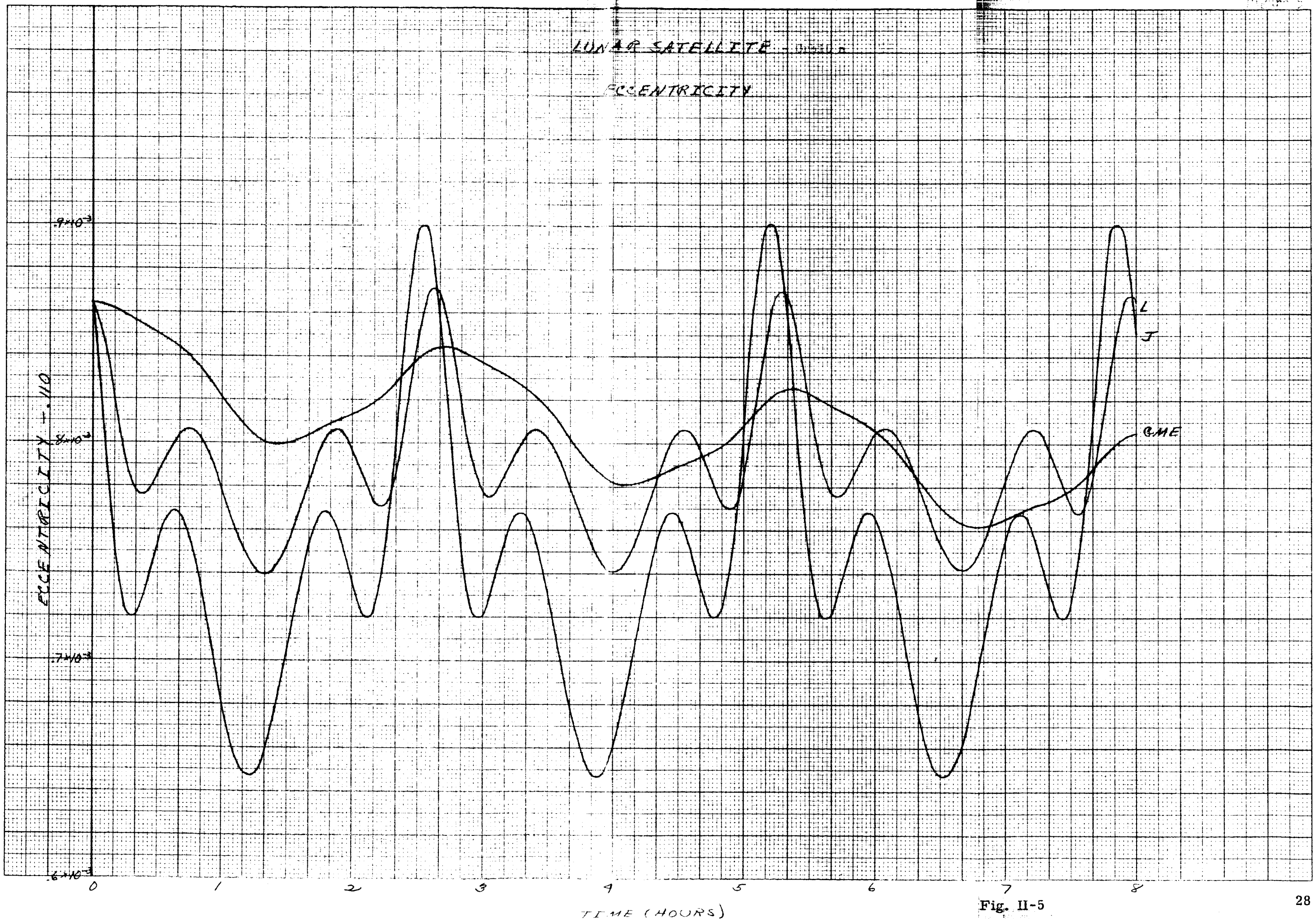
LUNAR SATELLITE
ECCENTRICITY
ECCENTRICITY + .110
9×10⁻³
8×10⁻³
7×10⁻³
6×10⁻³
0
1
2
3
4
5
6
7
8
TIME (HOURS)
L
J
GME

Fig. II-5

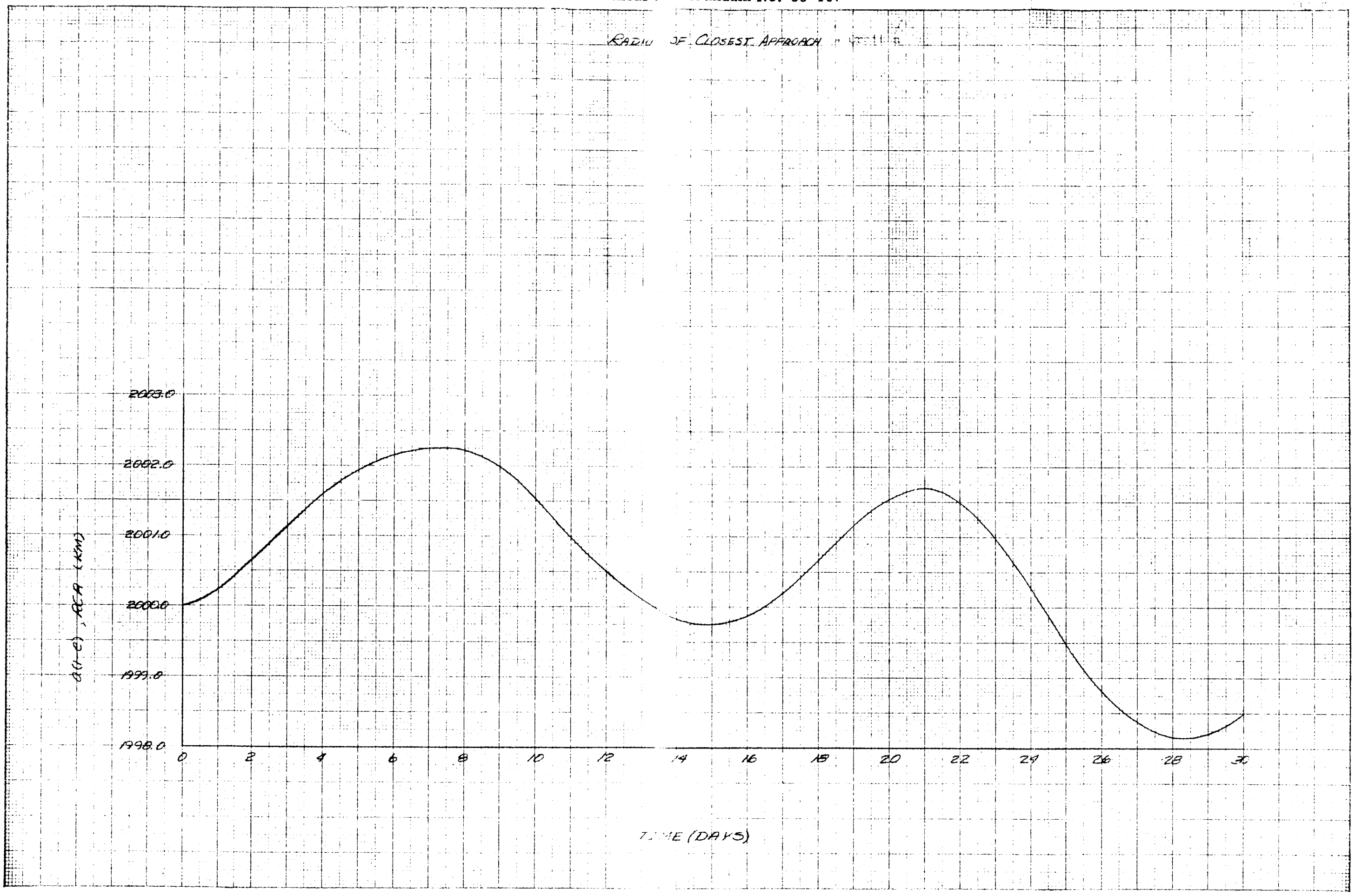
RADIUS OF CLOSEST APPROACH
2003.0
2002.0
2001.0
2000.0
1999.0
1998.0
0
2
4
6
8
10
12
14
16
18
20
22
24
26
28
30
TIME (DAYS)

Fig. II-4

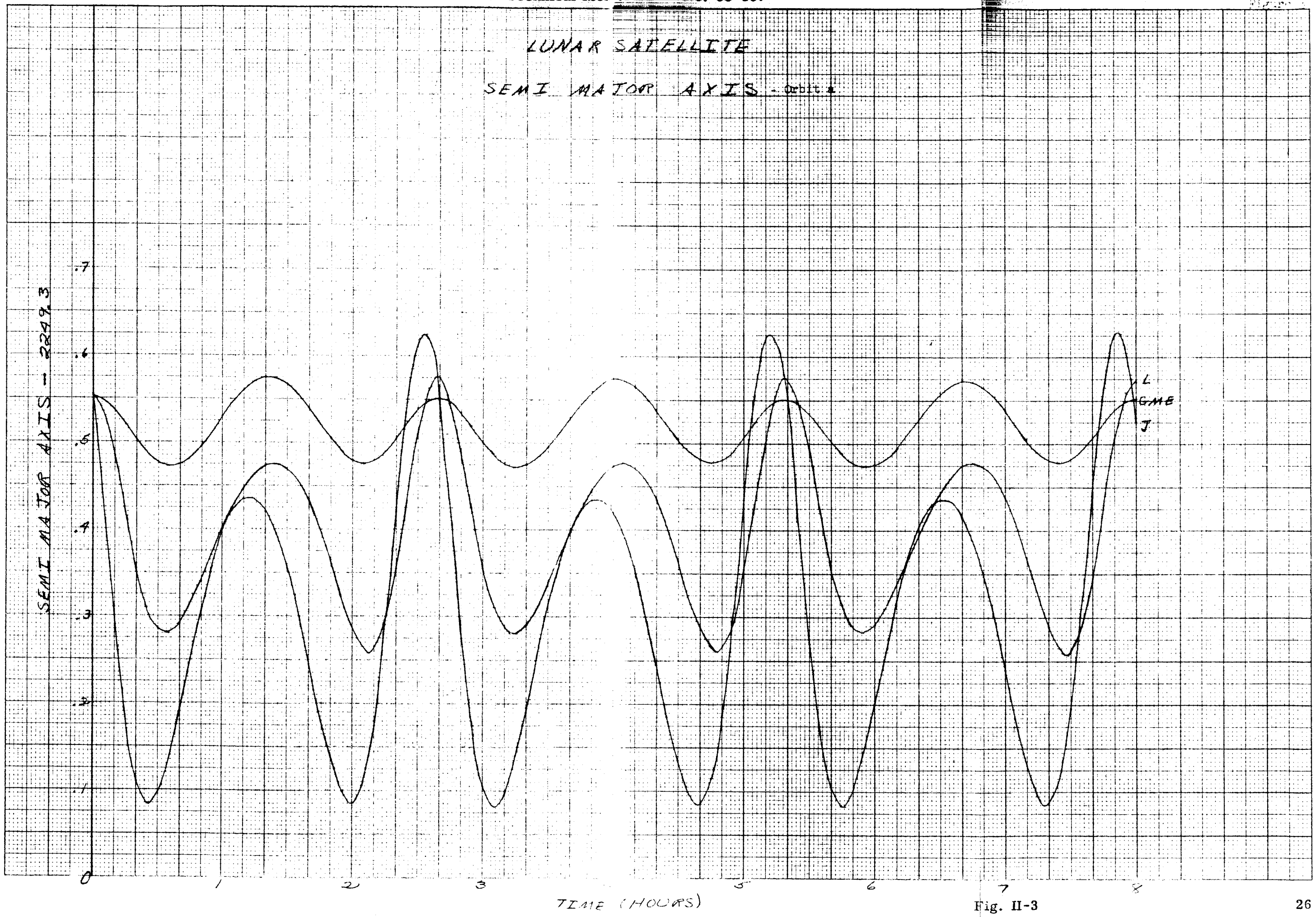
LUNAR SATELLITE
SEMI MAJOR AXIS - Orbit #
SEMI MAJOR AXIS - 2249.3
.7
.6
.5
.4
.3
.2
.1
0
1
2
3
5
6
7
8
TIME (HOURS)
L
GME
J

Fig. II-3

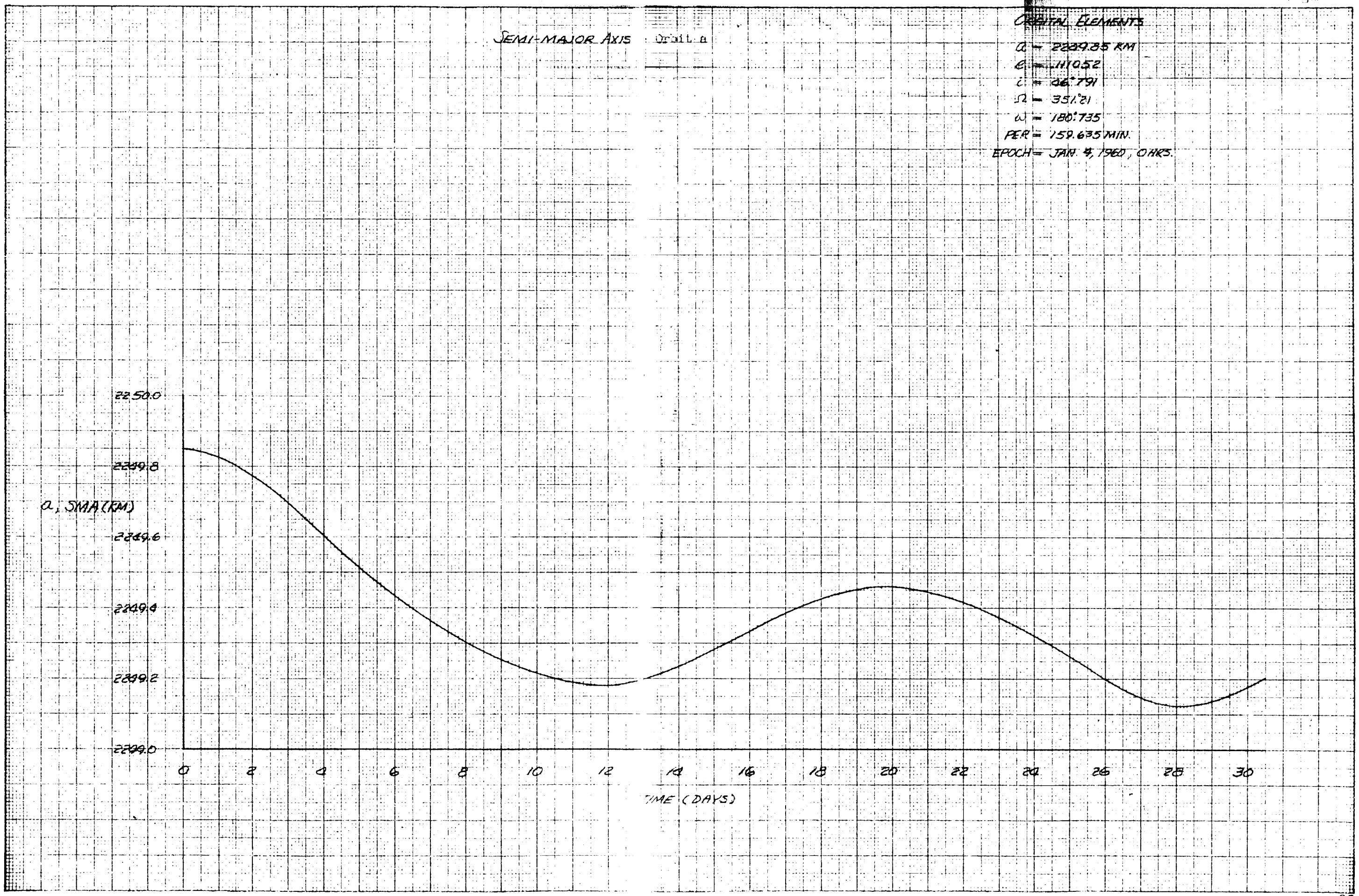
SEMI-MAJOR AXIS Orbit a
ORBITAL ELEMENTS
a = 2249.85 KM
e = .11052
i = 46°.791
Ω = 351°.21
ω = 180°.735
PER = 159.635 MIN.
EPOCH = JAN. 4, 1960, 0 HRS.
a, SMA (KM)
2250.0
2249.8
2249.6
2249.4
2249.2
2249.0
0
2
4
6
8
10
12
14
16
18
20
22
24
26
28
30
TIME (DAYS)

Fig. II-2

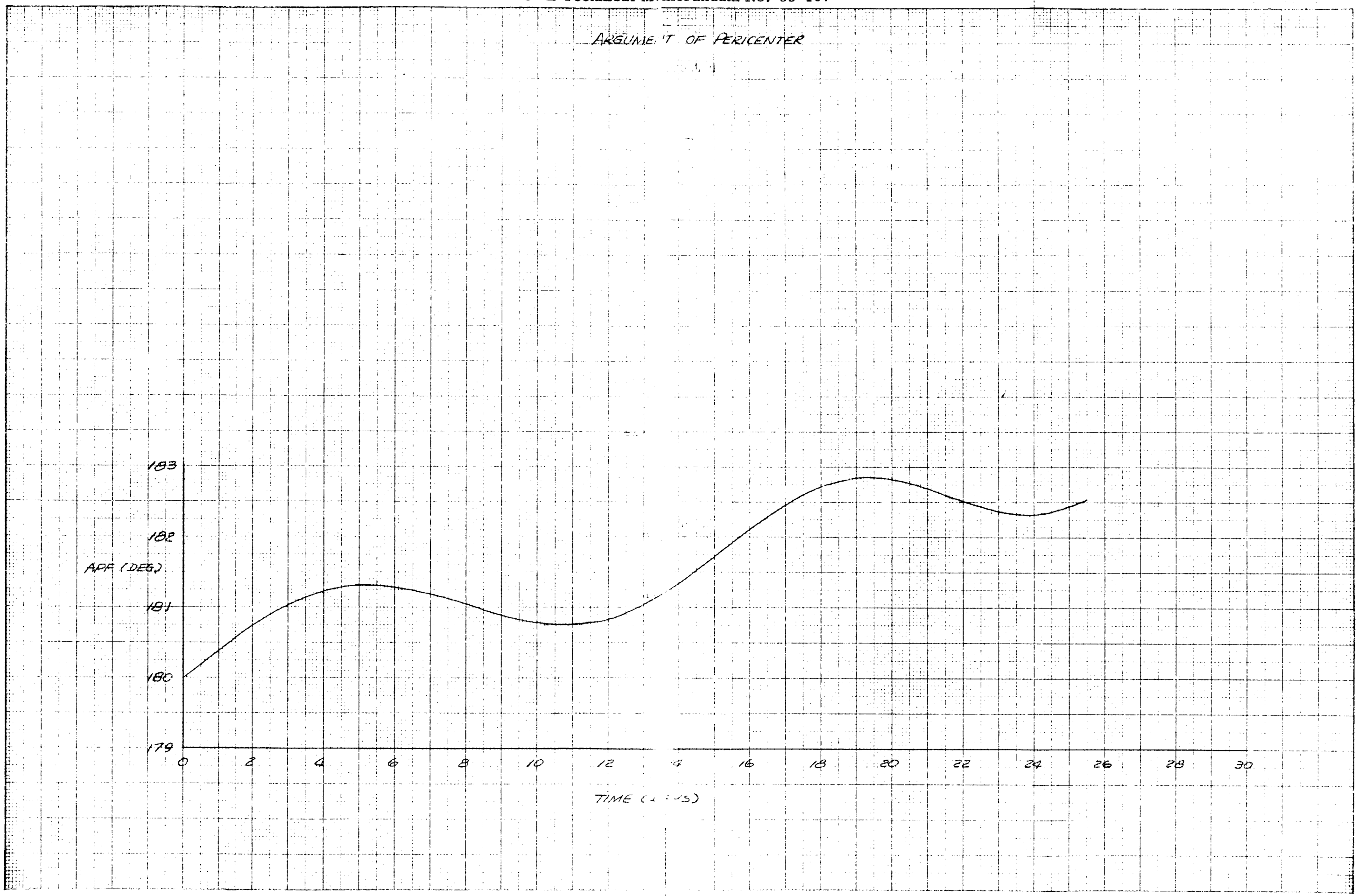
ARGUMENT OF PERICENTER
183
182
APF (DEG)
181
180
179
0
2
4
6
8
10
12
16
18
20
22
24
26
28
30
TIME

Fig. II-30

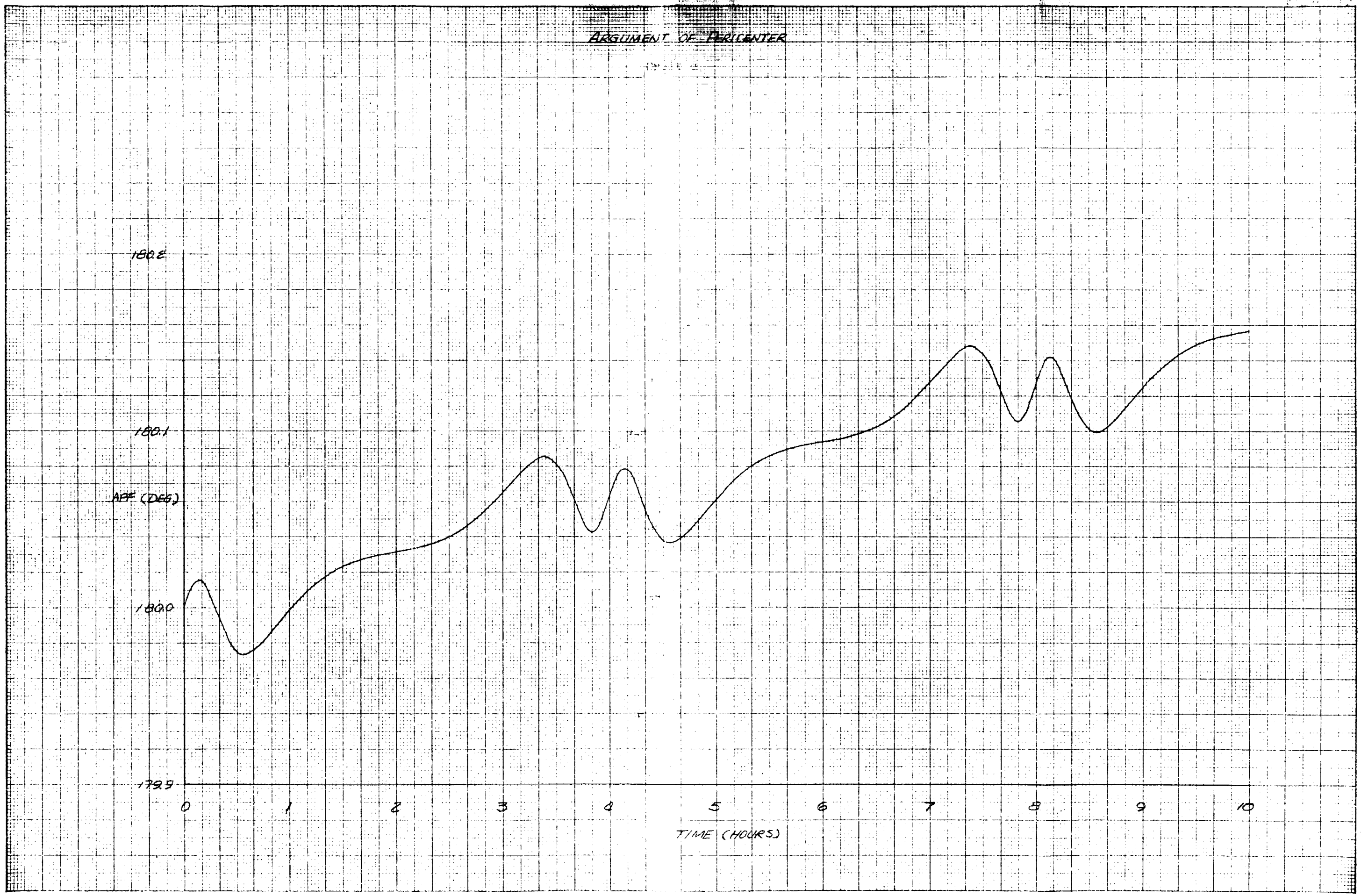
ARGUMENT OF PERICENTER
180.2
180.1
ADF (DEG)
180.0
179.9
0
1
2
3
4
5
6
7
8
9
10
TIME (HOURS)

Fig. II-29

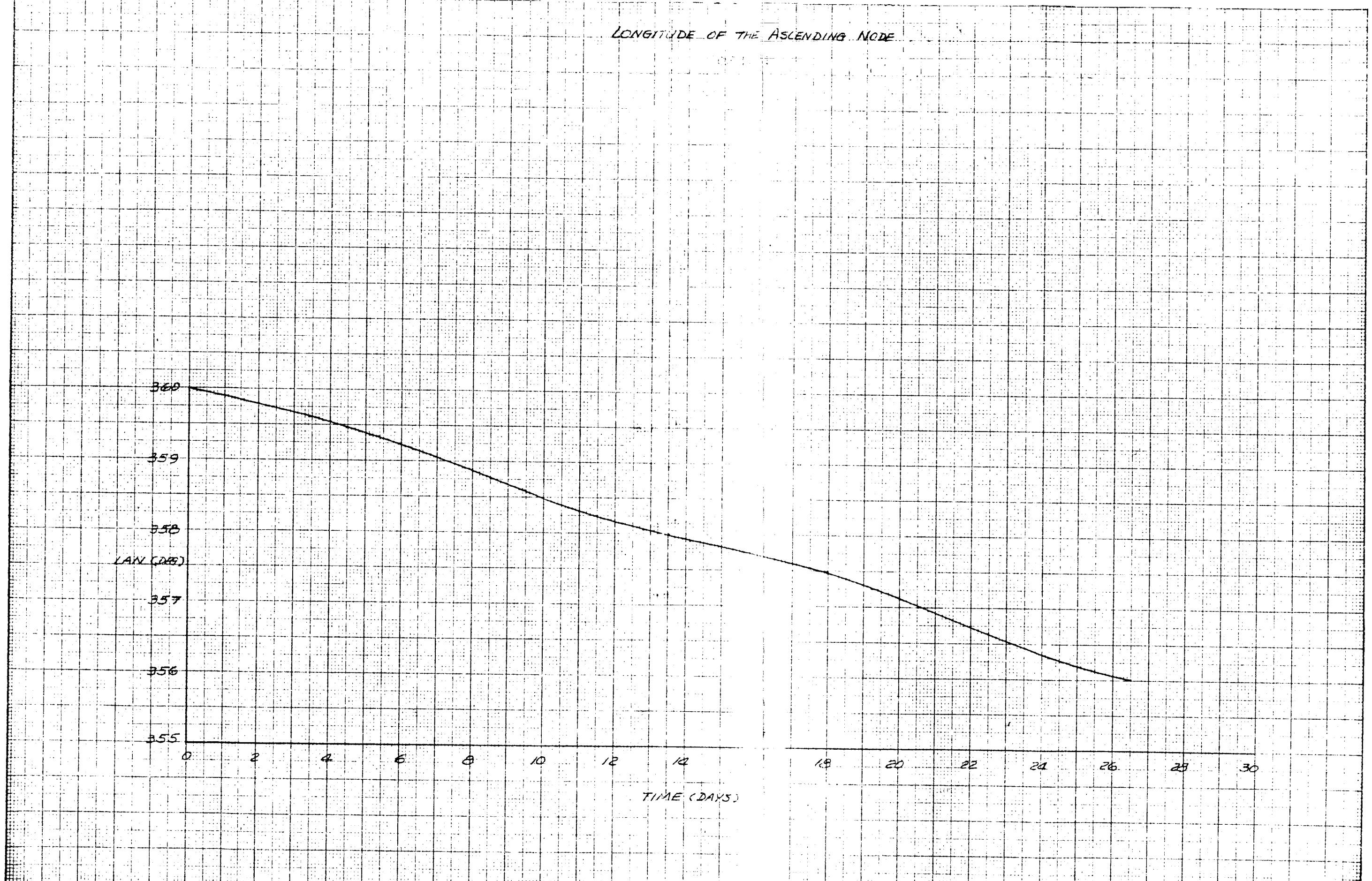
LONGITUDE OF THE ASCENDING NODE
360
359
358
LAN (DEG)
357
356
355
0
2
4
6
8
10
12
14
18
20
22
24
26
28
30
TIME (DAYS)

Fig. II-28

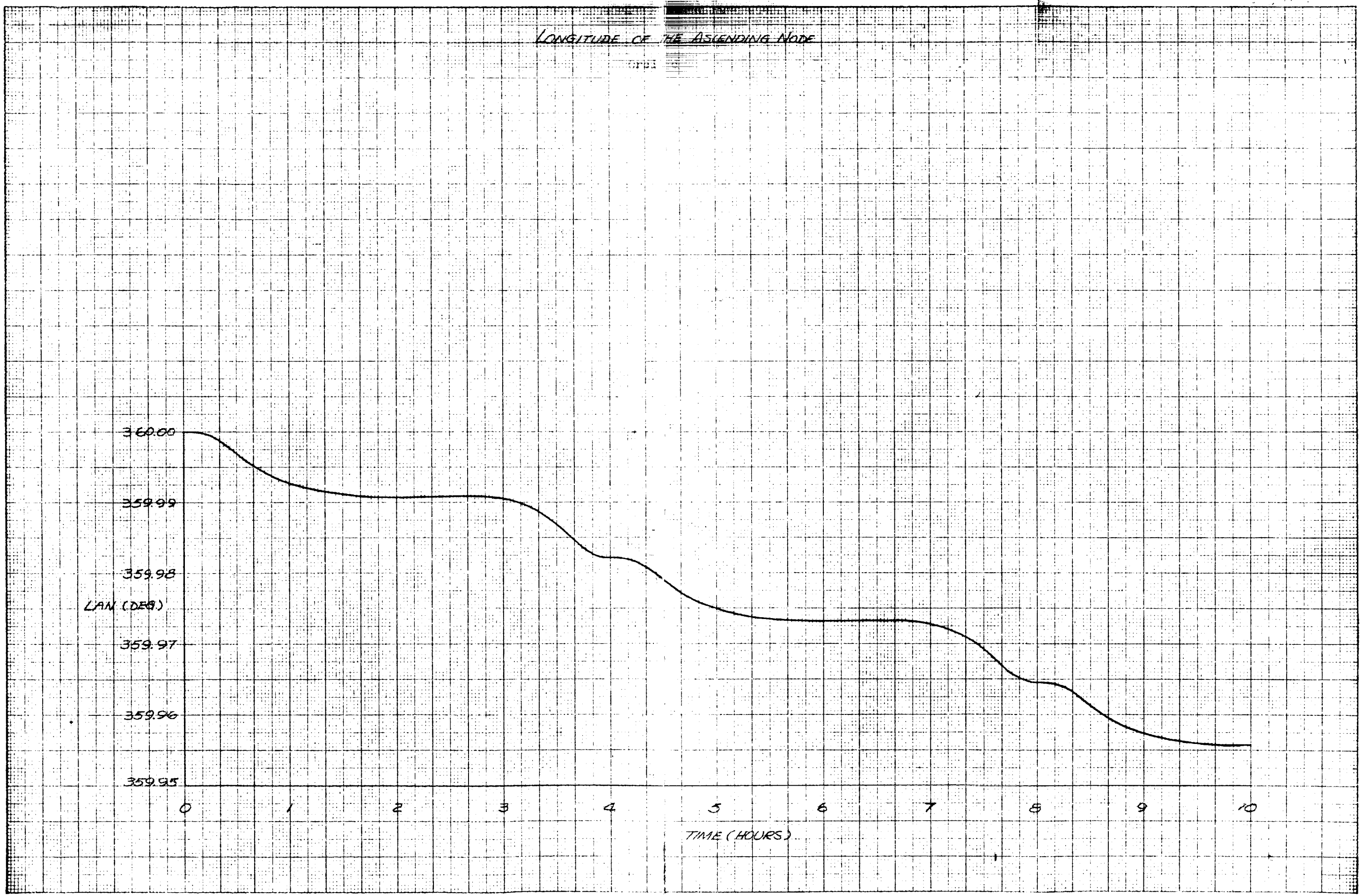
LONGITUDE OF THE ASCENDING NODE
360.00
359.99
359.98
LAN (DEG.)
359.97
359.96
359.95
0
1
2
3
4
5
6
7
8
9
10
TIME (HOURS)

Fig. II-2.7

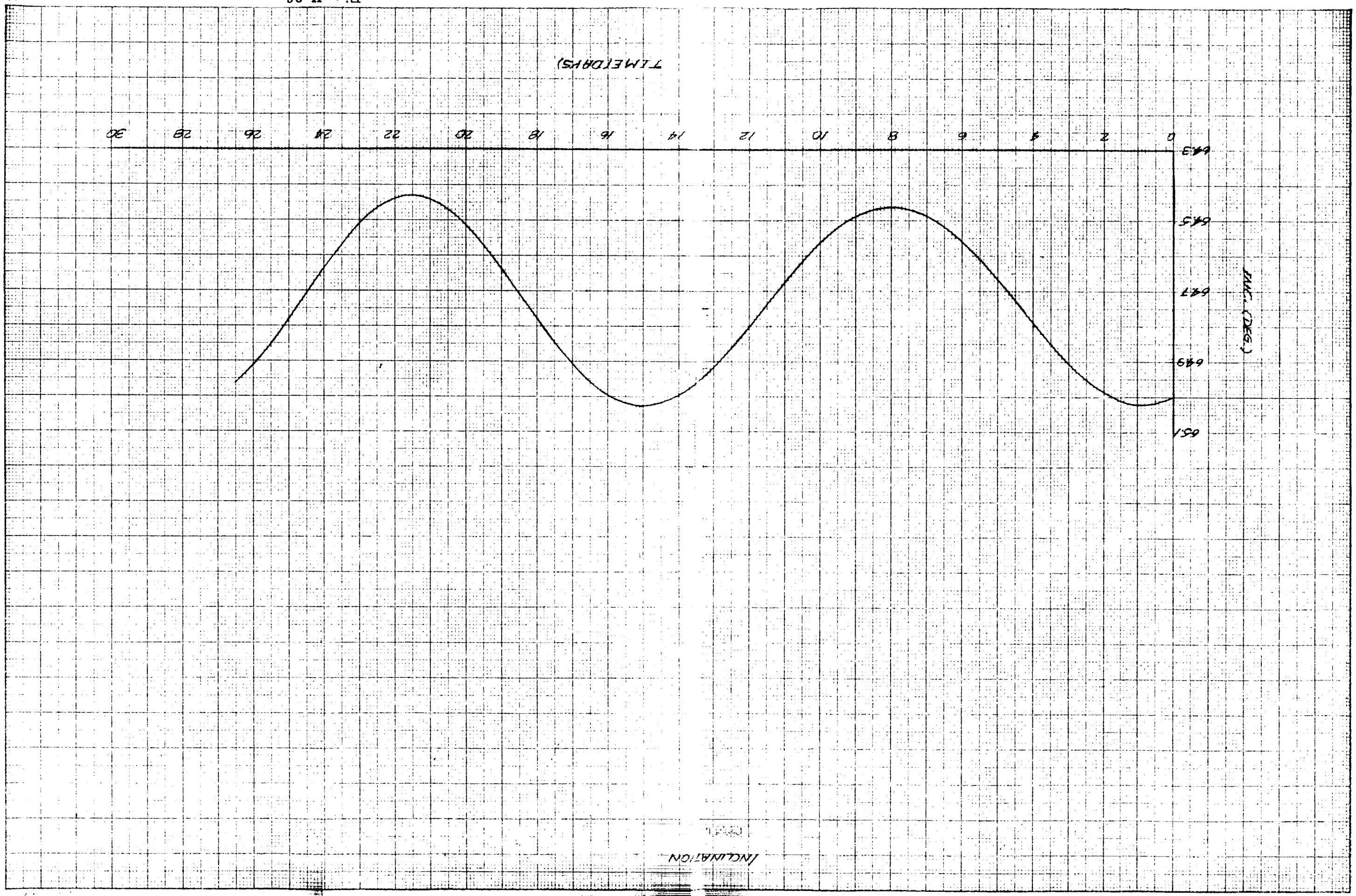
INCLINATION
(DEG.)
651
649
647
645
643
0
2
4
6
8
10
12
14
16
18
20
22
24
26
28
30
TIME(DAYS)

Fig. II-26

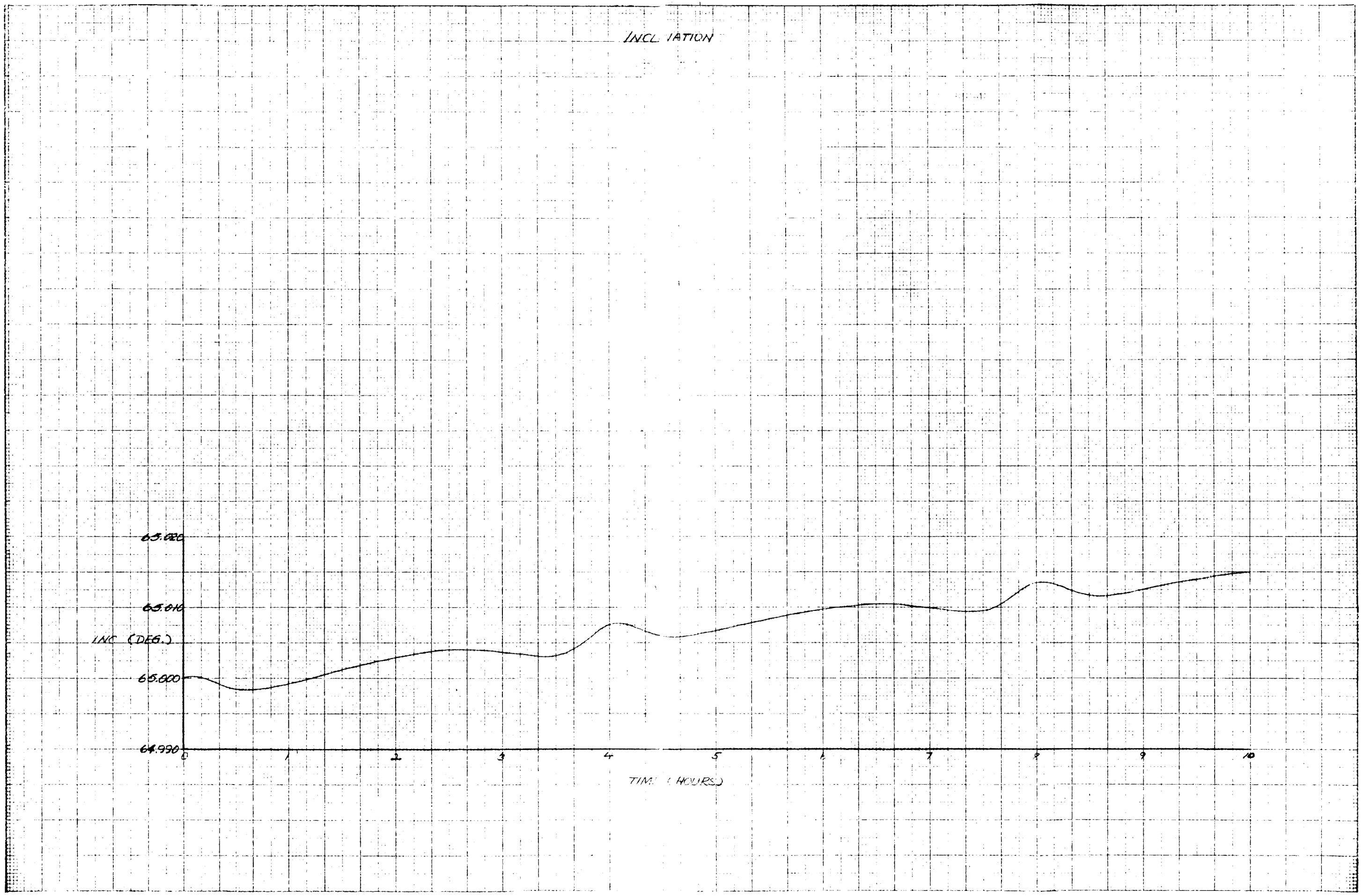
INCLINATION
65.020
65.010
INC (DEG.)
65.000
64.990
0
1
2
3
4
5
6
7
8
9
10
TIME (HOURS)

Fig. II-25

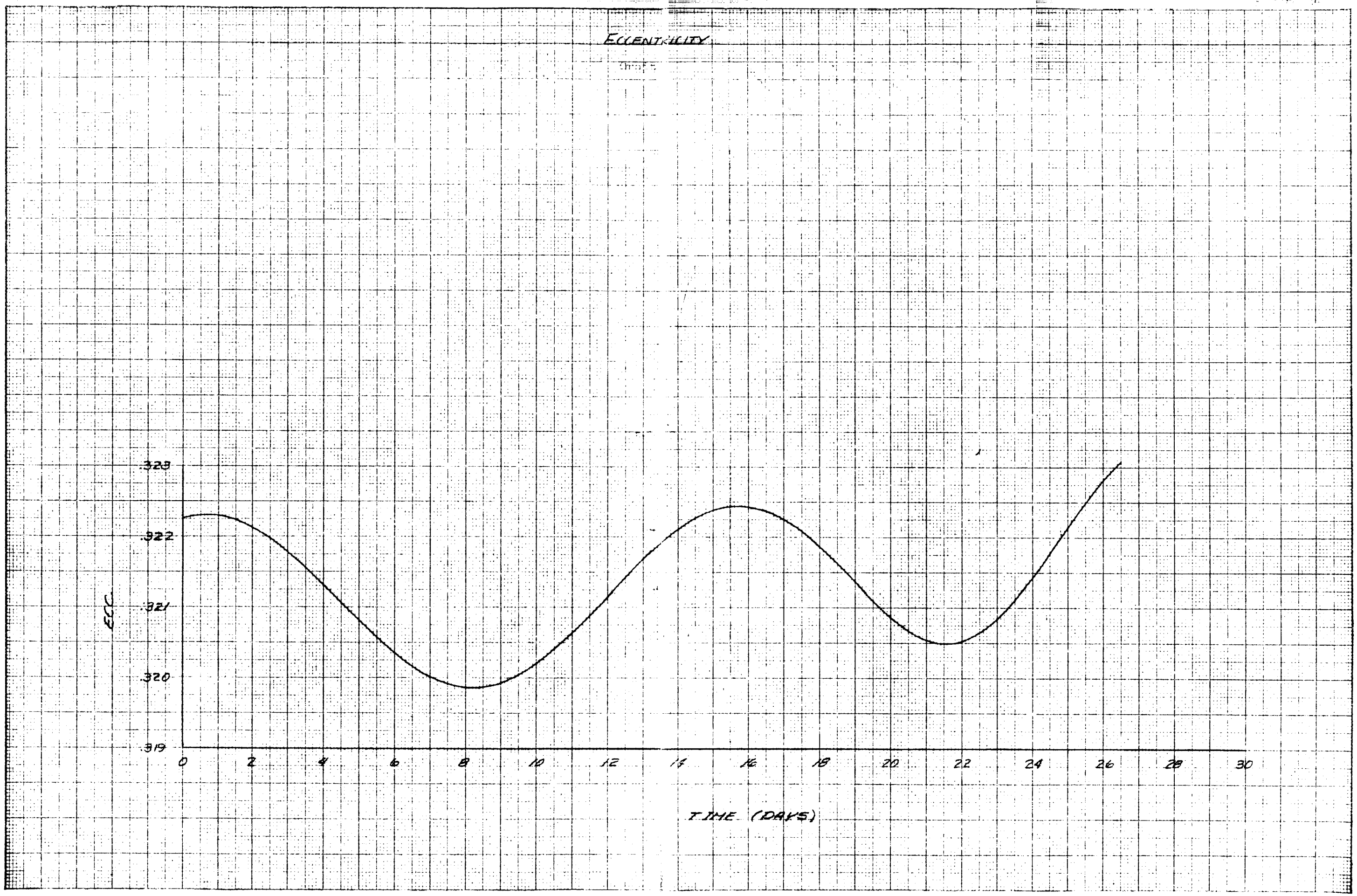
ECCENTRICITY
.323
.322
.321
.320
.319
ECC
0
2
4
6
8
10
12
14
16
18
20
22
24
26
28
30
TIME (DAYS)

Fig. II-24

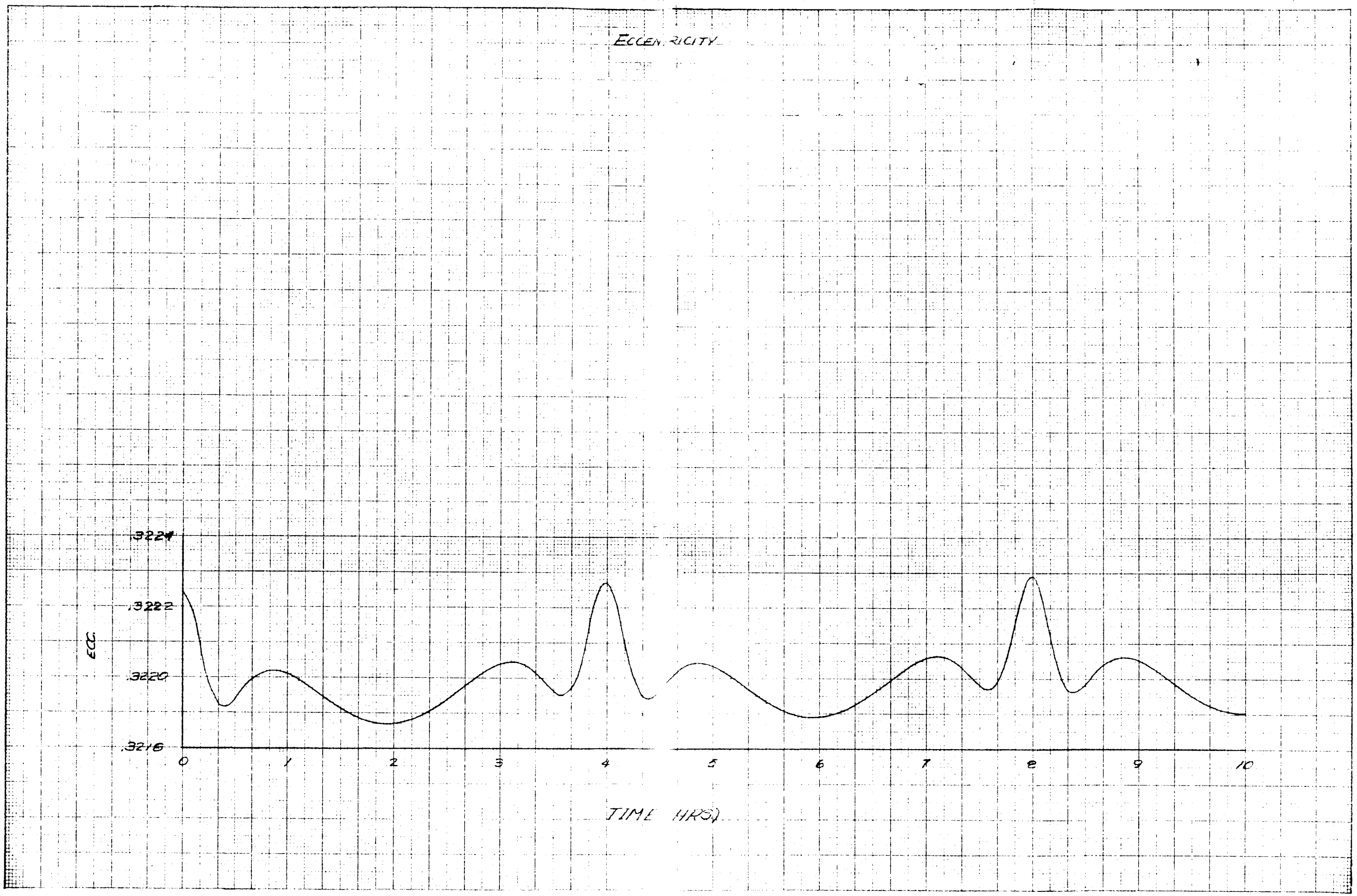
ECCENTRICITY
.3224
.3222
.3220
.3216
ECC
0
1
2
3
4
5
6
7
8
9
10
TIME (HRS)

Fig. II-23

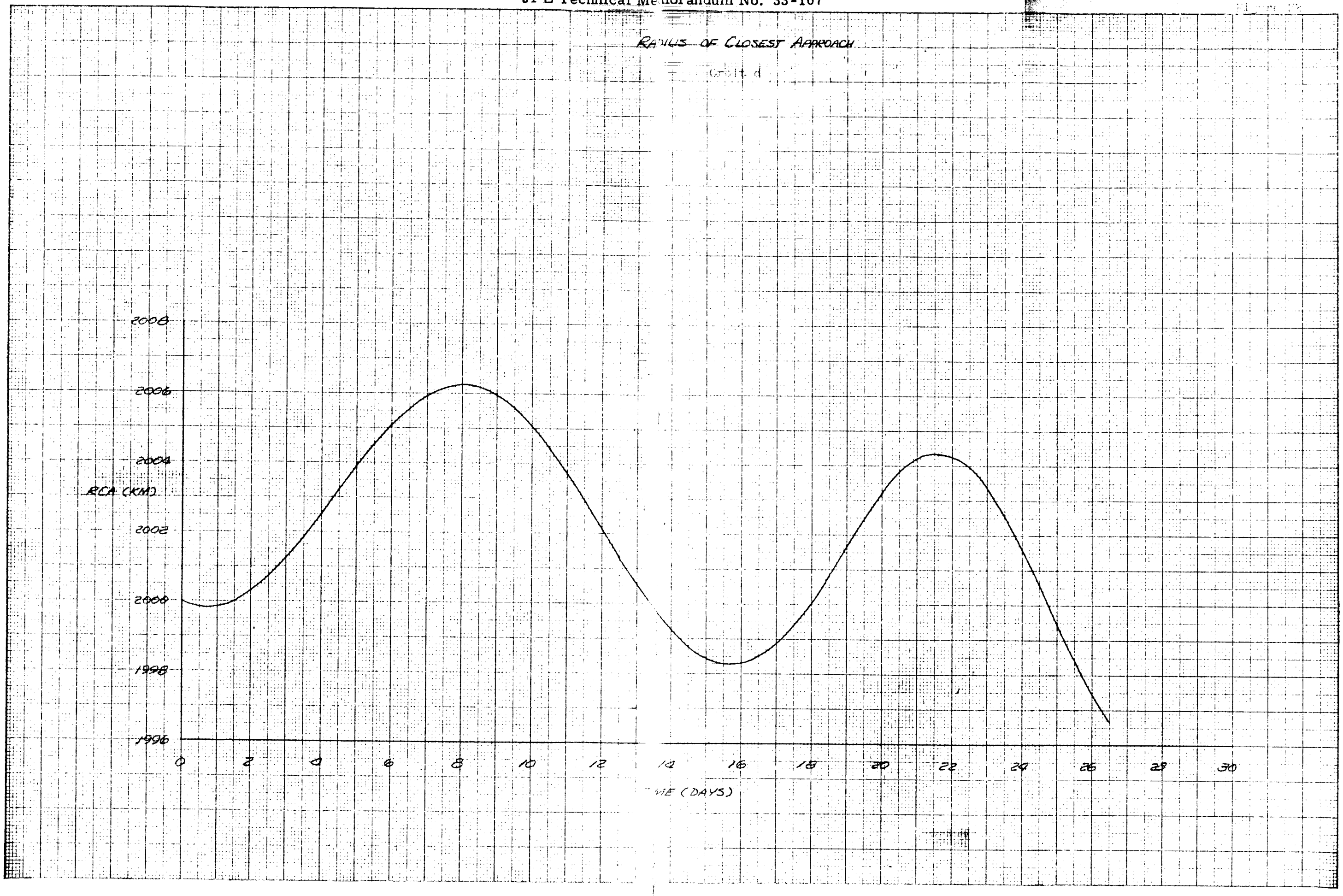

Fig. II-22

K+E 10 X 10 TO THE CM. 359T-14LG KEUFFEL & ESSER CO. ALBANENE ® MADE IN U.S.A.

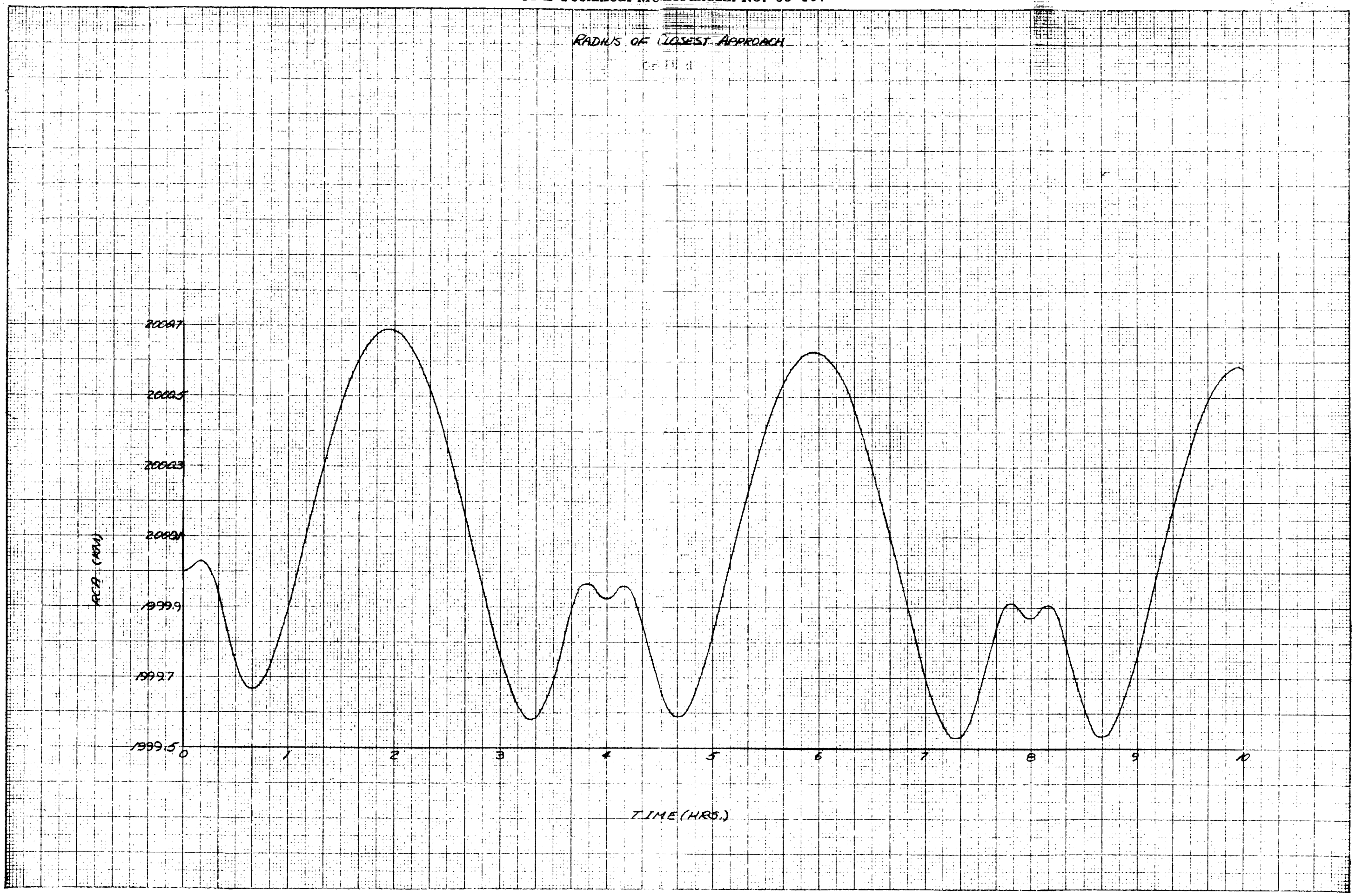
RADIUS OF CLOSEST APPROACH
2009.7
2009.5
2009.3
2009.1
1999.9
1999.7
1999.5
RCP (AU)
0
1
2
3
4
5
6
7
8
9
10
TIME (HRS.)

Fig. II-21

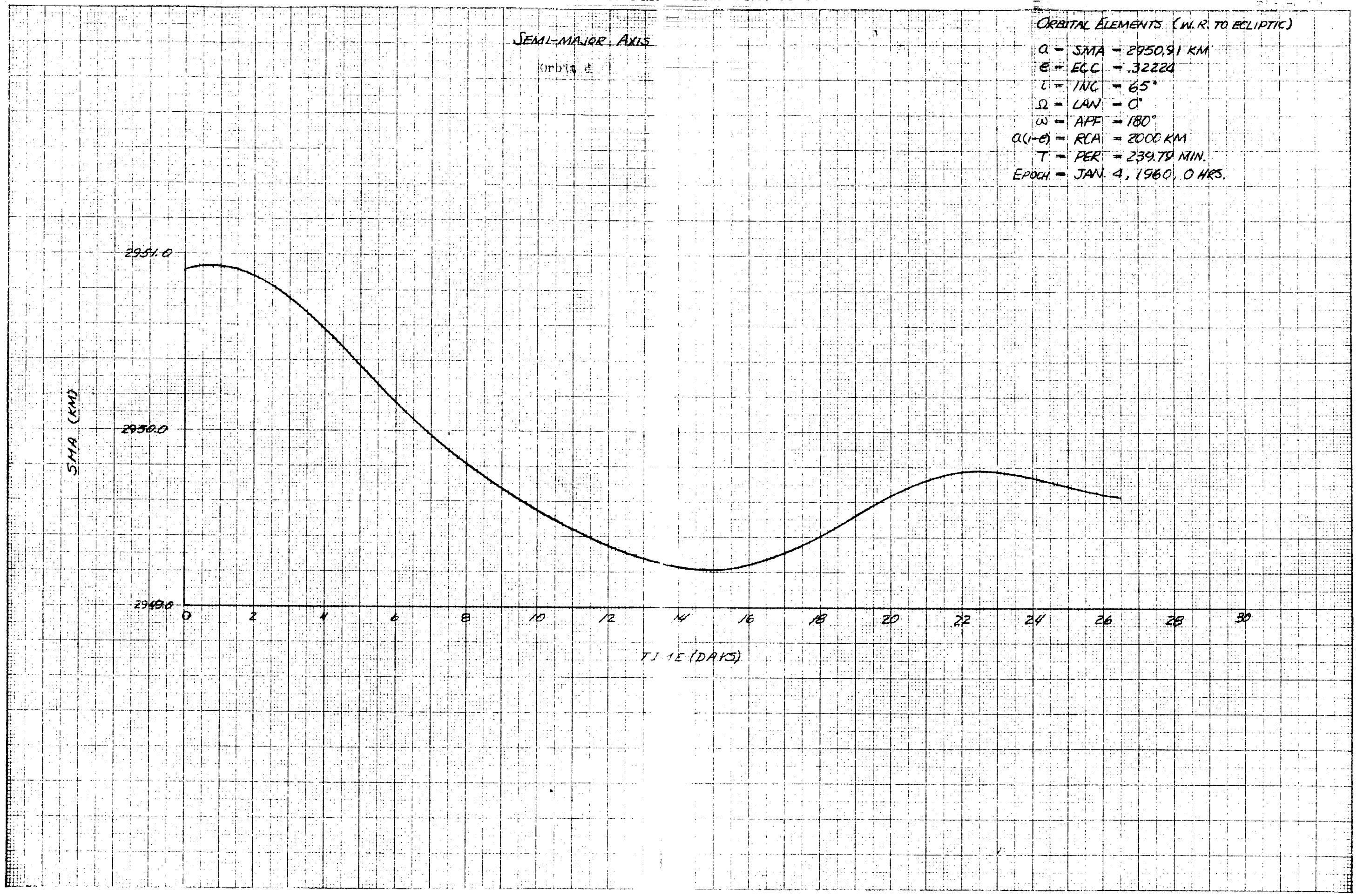
SEMI-MAJOR AXIS
Orbit 4
ORBITAL ELEMENTS (W.R. TO ECLIPTIC)
a - SMA - 2950.91 KM
e - ECC - .32224
i - INC - 65°
Ω - LAN - 0°
ω - APF - 180°
a(1-e) - RCA - 2000 KM
T - PER - 239.79 MIN.
EPOCH - JAN. 4, 1960, 0 HRS.
SMA (KM)
2951.0
2950.0
2949.0
0
2
4
6
8
10
12
14
16
18
20
22
24
26
28
30
TIME (DAYS)

Fig. II-20

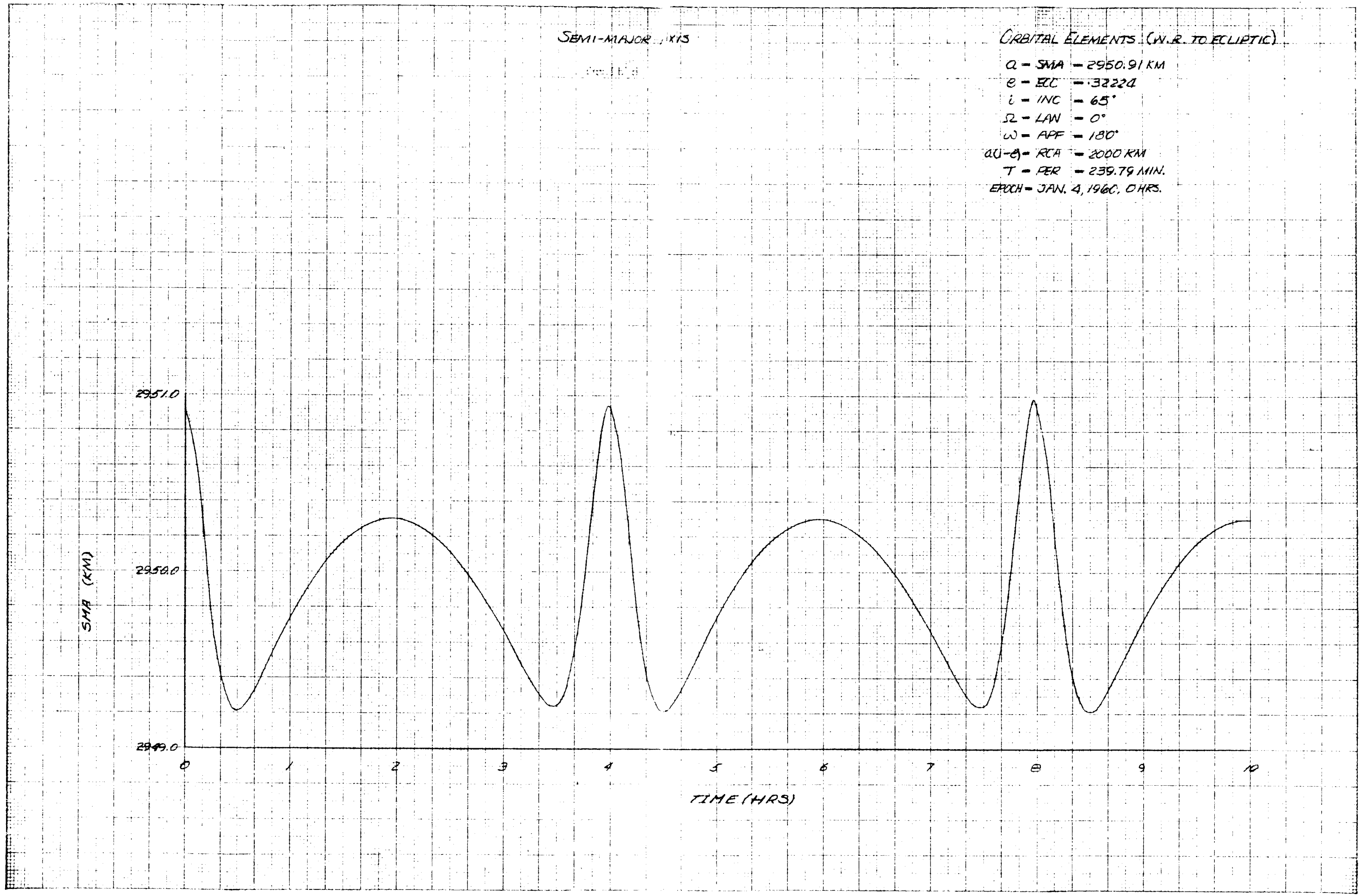
SEMI-MAJOR AXIS
ORBITAL ELEMENTS (W.R. TO ECLIPTIC)
a - SMA - 2950.91 KM
e - ECC - .32224
i - INC - 65°
Ω - LAN - 0°
ω - APF - 180°
a(1-e) - RCA - 2000 KM
T - PER - 239.79 MIN.
EPOCH - JAN. 4, 1960, 0 HRS.
2951.0
2950.0
2949.0
SMA (KM)
0
1
2
3
4
5
6
7
8
9
10
TIME (HRS)

Fig. II-19

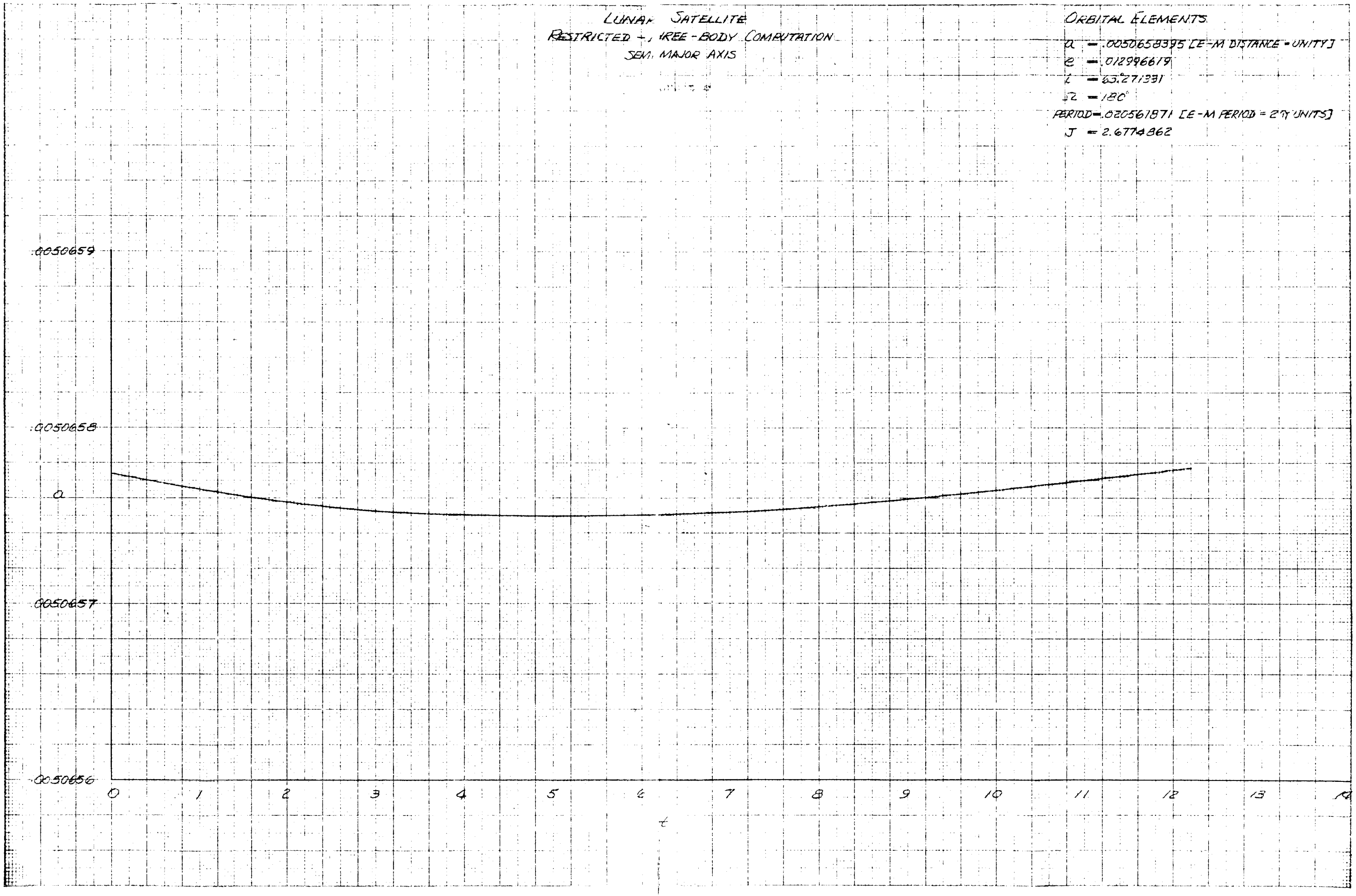
LUNAR SATELLITE
RESTRICTED 3, FREE-BODY COMPUTATION
SEMI MAJOR AXIS
ORBITAL ELEMENTS
a = .0050658395 [E-M DISTANCE = UNITY]
e = .012996619
i = 63.271331
Ω = 180°
PERIOD = .020561871 [E-M PERIOD = 2π UNITS]
J = 2.6774862
.0050659
.0050658
a
.0050657
.0050656
0
1
2
3
4
5
6
7
8
9
10
11
12
13
14
t

Fig. II-31

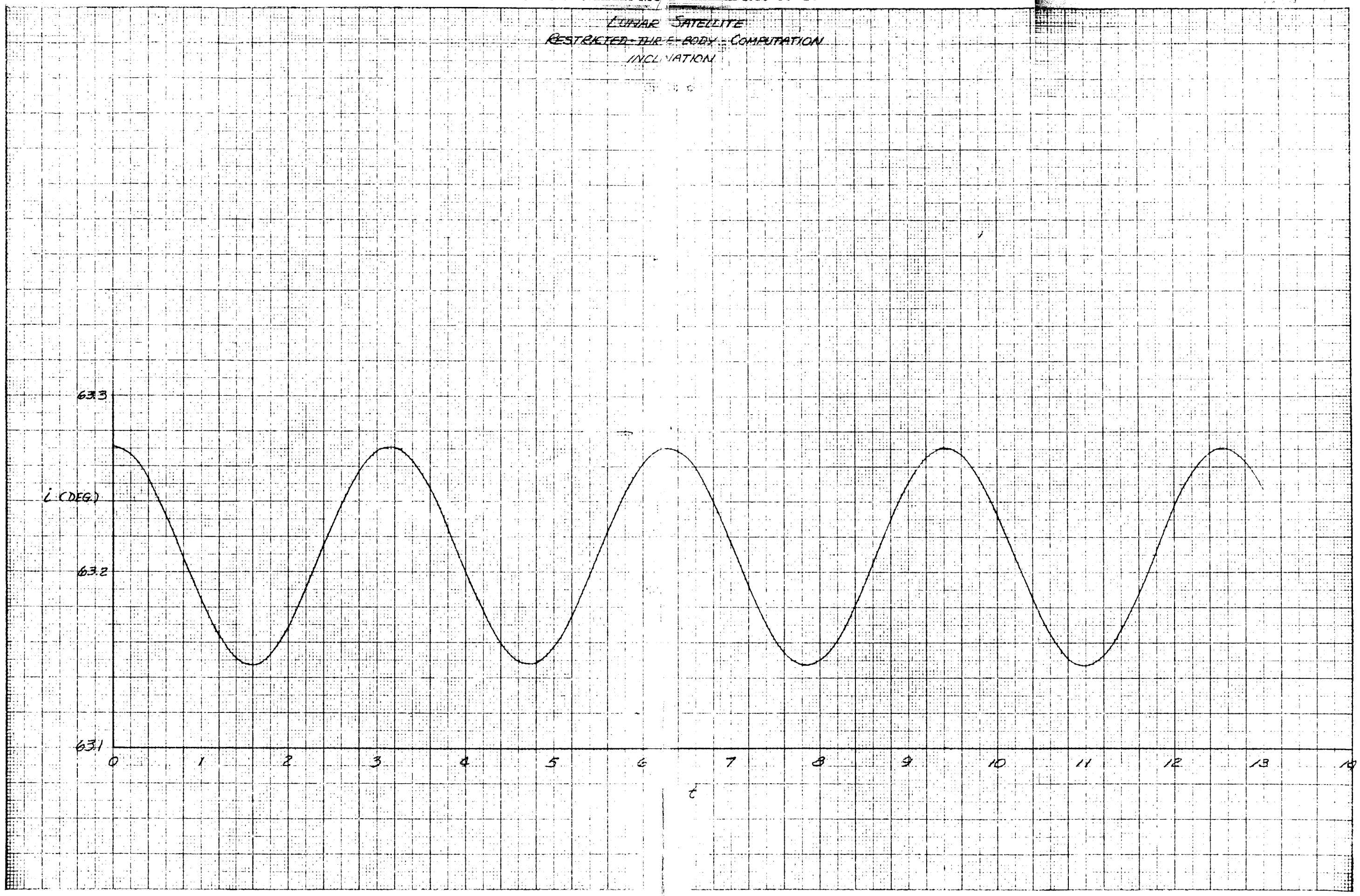
LUNAR SATELLITE
RESTRICTED-THREE-BODY-COMPUTATION
INCLINATION
633
i (DEG)
63.2
63.1
0
1
2
3
4
5
6
7
8
9
10
11
12
13
14
t

Fig. II-32

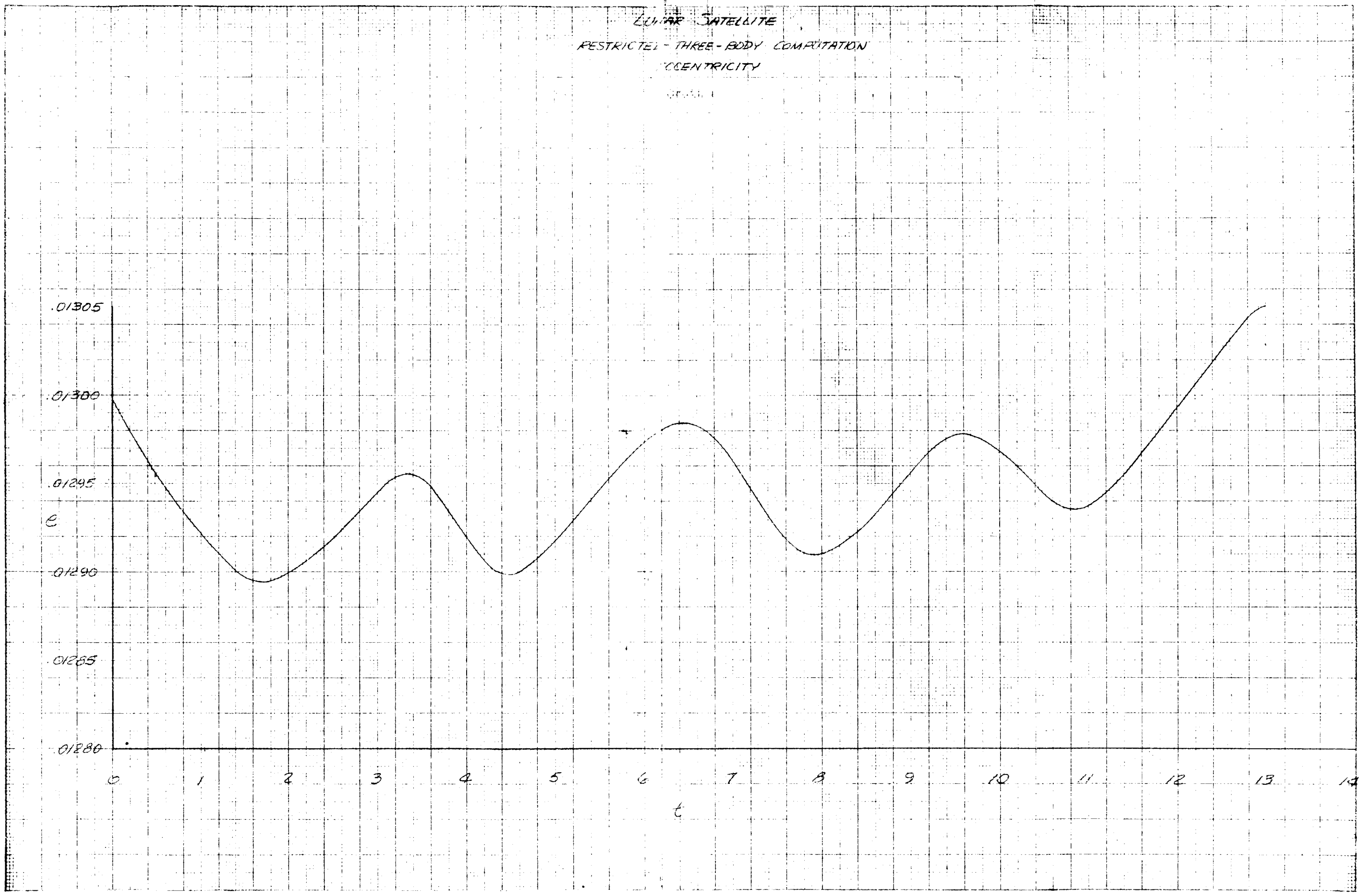
LUNAR SATELLITE
RESTRICTED - THREE - BODY COMPUTATION
ECCENTRICITY
.01305
.01300
.01295
e
.01290
.01285
.01280
0
1
2
3
4
5
6
7
8
9
10
11
12
13
14
t

Fig. II-33

III. THEORY OF ORBIT DETERMINATION

by J. D. Anderson

The usual orbit determination problem is to reduce a set of observations to a set of orbital parameters which describe, by means of a solution to the differential equations of motion, the orbit of the observed object for all time. In space flight problems the number of observations is large, and a weighted least squares estimator is used to obtain these parameters. In the case of a lunar satellite orbit, problems arise if the orbit determination is extended over many orbital periods because the solution to the equations of motion is obtained by a step-by-step numerical integration. The accuracy of these solutions is known to suffer an accumulative degradation as the solution is extended to future times, and so it is only reasonable to determine the orbit of the satellite over a limited number of orbits. However, if observations are continually available over many orbits, it is possible to compute an orbit every few days and thus always to have available a relatively accurate knowledge of the position and, if needed, the velocity of the orbiter. In addition, certain physical constants can be included in the estimation procedure as additional parameters. Of particular interest for a close satellite are the mass of the Moon and the second harmonic coefficients in the Legendre expansion of the Moon's potential function. For a distant satellite, the mass of the Earth and the Earth-Moon distance could also enter. An introduction of physical constants serves to provide a more realistic estimate of the satellite's position and velocity coordinates as well as to influence the parameter covariance matrix which describes the accuracy of the least

squares fit to the data. Without this influence an overly optimistic estimate of the accuracy of the orbit determination can result.

Besides providing an accurate ephemeris of the satellite for navigational and charting purposes, the orbit determination can provide useful information about the physical character of the Moon. Such a study requires the evaluation of long-term effects in the orbit and the selection of harmonic coefficients in the potential function that will describe the periodic motions of the orbital elements. It is proposed that mean elements, in other words elements averaged over one period of the satellite's motion, be used to determine the harmonic coefficients. Rates in these mean elements can be derived quite easily and then numerically integrated to yield the mean elements as a function of time. The observed values of the mean elements are obtained from the short-term orbit determination program discussed above and are available at various time points. Therefore, the fit of the computed elements to the observed elements along with the harmonic coefficients can be obtained in a minimum variance sense if the estimation errors in the elements are assumed not autocorrelated. Then the covariance matrix on all the mean element data consists of blocks down the diagonal, and it can be inverted by inverting each small block independently. If there are six orbital elements, for example, a 6 x 6 covariance matrix can be constructed at each mean element data point by applying the above short-term program. Then, because the elements are assumed uncorrelated between data time points, the larger covariance matrix of all data can be inverted by inverting each 6 x 6 matrix and by arranging them as blocks down the diagonal of the matrix. This assumption of independence seems reasonable if the raw data are

uncorrelated between mean element time points and if all significant physical constants are adjusted along with the orbital elements. The method of computing the mean orbital elements and their covariance matrix is described as follows:

The vector of orbit parameters e can be expressed either as a function of time t and the initial value e of the parameters at the epoch t_0 or equivalently as a function of the mean anomaly M. That is, $e = e(t, e_0)$ or $e = e'(M, e_0)$. The estimate e_0^* of the vector e_0 is obtained by the usual weighted least squares fit to data taken in the orbital pass associated with t_0. It is the above short-term program that is used for this purpose. Usually, a set of parameters other than e is used in this program, and the appropriate transformations must be available to go from one set to another. Designating the other set of parameters by q--for example, cartesian coordinates at time t--we also assume that increments in q and e can be related by the linear relation

$$\delta q = A \delta e \tag{1}$$

In addition, we assume that the inverse transformation exists.

$$\delta e = A^{-1} \delta q \tag{2}$$

In order to study long-term effects in e, the mean elements $\bar{e}$ are required for the orbit in question. By definition

$$\bar{e} = \frac{1}{2\pi} \int_0^{2\pi} e'(M, e_0)\, dM \tag{3}$$

In practice, the above integral will be evaluated numerically. Clearly, the estimate $\bar{e}^*$ of $\bar{e}$ is obtained by using the estimate of e_0 in (3)

$$\bar{e}^* = \frac{1}{2\pi}\int_0^{2\pi} e'(M, e_0^*)\, dM \tag{4}$$

The covariance matrix on this estimate (4) is obtained simply by subtracting (4) from (3) to obtain the error vector $\delta\bar{e}$.

$$\delta\bar{e} = \bar{e}^* - \bar{e} = \frac{1}{2\pi}\int_0^{2\pi} \left[e(M, e_0^*) - e(M, e_0)\right] dM \tag{5}$$

The error on the estimate of e_0 is

$$\delta e_0 = e_0^* - e_0 \tag{6}$$

and $\delta\bar{e}$ and δe_0 are linearly related by

$$\delta\bar{e} = \frac{1}{2\pi}\int_0^{2\pi} \frac{\partial e}{\partial e_0}\, \delta e_0\, dM \tag{7}$$

The matrix $\partial e/\partial e_0$ can be written as the product of three matrices; the matrix A^{-1} of (2) evaluated at t, the matrix U that maps the parameters q from t_0 to t ($\delta q = U\delta q_0$), and the matrix A_0 of (1) evaluated at t_0.

$$\frac{\partial e}{\partial e_0} = A^{-1}\, U\, A_0 \tag{8}$$

The matrix U is an output of the numerical integration trajectory program if q represents cartesian components of position and velocity. Because A_0 and δe_0 are constant over the interval $0 \leq M \leq 2\pi$, Eq. (7) can be written

$$\delta\bar{e} = \left[\frac{1}{2\pi}\int_0^{2\pi} A^{-1}\, U\, dM\right] A_0 \delta e_0 \tag{9}$$

or

$$\delta\bar{e} = \overline{(A^{-1}U)}\, A_0 \delta e_0 \tag{10}$$

where the averaged matrix in (10) is obtained numerically as with $\bar{e}$. From the short-term orbit determination program the covariance matrix Γ_0 is available for the estimate of the parameters q_0 at t_0. The corresponding covariance matrix Λ_0 for e_0 is from (2)

$$\Lambda_0 = \mathrm{Exp}\left\{\delta e_0 \delta e_0^{\,T}\right\} = A_0^{-1}\, \Gamma_0 (A_0^{-1})^T \tag{11}$$

Similarly, the covariance matrix $\bar{\Lambda}$ for $\bar{e}$ is

$$\bar{\Lambda} = \mathrm{Exp}\left\{\delta\bar{e}\, \delta\bar{e}^{\,T}\right\} = \overline{(A^{-1}U)}\, A_0 \Lambda_0 A_0^{\,T}\, \overline{(A^{-1}U)}^T \tag{12}$$

or by (11)

$$\bar{\Lambda} = \overline{(A^{-1}U)}\, \Gamma_0\, \overline{(A^{-1}U)}^T \tag{13}$$

Therefore, given either Λ_0 or Γ_0 the covariance matrix $\bar{\Lambda}$ for the mean orbital elements can be found.

IV. ACCURACY OF RADIO MEASUREMENTS

by J. P. Fearey, C. R. Gates, and T. W. Hamilton

Orbit determination of lunar satellites will be based primarily on radio measurements made from the Deep Space Instrumentation Facility (DSIF). (Note that optical and/or radio measurements made from the satellite itself, if available, would also be of great value in orbit determination.)

The DSIF consists of three stations, located in South Africa, Australia, and California, USA. Each station contains one or more steerable antennas 85 ft in diameter. (Antennas 210 ft in diameter are expected to be available in 1965.) The normal radio frequency of operation is about 2300 mc.

Angular measurements are obtained by measuring the angular attitude of the antenna. Some of the antennas have vertical and horizontal axes, yielding azimuth and elevation, while other of the antennas have equatorial mountings, yielding local hour angle and declination. The principal error in the measurements of angles is a low-frequency error in calibration, having an rms value of about 0.02 deg, and having an autocorrelation extending over one-half of one pass. It is hoped that this figure (0.02 deg) may in the future be reduced by 3 times. Higher frequency errors, such as servo jitter, are not as significant as the low-frequency error in the determination of orbits.

Range rate is determined by means of doppler shift, in which a continuous radio signal is sent to the spacecraft in which the signal is amplified and sent back to Earth and the transmitted and received signals are compared. The principal error in this system is the drift of the transmitter in the time

required for the signal to make a round trip from Earth to spacecraft. A design goal of 0.06 meters/sec rms has been established, and an accuracy of 0.02 meters/sec rms has been achieved in practice. Improvements of several times in this accuracy are achievable through the use of ultrastable frequency references.

Range is determined by measuring the round-trip transit time for a pulse chain, sent from Earth to spacecraft and back to Earth. The accuracy of range measurements depends on the system used. The error which principally affects orbit determination is apparently a bias or very-low-frequency error, having a correlation width of up to one day. The magnitude of this error may be 10 to 30 meters rms.

A final error source which is often of greater effect than those listed above is the uncertainties in the locations of the tracking stations. The current uncertainties appear to be on the order of 100-200 meters in latitude and longitude and 50 meters in altitude. Improvements are expected to be realized through the tracking of geodetic satellites.

It should be noted that angular measurements of the accuracy quoted above are of little value in the orbit determination of lunar satellites; range and range rate are the important data. In general, range rate is always available when range is available; however, the obtaining of range data requires substantially more equipment, especially in the spacecraft, than does the obtaining of range rate only. Preliminary thinking suggests that the addition of range data to range rate data will improve knowledge of the Earth-Moon phenomena, but will not improve knowledge of the orbit of a lunar satellite relative to the Moon.

V. ORBIT DETERMINATION

by J. D. Reichert

The purpose of this section is to present certain results obtained from an introductory approach to the problem of orbit determination of a lunar satellite from doppler data alone. To approach the problem first in a simple form, the model chosen eliminated many factors. Those factors eliminated were considered superfluous for an approach to the essence of the question in first approximation. The problem is considered from two different viewpoints: 1) GM of Moon certain, 2) GM of Moon uncertain. (GM is the universal gravitational constant times the mass of the Moon.)

A. The Model

It is presumed that the Earth, Moon, and probe are each point masses, with the Moon moving in a perfect circle about the Earth. The satellite moves in an elliptical orbit about the Moon as focus. The assumption of a point mass Moon eliminates perturbative effects resulting from the shape of the Moon. Since these effects are ignored, then it follows from Lorell (Ref. 1) and Lass and Solloway (Ref. 2) that, for the orbits considered here, it is quite proper also to ignore the effects of the Earth acting directly on the Moon. It is only when the major axis of the orbit becomes as large as twice the Moon's radius that the two types of effects become of comparable influence on the probe. The same references also show that the effects of the Sun are negligible for these orbits. Thus, consistent with the point-mass Moon approximation, the model ignores Earth-Sun-probe interactions. Hence, without loss of further generality

the Earth is considered fixed in space and the Keplerian orbital elements of the satellite will be constants of the motion (see Lass and Solloway, Ref. 2). The observer of the system is located at the center of the Earth and attempts to determine these constants of the motion from doppler data alone.

With a point-mass Moon, a terrestrial observer can receive data from the probe during the whole orbit and there is no occulting. It appears to make little difference whether one complete orbit or two half-orbits are observed, so this detail is of small importance.

A more complete study should allow for several observers on the surface of a rotating Earth. Such a study should likely indicate the possibility of more accurate determination of orbital elements because of parallax effects. At the same time, one might wish to give the Moon a spherical shape and add occulting time as a separate data type to further improve the orbital estimate.

It is very important to the model to have the Moon move around the Earth so that the observer may see the orbit from various orientations. Otherwise the problem is essentially the binary star problem and, as Moulton (Ref. 3) shows, degeneracies result which prohibit complete determination of the orbit.

The model chosen still possesses a certain degeneracy. Since the observer is situated in the Earth-Moon plane he can never distinguish between the true orbit and its reflection through the Earth-Moon plane. The reason is simple: he would receive exactly the same doppler signals from the two orbits. It is therefore presumed that one can determine from a priori information which of two possible orbits has occurred.

B. Mathematical Approach

1. Covariance Matrices

Denoting range rate, the time rate of change of distance between observer and probe, by $\dot{\rho}$, one obtains at any instant t_j:

$$d\dot{\rho}\Big)_{t = t_j} = \frac{\partial \dot{\rho}}{\partial \alpha_i}\Big)_{t = t_j} d\alpha_i \tag{1}$$

where the α_i are the orbital parameters. This equation relates errors in orbital parameters to errors in range rate. Imagining $d\dot{\rho}$ formed at various times, t_j, one may consider $d\dot{\rho}\Big)_{t = t_j}$ and $d\alpha_i$ to be elements of the column matrices $\overrightarrow{d\dot{\rho}}$ and $\overrightarrow{d\alpha}$ respectively. Then $\overrightarrow{d\alpha}$ is (n x 1) and $\overrightarrow{d\dot{\rho}}$ is (N x 1), where n is the number of orbital parameters containing errors and N is the number of observation times t_j. One may then rewrite (1) as

$$\overrightarrow{d\dot{\rho}} = A\overrightarrow{d\alpha} \tag{2}$$

where A is the (N x n) matrix such that $A_{ji} = \frac{\partial \dot{\rho}}{\partial \alpha_i}\Big)_{t = t_j}$.
Then multiply by the transpose of A to obtain

$$A^T \overrightarrow{d\dot{\rho}} = A^T A \overrightarrow{d\alpha} \tag{3}$$

Now if $A^T A$ is non-singular (it will be non-singular in the present case, in spite of the reflection degeneracy indicated above), then one may isolate $\overrightarrow{d\alpha}$ as

$$\overrightarrow{d\alpha} = (A^T A)^{-1} A^T \overrightarrow{d\dot{\rho}} \tag{4}$$

Then

$$\overrightarrow{d\alpha}\,\overrightarrow{d\alpha}^T = (A^TA)^{-1}\,A^T\,\overrightarrow{d\rho}\,\overrightarrow{d\rho}^T\,A\,(A^TA)^{-1} \tag{5}$$

where use was made of the fact that $(A^TA)^{-1} = \left[(A^TA)^{-1}\right]^T$.

Now performing an ensemble average in (5) one obtains

$$\overline{\overrightarrow{d\alpha}\,\overrightarrow{d\alpha}^T} \quad (A^TA)^{-1}\,A^T\,\overline{\overrightarrow{d\rho}\,\overrightarrow{d\rho}^T}\,A\,(A^TA)^{-1} \tag{6}$$

since A is a fixed matrix it is unaffected by the averaging process. Now by definition of the covariance matrices of parameters and data one finds:

$$\Lambda_\alpha = \overline{\overrightarrow{d\alpha}\,\overrightarrow{d\alpha}^T} \quad \text{and} \quad \Lambda_{\dot\rho} = \overline{\overrightarrow{d\dot\rho}\,\overrightarrow{d\dot\rho}^T} \tag{7}$$

Combining (6) and (7):

$$\Lambda_\alpha = (A^TA)^{-1}\,A^T\,\Lambda_{\dot\rho}\,A\,(A^TA)^{-1} \tag{8}$$

This is the desired formula. If now the assumption is made that data points are separated by sufficiently long times that errors in one point are uncorrelated with errors in the next, one may take $\Lambda_{\dot\rho}$ to be diagonal. If, further, one presumes that data errors are time-independent, then $\Lambda_{\dot\rho}$ may be written as

$$\Lambda_{\dot\rho} = \sigma^2 I \tag{9}$$

where σ^2 is a constant[4] and I is the (N x N) identity matrix. Then (8) and (9) combine to give immediately:

[4]For the results presented later, it was presumed that $\sigma^2 = (0.02\ \text{m/sec})^2$

$$\Lambda_\alpha = \sigma^2 (A^T A)^{-1} = \sigma^2 N^{-1} \tag{10}$$

where $\frac{1}{\sigma^2} N$ is the normal or information matrix and $N \equiv (A^T A)$.

Information may be added. The matrix N_1, obtained from one group of data points, may be added to the matrix N_2, obtained from a second group of data points, to give $N_3 = N_1 + N_2$. Then $\sigma^2 N_3^{-1}$ will be the covariance matrix resulting from use of both sets of data.

2. Mapping of Covariance Matrices

Often one obtains a covariance matrix on one set of orbital parameters and then wishes to map this matrix into the covariance matrix on another set of orbital elements. Observe that

$$\left.\frac{\partial \dot{\rho}}{\partial \alpha_i}\right)_{t = t_j} = \left.\frac{\partial \dot{\rho}}{\partial \alpha_k}\right)_{t = t_j} \frac{\partial \bar{\alpha}_k}{\partial \alpha_i} \tag{11}$$

As in obtaining Eq. (2) above, rewrite this in matrix form as $A = \bar{A}U$ where

$$U_{jk} = \frac{\partial \bar{\alpha}_j}{\partial \alpha_k} \tag{12}$$

Then

$$A^T A = U^T \bar{A}^T \bar{A} U \tag{13}$$

and

$$(A^T A)^{-1} = U^{-1} (\bar{A}^T \bar{A})^{-1} (U^T)^{-1} \tag{14}$$

Thus

$$(\bar{A}^T\bar{A})^{-1} = U\,(A^TA)^{-1}\,U^T \tag{15}$$

Comparison of (10) and (15) gives

$$\bar{\Lambda}_x = U\Lambda_x U^T \tag{16}$$

Notice that Λ_x maps like a contravariant tensor.

3. Coordinate Systems Used

There is a Moon-centered, non-rotating Cartesian coordinate system such that at $t = 0$, the $\bar{x}$ - axis passes through the Earth and the $\bar{y}$ - axis lies in the Earth-Moon plane, directed away from the direction of the Moon's orbital motion at $t = 0$. This coordinate system $(\bar{x}, \bar{y}, \bar{z})$ is referred to below as the <u>fixed</u> coordinate system.

A second coordinate system of interest is a Moon-centered Cartesian system such that the x-axis points to the lunar satellite at every instant and the y-axis lies in the Moon-satellite plane, always directed as the satellite moves. This coordinate system (x, y, z) is referred to below as the <u>rotating</u> coordinate system.

The third system used is a set of Keplerian orbital elements for the satellite motion. The elements are a - semimajor axis, ϵ - eccentricity, t_0 - time of perigee passage, and three Euler angles: Ω, ω, i. Ω is angle of ascending node measured, in the $\bar{x}$, $\bar{y}$, plane, from the $\bar{x}$-axis: $0 \leq \Omega \leq 2\pi$. Then i, the inclination angle, lies on the range $0 \leq i \leq \pi$ and is measured from

the $\bar{x}$, $\bar{y}$ plane positive in the positive $\bar{z}$-direction. Finally, ω, the argument of perigee passage, lies on the range $0 \leq \omega \leq 2\pi$ and is measured from the ascending node positive in the positive $\bar{z}$-direction.

To locate the probe in the Keplerian system it is necessary to know a, ϵ, t_0, Ω, ω, i, and the time $\hat{t}$. Thus, to relate the Cartesian coordinates to the Kepler coordinates, time must enter explicitly:

$$x = x(a, \epsilon, t_0, \Omega, \omega, i, \hat{t}), \text{ etc.}$$

Thus, the $\partial\bar{\alpha}_k/\partial\alpha_i$ occurring in Eq. (11) above must be evaluated at the time $\hat{t}$. The quantities $\hat{t}_i$ are various mapping times.

The reflection degeneracy mentioned in Section VA may be expressed in these coordinate systems as inability to distinguish $\bar{z}$ for the probe from $-\bar{z}$ or as inability to distinguish between the coordinates (Ω, ω) and $(\Omega + \pi, \omega + \pi)$. The results presented below were obtained from calculations in the Keplerian system and were then mapped into the two Cartesian systems. It was discovered that, for this model, one could write

$$\dot{\rho} \equiv \frac{\dot{\vec{r}} \cdot \vec{r}}{|\vec{r}|} = -\left[\Omega \frac{\partial \rho}{\partial \Omega} + \frac{\partial \rho}{\partial t_0}\right] \tag{17}$$

where $\rho \equiv |\vec{r}|$ is the range or distance from observer to probe and $\vec{r}$ is a vector from center of Earth to probe; Ω is the constant angular velocity of the Moon. This relation gave considerable simplification to the algebra of the problem.

C. The Orbits Considered

The covariance matrices for several different orbits have been obtained under various conditions. The discussion and graphs which follow are based on the following orbits, where h denotes the height of probe above surface of Moon at periselene.

1. $h = 50$ km, $a = 1986.6666$ km, $i = 45$ deg, $e = 0.1$, $\Omega = 0$, $\omega = 45°$, $t_0 = 100$ sec.
2. $h = 50$ km, $a = 1986.6666$ km, $i = 60$ deg, other parameters same as for orbit 1.
3. $h = 150$ km, $a = 2097.7777$ km, $i = 45$ deg, other parameters same as for orbit 1.
4. $h = 150$ km, $a = 2097.7777$ km, $i = 60$ deg, other parameters same as for orbit 1.
5. $h = 250$ km, $a = 2208.8888$ km, $i = 45$ deg, other parameters same as for orbit 1.
6. $h = 250$ km, $a = 2208.8888$ km, $i = 60$ deg, other parameters same as for orbit 1.
7. $h = 1000$ km, $a = 3042.2222$, $i = 45$ deg, other parameters same as for orbit 1.
8. $h = 1000$ km, $a = 3042.2222$, $i = 60$ deg, other parameters same as for orbit 1.
9. $h = 100$ km, $a = 1938.0000$ km, $i = 45$ deg, $\epsilon = 0.0516$, $\Omega = 0$, $\omega = 45$ deg, $t_0 = 0$.

D. The Sampling Procedure

Information about each orbit was collected in several ways, taking advantage of the procedure indicated above for adding information. The month was divided into twenty-one viewing periods, each period being approximately two hours long. These periods were separated by 114860 sec (≈31.9 hr), measured from the beginning of one view period to the beginning of the next view period. During each view period exactly 20 data points were used with separation 383 sec (≈6.4 min). Thus the 20 points in each view period were evenly spaced over a period of 7277 sec (≈2.02 hr). It is of interest to compare the length of a view period with the period, τ, of the orbits investigated:

	Seconds	Hours	Fraction of orbit seen in one view period
Length of view period	7277	2.02	
τ for orbits 1 and 2	8631	2.40	0.84
τ for orbits 3 and 4	9368	2.60	0.78
τ for orbits 5 and 6	10118	2.80	0.72
τ for orbits 7 and 8	16353	4.54	0.44
τ for orbit 9	7657	2.13	0.95

For convenience the view periods are referred to as "passes" and the passes are numbered from 1 to 21. Now the methods for examining the orbit considered here are:

Sampling mode	Data combined from the following passes	Comment
1	first pass	orbit viewed on edge, periselene nearest observer[5]
2	sixth	orbit viewed broadside
3	eleventh	orbit viewed on edge, apselene nearest observer
4	sixteenth	orbit viewed broadside
5	twenty-first	orbit viewed on edge, periselene nearest observer
6	all twenty-one passes	
7	first eleven passes in month	
8	last eleven passes in month	
9	the eleven passes at the center of the month (6, 7, 8, 9, 10, 11, 12, 13, 14, 15, 16)	
10	first and sixth	
11	first and sixteenth	
12	sixth and eleventh	
13	sixth and sixteenth	
14	first and eleventh	

These mode numbers appear as abscissas on several of the graphs which follow. Dashed lines on the graphs separate the plotted points into groups computed on the basis of the same number of observations.

[5] The orbit appears on edge in this case because $\Omega = 0$ and the $\bar{x}$-axis passes through the center of the Earth at $t = 0$.

E. Results

Certain results are presented in Tables V-1 through V-8, which accompany Fig. V-1 through V-27. It is hoped that the results illustrated can be of value in estimating accuracy to be expected in locating a lunar probe. As a check on the construction of the program, one set of equations was programmed for the IBM 7090 at JPL, while another set, of different algebraic form, was programmed by another programmer for the IBM 1620 at JPL. The results from the two programs agree.

The results from this model have been compared with results for the same orbit, sampled in the same way, obtained from the JPL Ranger Orbit Determination Program. For the check the Ranger Program ignored mass of Moon uncertainties, station location uncertainties, etc. The results were found to be in good agreement, suggesting that the model assumed here is a satisfactory first approximation. A tracking accuracy of 0.02 m/sec was assumed.

The first set of figures (Fig. V-1 through V-27) is accompanied by the results from which the graphs were drawn. The figures illustrate how the diagonal elements of the covariance matrices depend on h, i, and sampling mode. In each of these graphs the abscissa is h, the height above the surface of the Moon at periselene. (The radius of the Moon is 1738 km.) The ordinate is the variance, σ, or diagonal element in the covariance matrix, corresponding to the quantity indicated by the subscript. As indicated on the figures, the mapping time for the quantities σ_x, σ_y, σ_z and $\sigma_{\bar{x}}$, $\sigma_{\bar{y}}$, $\sigma_{\bar{z}}$ is $\hat{t}=0$ sec. This is the first of the month, at which time the observer sees the orbit on edge, since $\Omega = 0$ and the $\bar{x}$-axis passes through the Earth at time $t=0$.

The most striking feature of the first twenty-seven figures is that they all look very much the same. Note that σ_i (mass of Moon estimated) and σ_z (mass of Moon estimated) are also plotted on a log scale. Indicated as a parameter on the graphs is the sampling mode explained earlier. It is quite understandable that the curves resulting from sampling modes using several passes should yield smaller variances than modes utilizing fewer passes. The uncertainties must decrease as more information is considered. However, by observing the same pass Q different times, one might expect the variance to decrease by a factor of $1/\sqrt{Q}$. Now one should hope that information gained from twenty different passes should be better than information obtained twenty times for the same pass. To illustrate this point, one may consider Fig. V-1. For mode 1, based on one pass, $\sigma_a = 12.337$ m for $i = 45$ deg yielding $\sigma_a/\sqrt{20} = 2.76$ m. On the other hand, for mode 6, based on twenty passes, $\sigma_a = 1.456$ m for $i = 45$ deg, which is smaller than 2.76 m by a factor of 0.53, showing that it is profitable to sample several different passes.

On these same graphs, one may observe that the variances change only slightly between $i = 45$ and $i = 60$ deg. It appears that variances are about the same or are slightly larger for $i = 45$ deg for most of the parameters, but that Ω, ω, i, z, and $\bar{z}$ may have slightly smaller variances for the $i = 45$ deg case. The main conclusion, however, appears that there is little difference in the $i = 45$ and the $i = 60$ deg cases for these orbits.

Still considering this first set of graphs, one must give some consideration to the apparent increase of the variances with increasing h. A possible explanation for the rise is that smaller fractions of an orbit are seen during a

view period for the larger orbits. This may explain the rise in part, but it can be argued that the increase is real. For example, consider Fig. V-1 again. See that, for h = 1000 km, one obtains a smaller variance for mode 10 than from mode 1 by more than the expected factor of $1/\sqrt{2}$. It seems clear, therefore, that mode 10 gives a smaller σ_a than two sets of observations of the first pass and also, then, smaller than the first pass plus twenty additional points necessary to complete the first 4.5-hour orbit of the month. However, σ_a for mode 10 for h = 1000 km is greater than σ_a for mode 1 for h = 50 km, even though twice as many data points were used for mode 10. This and similar results from the other figures seem to indicate that the variances are really larger for the larger orbits no matter whether different-sized orbits are sampled with density of observations made equal or made inversely proportional to the periods.

Now, Fig. V-28 shows the variances of the Keplerian elements as a function of sampling mode. The dashed lines separate points obtained from different numbers of passes. The orbit considered has h = 150 km, i = 45 deg. Considering first the results of using only one pass of data, it is of interest to note the periodic character of the variances in the course of the month. Note further that the variance on i is smallest when the orbit is viewed broadside, while for the other elements, the variance is smallest when the orbit is viewed on edge. Observe that when eleven passes are used, the variances are the same for modes 7, 8, and 9. Finally, it is of interest to note that the variances are large in modes 13 and 14 for the orientation angles, Ω, ω, and i. They are larger in these two cases than in the modes 10, 11, and 12, because information

is obtained from the orbit twice in the same aspect; i.e., pass 6 and pass 16 are both broadside passes, while pass 1 and pass 11 are both on edge. To determine the orientation well one needs both broadside and on-edge passes.

Now Fig. V-29 shows the diagonal elements, μ, of the normal matrices[6] obtained for 21 separate passes during the month. The orbit illustrated was orbit 9. These quantities, μ, offer some measure of the absorption of information. A larger value of μ indicates the presence of more information on that quantity. Note that all are periodic and that μ_Ω and μ_i are in phase with each other but out of phase with the other quantities. It appears that most information relative to i and Ω is obtained when the orbit is viewed broadside, whereas on-edge orbits offer the most information about the other parameters. Then Fig. V-30 shows a similar plot (on log scale) of the corresponding variances, σ, of the quantities. The complicated appearance of these curves, compared to those in Fig. V-29 is related to the presence of cross-correlation terms. Note that σ_a, σ_ϵ, and σ_{t_o} are roughly constant through the month.

Figure V-31 shows the variances on x, y, z, $\bar{x}$, $\bar{y}$, and $\bar{z}$, based on sampling mode 6, mapped to pass 11, in the center of the month. The variances are plotted vs the eccentric anomaly of the probe during pass 11.

Now Fig. V-32 through V-36 show how certain of the elements of the correlation matrix, P (the normalized covariance matrix), change with

[6]The normal or information matrix is the inverse of the covariance matrix.

sampling mode. The elements plotted are $P_{a\epsilon}$, P_{ai}, $P_{\Omega i}$, $P_{\omega i}$, and $P_{\omega\Omega}$. For each quantity the correlations are shown when mass of Moon is not estimated (6 x 6) and when mass of Moon is estimated (7 x 7). Notice that, for single passes, a and ϵ are most correlated, when mass of Moon is not estimated, precisely where they are least correlated when the mass of the Moon is estimated. On the other hand, for single passes, the other correlations plotted tend to be in phase for the two cases. Note that correlations appear to be independent of the set of 11 passes one considers. One further interesting result of the plots is the tendency to peak at mode 13, which combines information from the two broadside passes. Compare Fig. V-32 and V-33 with Fig. V-34 and V-35 in this regard to see an important difference between estimating or not estimating GM of the Moon. Finally, compare modes 10, 11, and 12 in Fig. V-36 with modes 13 and 14 to see the importance of combining two orbits of unlike aspect (one broadside and one on-edge) for removing the correlations between Ω and ω. The same is true for ω and i as Fig. V-35 indicates. On the other hand, Fig. V-34 suggests that high correlation between Ω and i is not present unless two broadside passes were combined.

In passing, one might observe from Fig. V-1 through V-27 that $\sigma_x \approx \sigma_a$ and $\sigma_z \approx a\sigma_i$, as one might expect. Up to this point, very little has been remarked concerning the magnitudes of the variances. This information is contained in detail in the data sheets (Tables V-1 through V-8) accompanying Fig. V-1 through V-27 and needs little explanation. In a few words, the results of this study seem to indicate that the probes studied can be located to within

several kilometers with two hours worth of data and to within a few meters with 10 times that much data.

REFERENCES

1. Lorell, J., Characteristics of Lunar Satellite Orbits, JPL Technical Memorandum 312-164, Jet Propulsion Laboratory, Pasadena, Calif., February 20, 1962.

2. Lass, H., and Solloway, C. B., "Motion of a Satellite of the Moon," Journal of the American Rocket Society, February 1961.

3. Moulton, F. R., An Introduction to Celestial Mechanics, the Macmillan Company, 1914.

Table V-1. Variances of Keplerian elements ($i = 45°$)[a]
(mass of the Moon not estimated)

$\Omega = 0$, $t_0 = 100$ sec., $\omega = 45°$

	h = 50 km	150 km	250 km	1000 km
Information from 20 points (~1 orbit), sampling mode 1				
σ_a	3.810×10^{-3} km	4.1088×10^{-3}	4.449×10^{-3}	1.2337×10^{-2}
σ_ϵ	6.177×10^{-6}	7.255×10^{-6}	8.041×10^{-6}	1.2906×10^{-5}
σ_{t_0}	6.580×10^{-2} sec	9.581×10^{-2}	1.5832×10^{-1}	1.1243
σ_Ω	9.632×10^{-4} rad	9.817×10^{-4}	1.4788×10^{-3}	8.715×10^{-3}
σ_ω	6.568×10^{-4} rad	6.475×10^{-4}	8.986×10^{-4}	5.566×10^{-3}
σ_i	1.6901×10^{-3} rad	2.390×10^{-3}	3.695×10^{-3}	1.3489×10^{-2}
Information from 40 points (~2 orbits), sampling mode 10				
σ_a	2.726×10^{-3}	3.135×10^{-3}	3.368×10^{-3}	6.683×10^{-3}
σ_ϵ	3.873×10^{-6}	4.021×10^{-6}	4.248×10^{-6}	6.206×10^{-6}
σ_{t_0}	4.302×10^{-2}	4.935×10^{-2}	5.450×10^{-2}	1.1358×10^{-1}
σ_Ω	1.0464×10^{-5}	1.0929×10^{-5}	1.1729×10^{-5}	1.3089×10^{-5}
σ_ω	3.434×10^{-5}	3.510×10^{-5}	3.511×10^{-5}	5.202×10^{-5}
σ_i	5.758×10^{-6}	5.944×10^{-6}	6.079×10^{-6}	7.601×10^{-6}
Information from 220 points (~11 orbits), sampling mode 7				
σ_a	1.1136×10^{-3}	1.2112×10^{-3}	1.3161×10^{-3}	2.046×10^{-3}
σ_ϵ	1.6472×10^{-6}	1.6981×10^{-6}	1.7695×10^{-6}	2.047×10^{-6}
σ_{t_0}	1.8083×10^{-2}	2.039×10^{-2}	2.276×10^{-2}	4.269×10^{-2}
σ_Ω	4.501×10^{-6}	4.611×10^{-6}	4.718×10^{-6}	5.503×10^{-6}
σ_ω	1.4555×10^{-5}	1.4842×10^{-5}	1.5165×10^{-5}	1.7676×10^{-5}
σ_i	2.535×10^{-6}	2.622×10^{-6}	2.693×10^{-6}	3.1324×10^{-6}
Information from 420 points (~21 orbits), sampling mode 6				
σ_a	8.178×10^{-4}	8.764×10^{-4}	9.355×10^{-4}	1.4563×10^{-3}
σ_ϵ	1.2142×10^{-6}	1.2260×10^{-6}	1.2728×10^{-6}	1.4793×10^{-6}
σ_{t_0}	1.3143×10^{-2}	1.4860×10^{-2}	1.6536×10^{-2}	3.086×10^{-2}
σ_Ω	3.244×10^{-6}	3.310×10^{-6}	3.403×10^{-6}	1.2474×10^{-5}
σ_ω	1.0822×10^{-5}	1.0940×10^{-5}	1.1266×10^{-5}	1.2988×10^{-5}
σ_i	1.7937×10^{-6}	1.8408×10^{-6}	1.8915×10^{-6}	2.223×10^{-6}

[a]Data plotted in Fig. V-1 through V-6.

Table V-2. Variances of Keplerian elements ($i = 60°$)[a]
(mass of the Moon not estimated)

$\Omega = 0$, $t_0 = 100$ sec., $\omega = 45°$

Information from 20 points (~1 orbit), sampling mode 1

σ_a	3.808×10^{-3} km	4.107×10^{-3}	4.446×10^{-3}	1.2594×10^{-2}
σ_ϵ	6.175×10^{-6}	7.254×10^{-6}	8.042×10^{-6}	1.3171×10^{-5}
σ_{t_0}	6.572×10^{-2} sec	9.558×10^{-2}	1.5791×10^{-1}	1.1531
σ_Ω	6.408×10^{-4} rad	6.588×10^{-4}	9.926×10^{-4}	6.061×10^{-3}
σ_ω	3.003×10^{-4} rad	2.866×10^{-4}	3.900×10^{-4}	2.420×10^{-3}
σ_i	1.3791×10^{-3} rad	1.9498×10^{-3}	3.013×10^{-3}	1.1354×10^{-2}

Information from 40 points (~2 orbits), sampling mode 10

σ_a	3.009×10^{-3}	3.479×10^{-3}	3.765×10^{-3}	6.771×10^{-3}
σ_ϵ	4.228×10^{-6}	4.328×10^{-6}	4.562×10^{-6}	6.526×10^{-6}
σ_{t_0}	4.815×10^{-2}	5.475×10^{-2}	5.979×10^{-2}	1.1759×10^{-1}
σ_Ω	6.284×10^{-6}	6.494×10^{-6}	6.885×10^{-6}	7.911×10^{-6}
σ_ω	3.695×10^{-5}	3.855×10^{-5}	3.865×10^{-5}	5.031×10^{-5}
σ_i	4.674×10^{-6}	4.805×10^{-6}	4.898×10^{-6}	6.196×10^{-6}

Information from 220 points (~11 orbits), sampling mode 7

σ_a	1.2129×10^{-3}	1.3174×10^{-3}	1.4465×10^{-3}	2.245×10^{-3}
σ_ϵ	1.7853×10^{-6}	1.8311×10^{-6}	1.9272×10^{-6}	2.229×10^{-6}
σ_{t_0}	2.003×10^{-2}	2.260×10^{-2}	2.522×10^{-2}	4.716×10^{-2}
σ_Ω	2.729×10^{-6}	2.794×10^{-6}	2.855×10^{-6}	3.341×10^{-6}
σ_ω	1.5395×10^{-5}	1.5878×10^{-5}	1.6209×10^{-5}	1.8922×10^{-5}
σ_i	2.063×10^{-6}	2.158×10^{-6}	2.189×10^{-6}	2.554×10^{-6}

Information from 420 points (~21 orbits), sampling mode 6

σ_a	8.964×10^{-4}	9.573×10^{-4}	1.0282×10^{-3}	1.6200×10^{-3}
σ_ϵ	1.3263×10^{-6}	1.3304×10^{-6}	1.3918×10^{-6}	1.6195×10^{-6}
σ_{t_0}	1.4623×10^{-2}	1.6544×10^{-2}	1.8455×10^{-2}	3.437×10^{-2}
σ_Ω	1.9432×10^{-6}	1.9915×10^{-6}	2.045×10^{-6}	2.370×10^{-6}
σ_ω	1.1246×10^{-5}	1.1670×10^{-5}	1.2020×10^{-5}	1.3913×10^{-5}
σ_i	1.4571×10^{-6}	1.4973×10^{-6}	1.5362×10^{-6}	1.3104×10^{-6}

[a]Data plotted in Fig. V-1 through V-6.

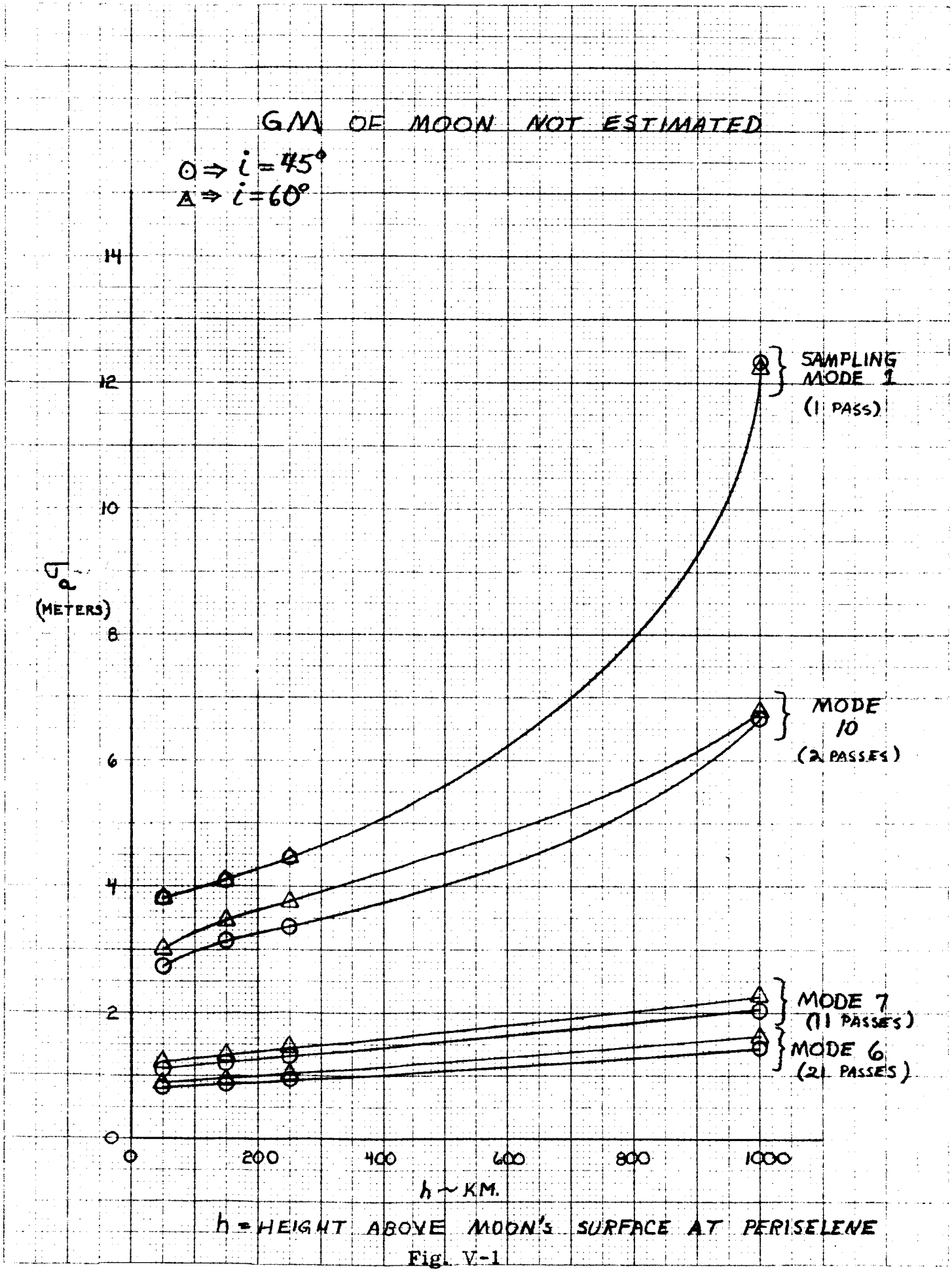
GM OF MOON NOT ESTIMATED
⊙ ⇒ i = 45°
△ ⇒ i = 60°
SAMPLING MODE 1 (1 PASS)
MODE 10 (2 PASSES)
MODE 7 (11 PASSES)
MODE 6 (21 PASSES)
σa (METERS)
0
2
4
6
8
10
12
14
0
200
400
600
800
1000
h ~ KM.
h = HEIGHT ABOVE MOON'S SURFACE AT PERISELENE

Fig. V-1

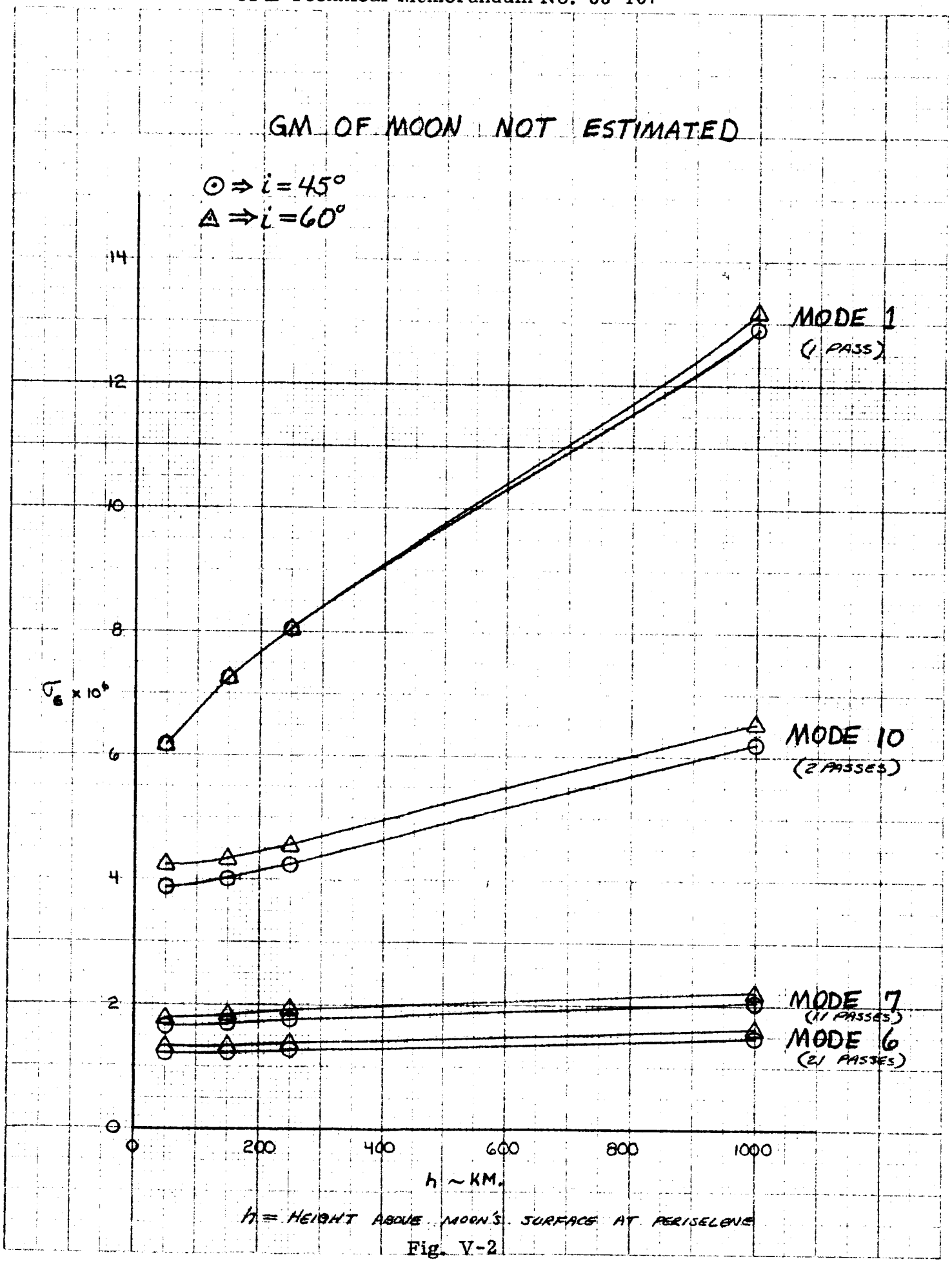
GM OF MOON NOT ESTIMATED
⊙ ⇒ i = 45°
△ ⇒ i = 60°
MODE 1
(1 PASS)
MODE 10
(2 PASSES)
MODE 7
(11 PASSES)
MODE 6
(21 PASSES)
σ6 × 10⁶
0
2
4
6
8
10
12
14
0
200
400
600
800
1000
h ~ KM.
h = HEIGHT ABOVE MOON'S SURFACE AT PERISELENE

Fig. V-2

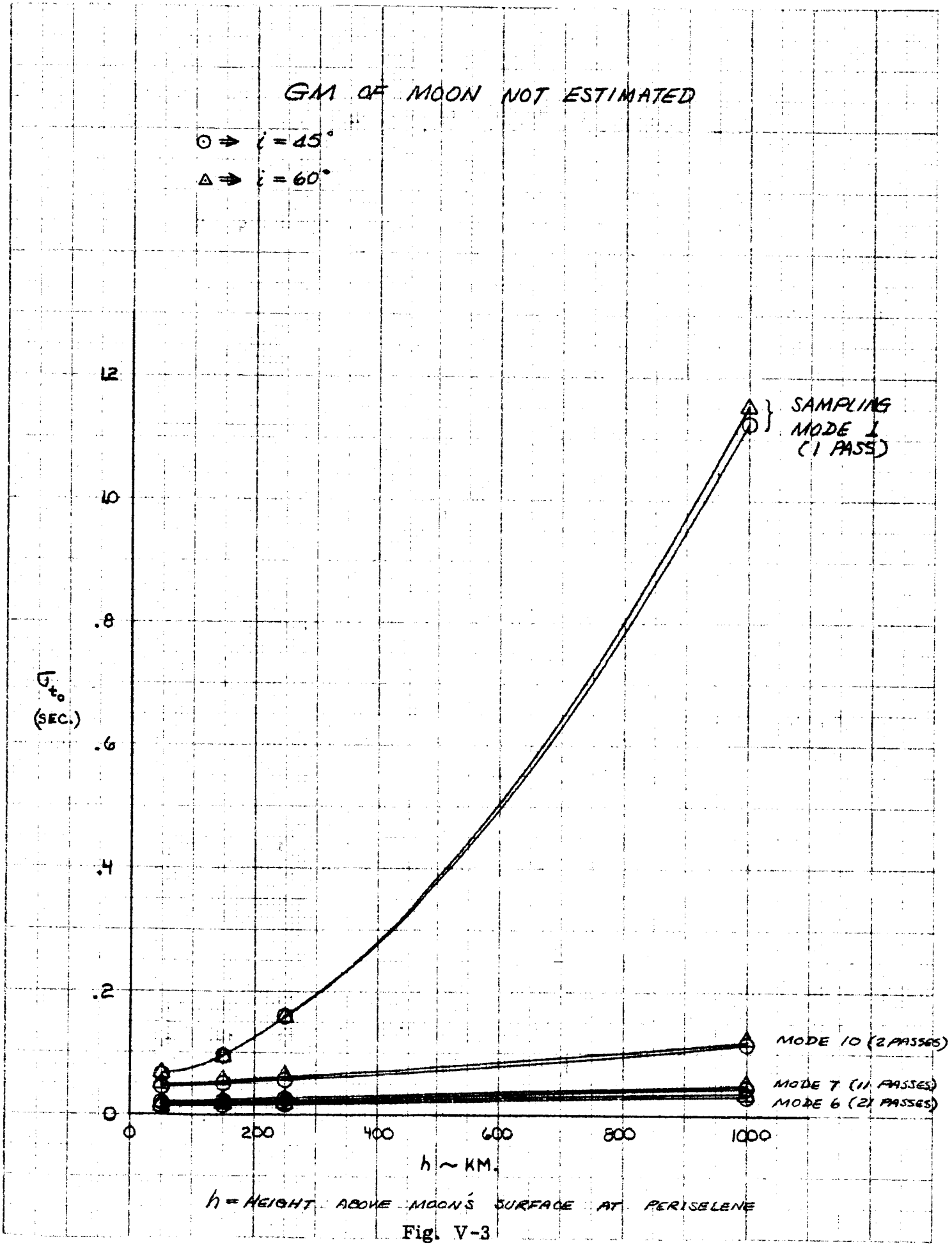
GM OF MOON NOT ESTIMATED
⊙ ⇒ i = 45°
△ ⇒ i = 60°
SAMPLING MODE 1 (1 PASS)
MODE 10 (2 PASSES)
MODE 7 (11 PASSES)
MODE 6 (21 PASSES)
σ_{t_0} (SEC.)
1.2
1.0
.8
.6
.4
.2
0
0
200
400
600
800
1000
h ~ KM.
h = HEIGHT ABOVE MOON'S SURFACE AT PERISELENE

Fig. V-3

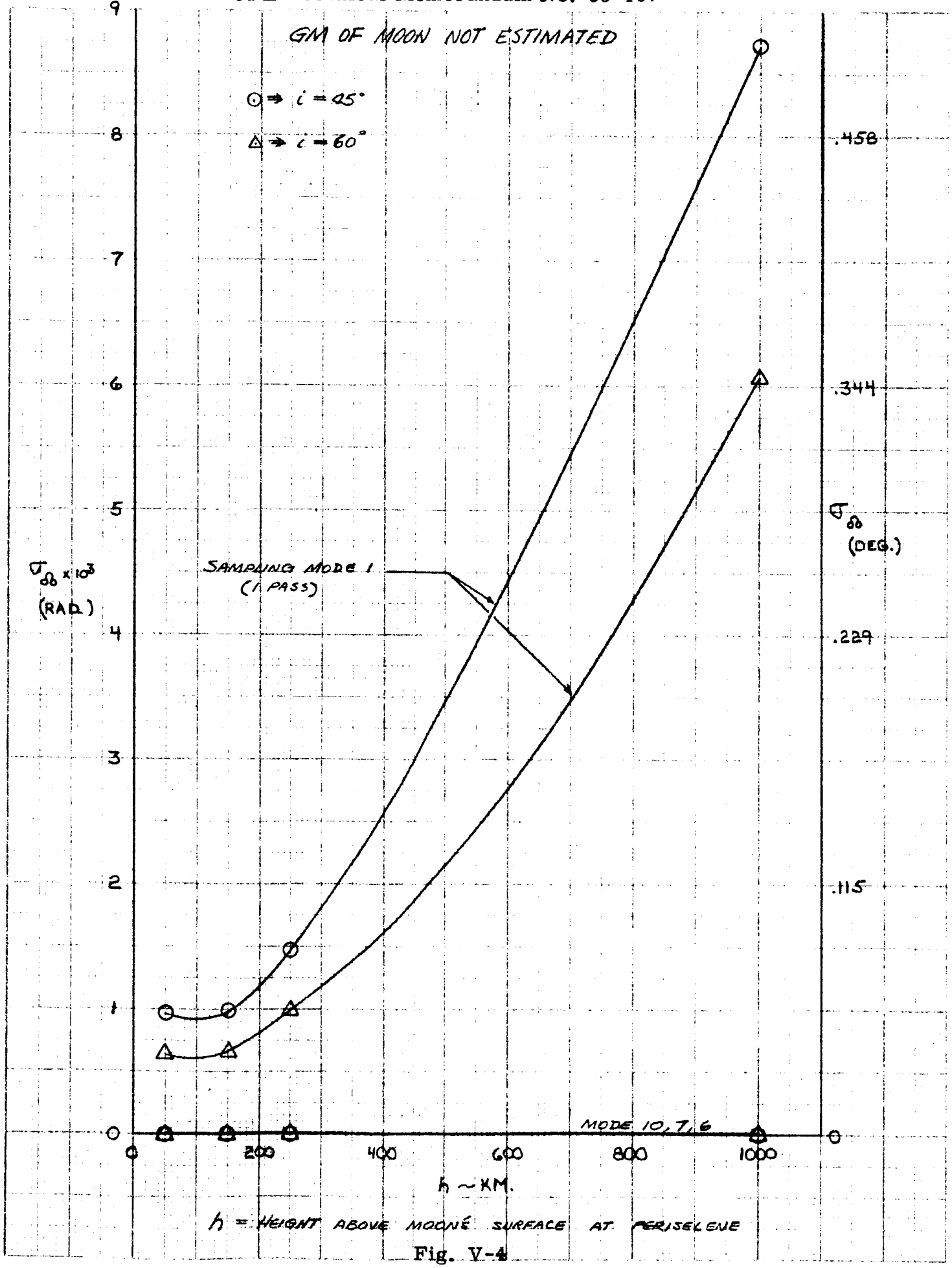
GM OF MOON NOT ESTIMATED
⊙ → i = 45°
△ → i = 60°
SAMPLING MODE 1
(1 PASS)
MODE 10, 7, 6
σδδ x 10³
(RAD.)
σδδ
(DEG.)
9
8
7
6
5
4
3
2
1
0
.458
.344
.229
.115
0
0
200
400
600
800
1000
h ~ KM.
h = HEIGHT ABOVE MOONÉ SURFACE AT PERISELENE

Fig. V-4

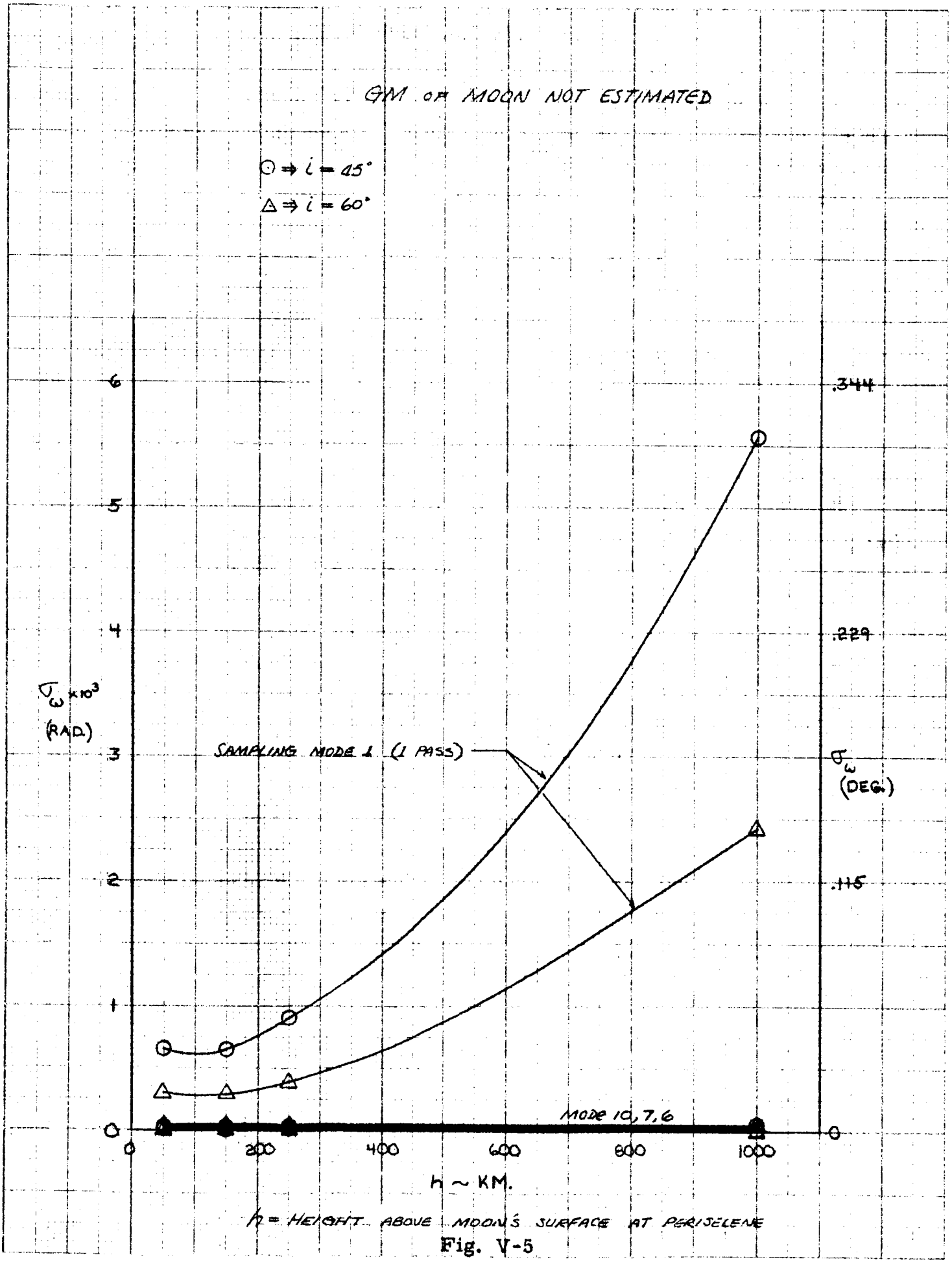
GM OF MOON NOT ESTIMATED
⊙ ⇒ i = 45°
△ ⇒ i = 60°
SAMPLING MODE 1 (1 PASS)
MODE 10, 7, 6
σω x10³ (RAD.)
σω (DEG.)
0
1
2
3
4
5
6
.115
.229
.344
0
200
400
600
800
1000
h ~ KM.
h = HEIGHT ABOVE MOON'S SURFACE AT PERISELENE

Fig. V-5

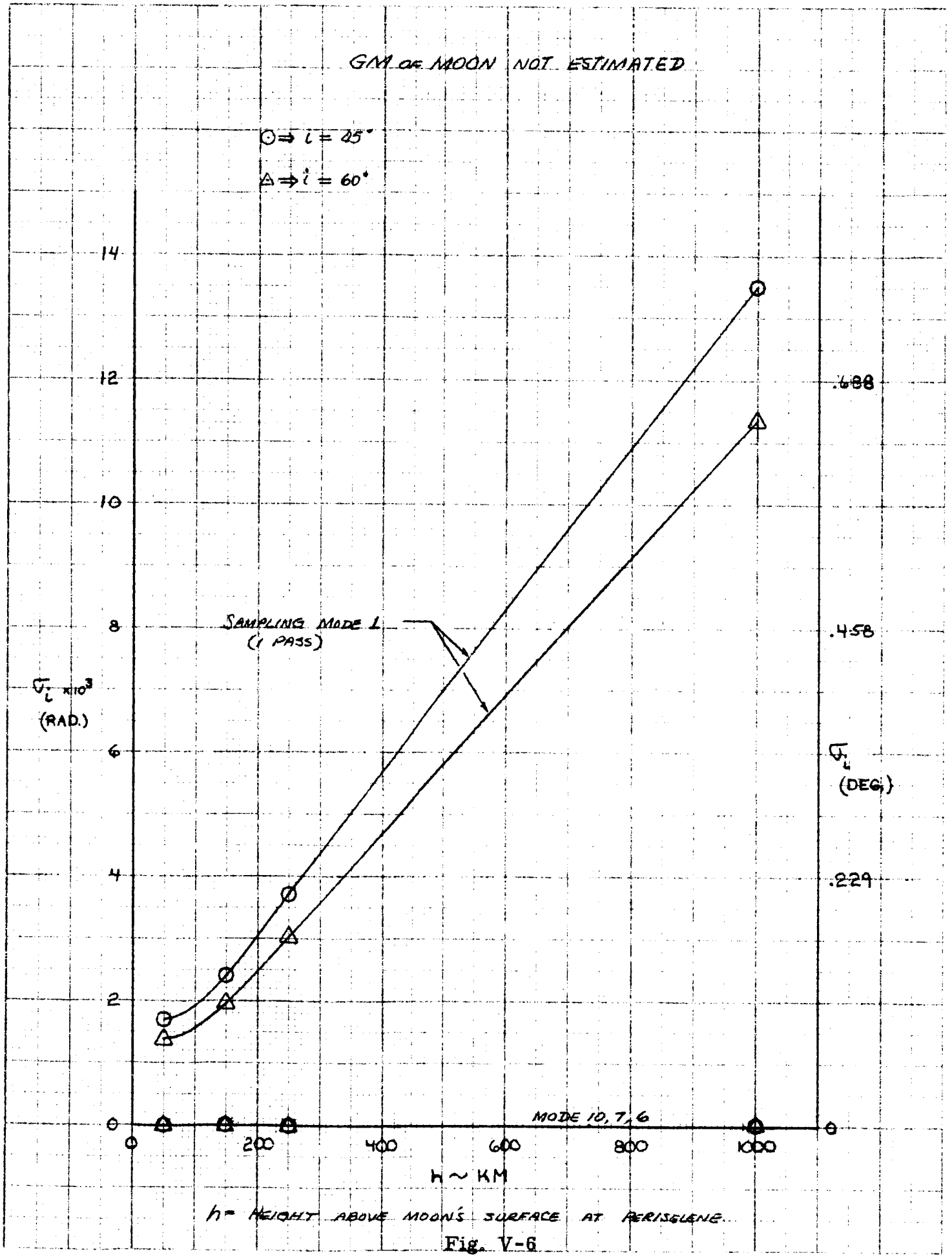
GM OF MOON NOT ESTIMATED
⊙ ⇒ i = 25°
△ ⇒ i = 60°
14
12
10
8
6
4
2
0
.688
.458
.229
0
$\sigma_L \times 10^3$ (RAD.)
σ_L (DEG.)
SAMPLING MODE 1 (1 PASS)
MODE 10, 7, 6
0
200
400
600
800
1000
h ~ KM
h = HEIGHT ABOVE MOON'S SURFACE AT PERISELENE.

Fig. V-6

Table V-3. Variances of Keplerian elements (i = 45°)[a]
(mass of the Moon estimated)

$\Omega = 0$, $t_0 = 100$ sec, $\omega = 45°$

	h = 50 km	150 km	250 km	1000 km
Information from 20 points (~ 1 orbit), sampling mode 1				
σ_a	1.9653×10^{-2} km	2.444×10^{-2}	2.973×10^{-2}	1.3898×10^{-1}
σ_ϵ	7.129×10^{-6}	9.970×10^{-6}	1.2934×10^{-5}	2.393×10^{-5}
σ_{t_0}	9.804×10^{-2} sec	1.0745×10^{-1}	1.5878×10^{-1}	1.8061
σ_Ω	1.2241×10^{-3} rad	1.1193×10^{-3}	1.4851×10^{-3}	2.640×10^{-2}
σ_ω	8.166×10^{-4} rad	7.427×10^{-4}	9.370×10^{-4}	1.7700×10^{-2}
σ_i	1.7288×10^{-3} rad	2.880×10^{-3}	5.115×10^{-3}	2.197×10^{-2}
σ_{GM}	1.1983×10^{-1} km^3/sec^2	1.4056×10^{-1}	1.6108×10^{-1}	6.945×10^{-1}
Information from 40 points (~ 2 orbits), sampling mode 10				
σ_a	9.664×10^{-3}	1.0486×10^{-2}	1.1239×10^{-2}	2.409×10^{-2}
σ_ϵ	3.873×10^{-6}	4.037×10^{-6}	4.284×10^{-6}	7.628×10^{-6}
t_0	5.141×10^{-2}	6.078×10^{-2}	6.877×10^{-2}	1.5739×10^{-1}
σ_Ω	1.0465×10^{-5}	1.0969×10^{-5}	1.1860×10^{-5}	6.547×10^{-5}
σ_ω	4.322×10^{-5}	4.233×10^{-5}	4.322×10^{-5}	6.419×10^{-5}
σ_i	6.185×10^{-6}	6.214×10^{-6}	6.266×10^{-6}	1.1737×10^{-5}
σ_{GM}	6.416×10^{-2}	6.515×10^{-2}	6.598×10^{-2}	9.315×10^{-2}
Information from 220 points (~11 orbits), sampling mode 7				
σ_a	4.074×10^{-3}	4.340×10^{-3}	4.624×10^{-3}	7.349×10^{-3}
σ_ϵ	1.6478×10^{-6}	1.6981×10^{-6}	1.7695×10^{-6}	2.060×10^{-6}
t_0	2.138×10^{-2}	2.340×10^{-2}	2.540×10^{-2}	4.814×10^{-2}
σ_Ω	4.506×10^{-6}	4.622×10^{-6}	4.739×10^{-6}	5.546×10^{-6}
σ_ω	1.6946×10^{-5}	1.7079×10^{-5}	1.7040×10^{-5}	2.014×10^{-5}
σ_i	2.707×10^{-6}	2.791×10^{-6}	2.898×10^{-6}	3.269×10^{-6}
σ_{GM}	2.708×10^{-2}	2.768×10^{-2}	2.827×10^{-2}	3.233×10^{-2}
Information from 420 points (~21 orbits), sampling mode 6				
σ_a	2.936×10^{-3}	3.234×10^{-3}	3.423×10^{-3}	5.307×10^{-3}
σ_ϵ	1.2142×10^{-6}	1.2262×10^{-6}	1.2730×10^{-6}	1.4846×10^{-6}
t_0	1.5510×10^{-2}	1.7628×10^{-2}	1.8850×10^{-2}	3.554×10^{-2}
σ_Ω	3.228×10^{-6}	3.3148×10^{-6}	3.409×10^{-6}	3.965×10^{-6}
σ_ω	1.2337×10^{-5}	1.2834×10^{-5}	1.2762×10^{-5}	1.4951×10^{-5}
σ_i	1.9224×10^{-6}	1.9708×10^{-6}	2.038×10^{-6}	2.352×10^{-6}
σ_{GM}	1.9708×10^{-2}	2.042×10^{-2}	2.070×10^{-2}	2.390×10^{-2}

[a]Data plotted in Fig. V-7 through V-14.

Table V-4. Variances of Keplerian elements (i = 60°)[a]
(mass of the Moon estimated)

$\Omega = 0$, $t_0 = 100$ sec, $\omega = 45°$

	h = 50 km	150 km	250 km	1000 km
Information from 20 points (~ 1 orbit) sampling mode 1				
σ_a	1.9648×10^{-2}	2.441×10^{-2}	2.969×10^{-2}	1.9348×10^{-1}
σ_ϵ	7.120×10^{-6}	9.954×10^{-6}	1.2917×10^{-5}	2.891×10^{-5}
σ_{t_0}	9.804×10^{-2}	1.0733×10^{-1}	1.5861×10^{-1}	2.544
σ_Ω	8.199×10^{-4}	7.499×10^{-4}	9.972×10^{-4}	2.588×10^{-2}
σ_ω	3.630×10^{-4}	3.296×10^{-4}	3.900×10^{-4}	1.1519×10^{-2}
σ_i	1.4101×10^{-3}	2.347×10^{-3}	4.167×10^{-3}	2.547×10^{-2}
σ_{GM}	1.1978×10^{-1}	1.4043×10^{-1}	1.6089×10^{-1}	9.816×10^{-1}
Information from 40 points (~ 2 orbits), sampling mode 10				
σ_a	1.1145×10^{-2}	1.2010×10^{-2}	1.2723×10^{-2}	2.511×10^{-2}
σ_ϵ	4.253×10^{-6}	4.381×10^{-6}	4.628×10^{-6}	8.086×10^{-6}
σ_{t_0}	5.859×10^{-2}	6.735×10^{-2}	7.452×10^{-2}	1.6834×10^{-1}
σ_Ω	6.289×10^{-6}	6.532×10^{-6}	6.954×10^{-6}	7.914×10^{-6}
σ_ω	4.383×10^{-5}	4.609×10^{-5}	4.682×10^{-5}	6.574×10^{-5}
σ_i	4.844×10^{-6}	4.914×10^{-6}	4.974×10^{-6}	8.110×10^{-6}
σ_{GM}	7.078×10^{-2}	7.118×10^{-2}	7.125×10^{-2}	9.660×10^{-2}
Information from 220 points (~ 11 orbits), sampling mode 7				
σ_a	4.616×10^{-3}	4.842×10^{-3}	5.095×10^{-3}	8.115×10^{-3}
σ_ϵ	1.7960×10^{-6}	1.8353×10^{-6}	1.9320×10^{-6}	2.272×10^{-6}
σ_{t_0}	2.413×10^{-2}	2.609×10^{-2}	2.811×10^{-2}	5.306×10^{-2}
σ_Ω	2.729×10^{-6}	2.794×10^{-6}	2.859×10^{-6}	3.350×10^{-6}
σ_ω	1.8149×10^{-5}	1.8134×10^{-5}	1.8030×10^{-5}	2.124×10^{-5}
σ_i	2.137×10^{-6}	2.201×10^{-6}	2.277×10^{-6}	2.613×10^{-6}
σ_{GM}	2.956×10^{-2}	2.982×10^{-2}	3.015×10^{-2}	3.459×10^{-2}
Information from 420 points (~ 21 orbits), sampling mode 6				
σ_a	3.328×10^{-3}	3.663×10^{-3}	3.822×10^{-3}	6.080×10^{-3}
σ_ϵ	1.3324×10^{-6}	1.3361×10^{-6}	1.3957×10^{-6}	1.6411×10^{-6}
σ_{t_0}	1.7495×10^{-2}	1.9872×10^{-2}	2.111×10^{-2}	3.960×10^{-2}
σ_Ω	1.9020×10^{-6}	1.9915×10^{-6}	2.045×10^{-6}	2.373×10^{-6}
σ_ω	1.3218×10^{-5}	1.377×10^{-5}	1.3582×10^{-5}	1.5867×10^{-5}
σ_i	1.5130×10^{-6}	1.5541×10^{-6}	1.6009×10^{-6}	1.8674×10^{-6}
σ_{GM}	2.148×10^{-2}	2.230×10^{-2}	2.236×10^{-2}	2.580×10^{-2}

[a] Data plotted in Fig. V-7 through V-14.

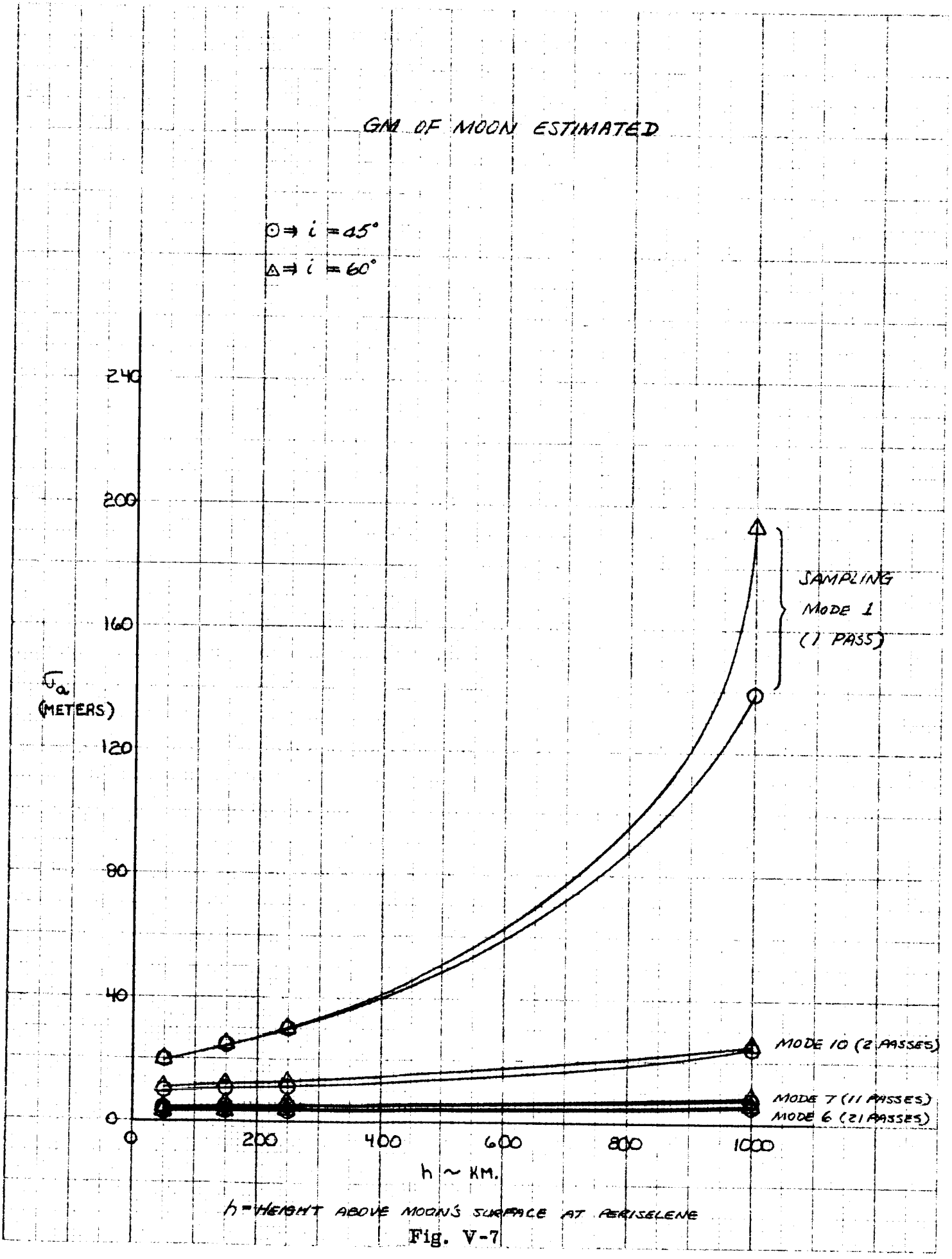
GM OF MOON ESTIMATED
⊙ ⇒ i = 45°
△ ⇒ i = 60°
240
200
160
120
80
40
0
σa
(METERS)
SAMPLING
MODE 1
(1 PASS)
MODE 10 (2 PASSES)
MODE 7 (11 PASSES)
MODE 6 (21 PASSES)
0
200
400
600
800
1000
h ~ KM.
h = HEIGHT ABOVE MOON'S SURFACE AT PERISELENE

Fig. V-7

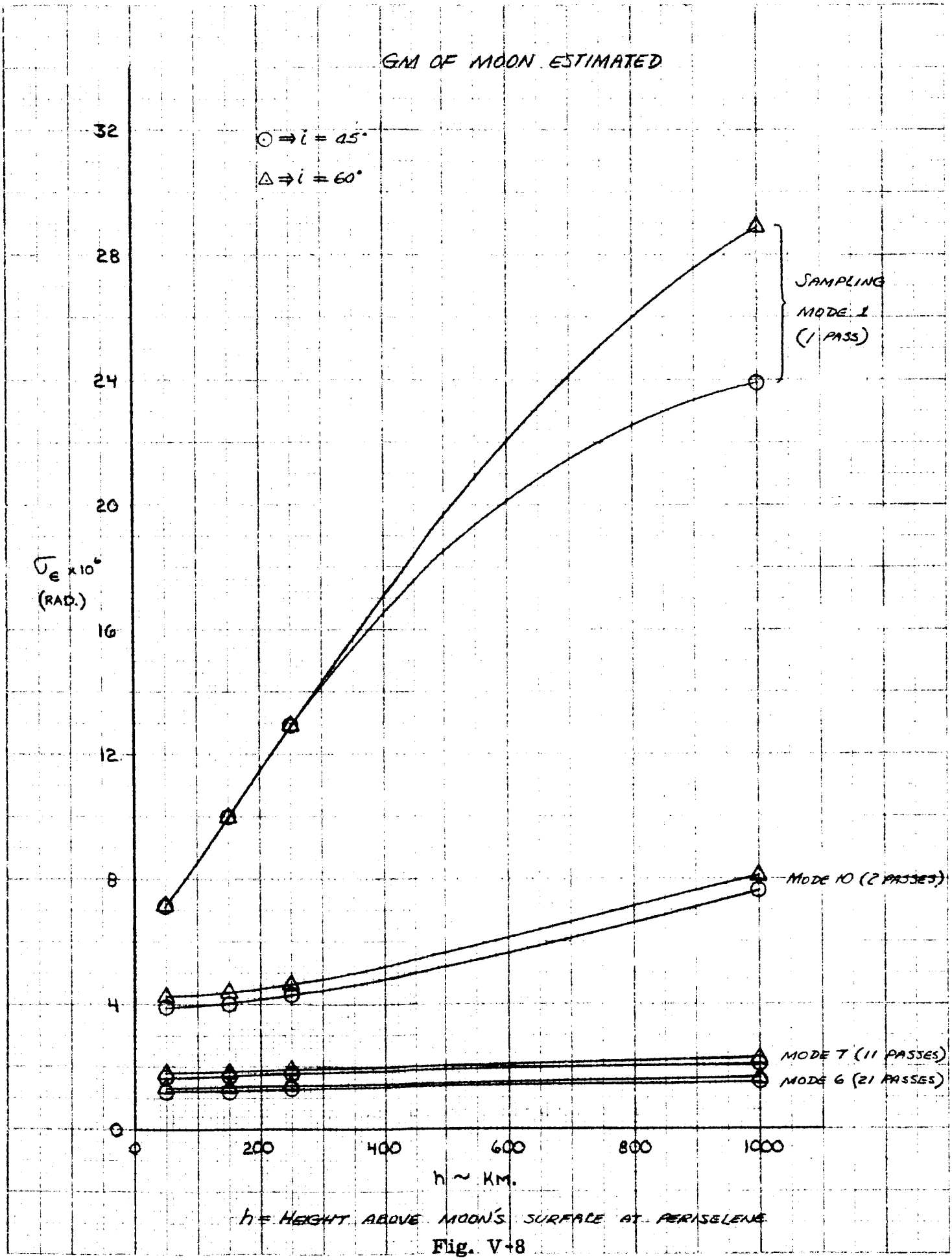
GM OF MOON ESTIMATED
⊙ ⇒ i = 45°
△ ⇒ i = 60°
SAMPLING MODE 1 (1 PASS)
MODE 10 (2 PASSES)
MODE 7 (11 PASSES)
MODE 6 (21 PASSES)
σ_ε x 10⁶ (RAD.)
0
4
8
12
16
20
24
28
32
0
200
400
600
800
1000
h ~ KM.
h = HEIGHT ABOVE MOON'S SURFACE AT PERISELENE

Fig. V-8

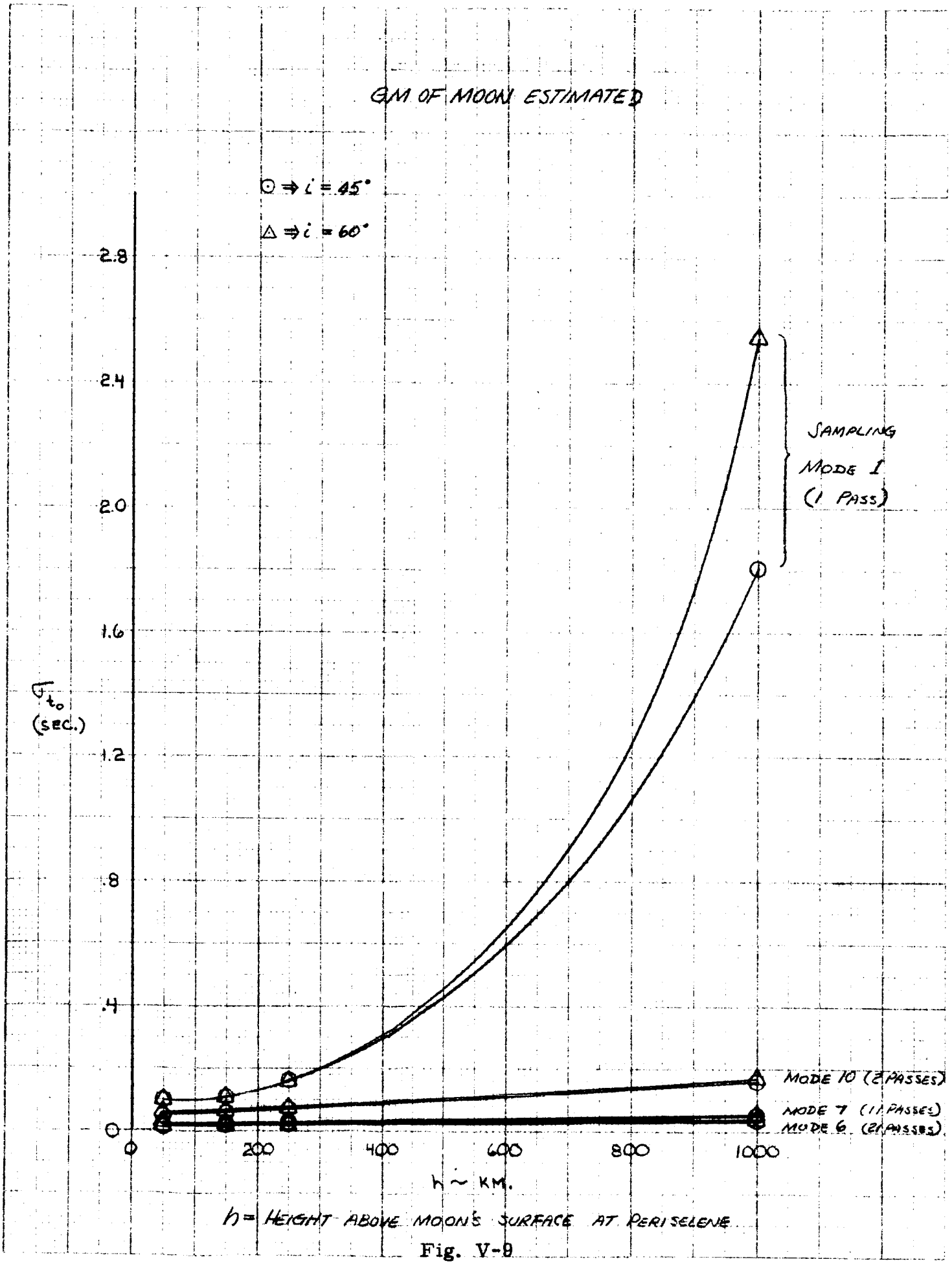
GM OF MOON ESTIMATED
⊙ ⇒ i = 45°
△ ⇒ i = 60°
2.8
2.4
2.0
1.6
1.2
.8
.4
0
σ_t0 (SEC.)
SAMPLING MODE 1 (1 PASS)
MODE 10 (2 PASSES)
MODE 7 (1 PASSES)
MODE 6 (2 PASSES)
0
200
400
600
800
1000
h ~ KM.
h = HEIGHT ABOVE MOON'S SURFACE AT PERISELENE

Fig. V-9

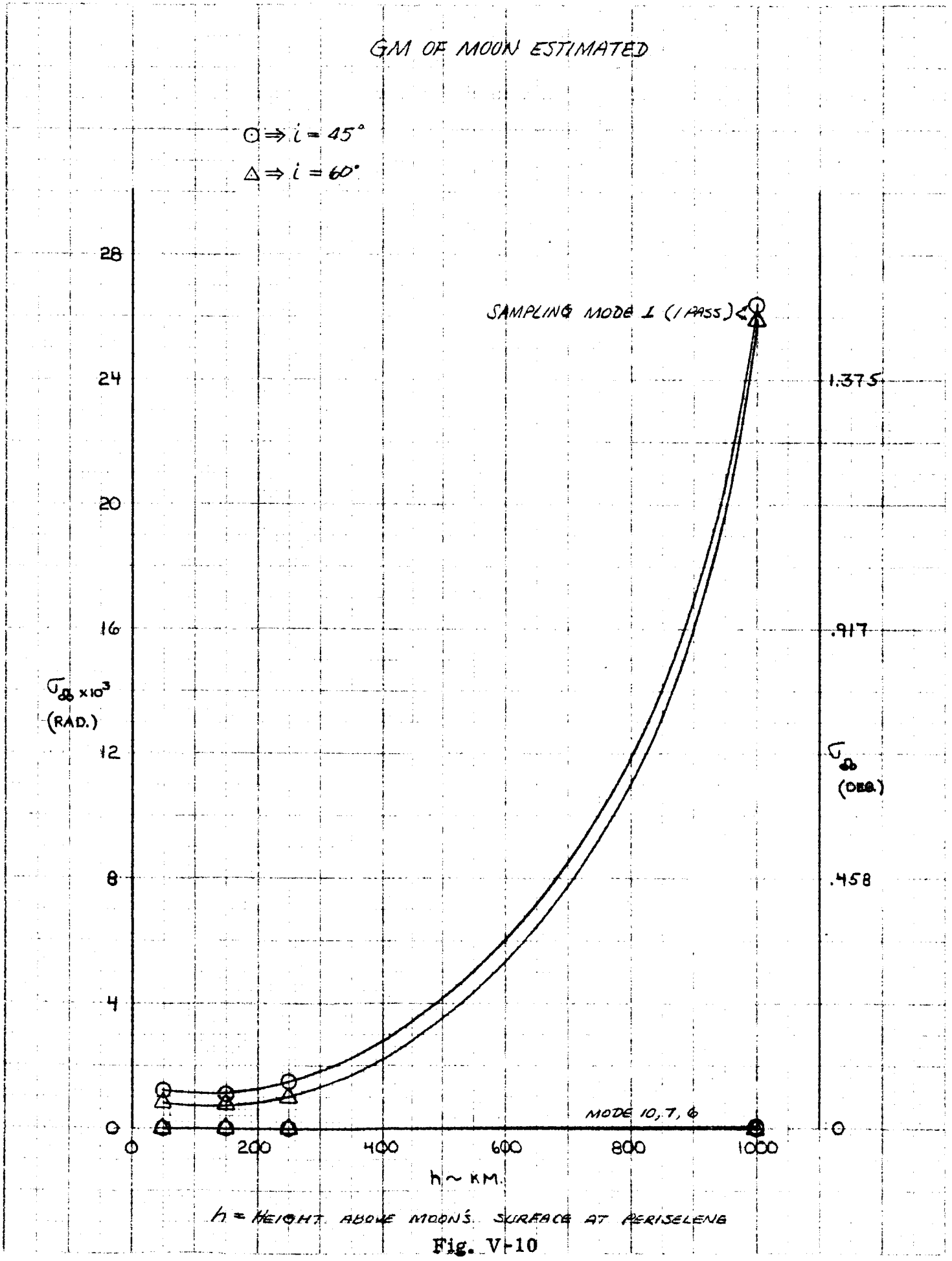
GM OF MOON ESTIMATED
⊙ ⇒ i = 45°
△ ⇒ i = 60°
SAMPLING MODE 1 (1 PASS)
MODE 10, 7, 6
28
24
20
16
12
8
4
0
$\sigma_{\Omega} \times 10^3$ (RAD.)
1.375
.917
.458
0
σ_{Ω} (DEG.)
0
200
400
600
800
1000
h ~ KM.
h = HEIGHT ABOVE MOON'S SURFACE AT PERISELENE

Fig. V-10

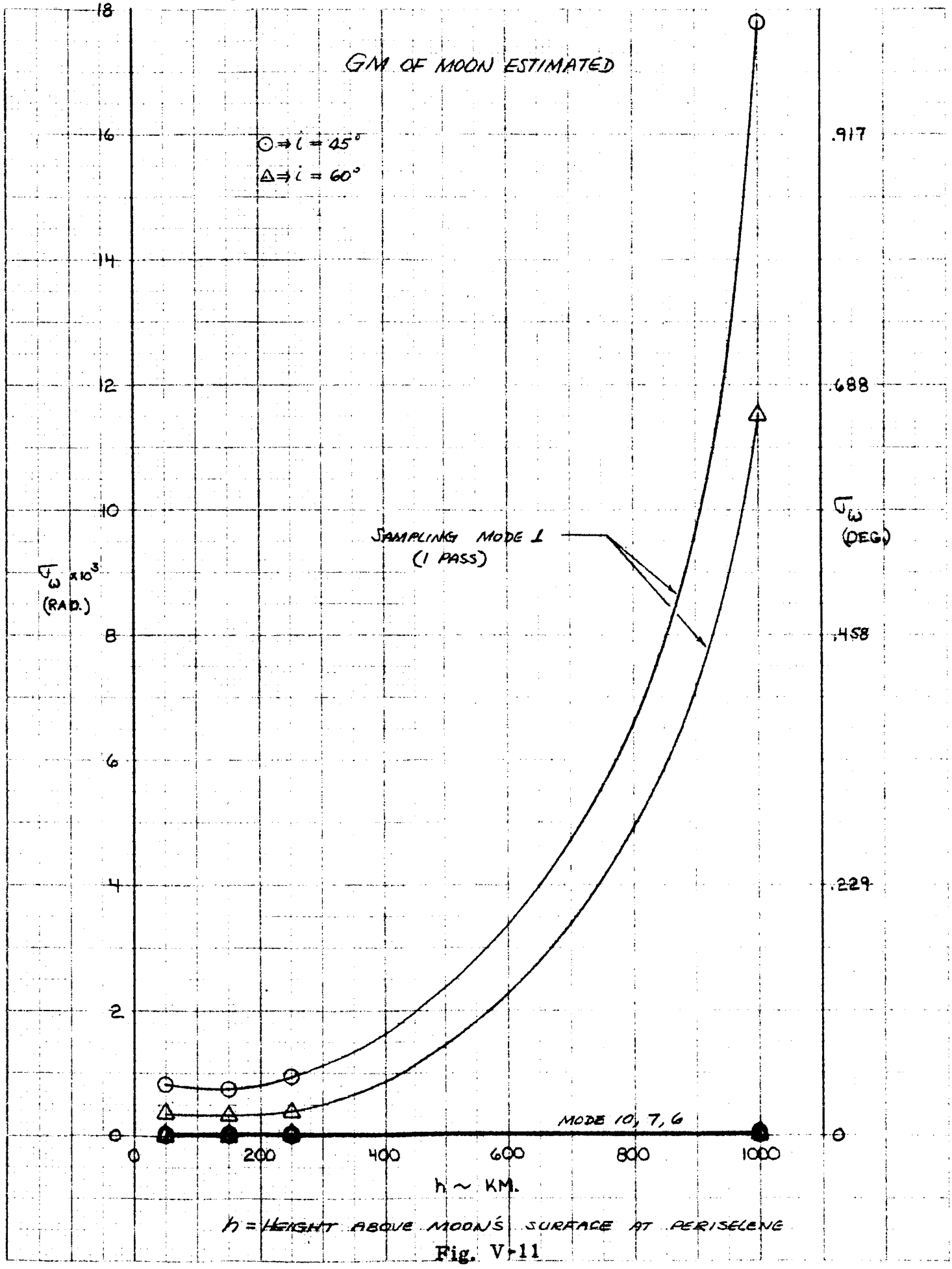
GM OF MOON ESTIMATED
⊙ ⇒ i = 45°
△ ⇒ i = 60°
SAMPLING MODE 1
(1 PASS)
MODE 10, 7, 6
σω ×10³
(RAD.)
σω
(DEG.)
18
16
14
12
10
8
6
4
2
0
.917
.688
.458
.229
0
0
200
400
600
800
1000
h ~ KM.
h = HEIGHT ABOVE MOON'S SURFACE AT PERISELENE

Fig. V-11

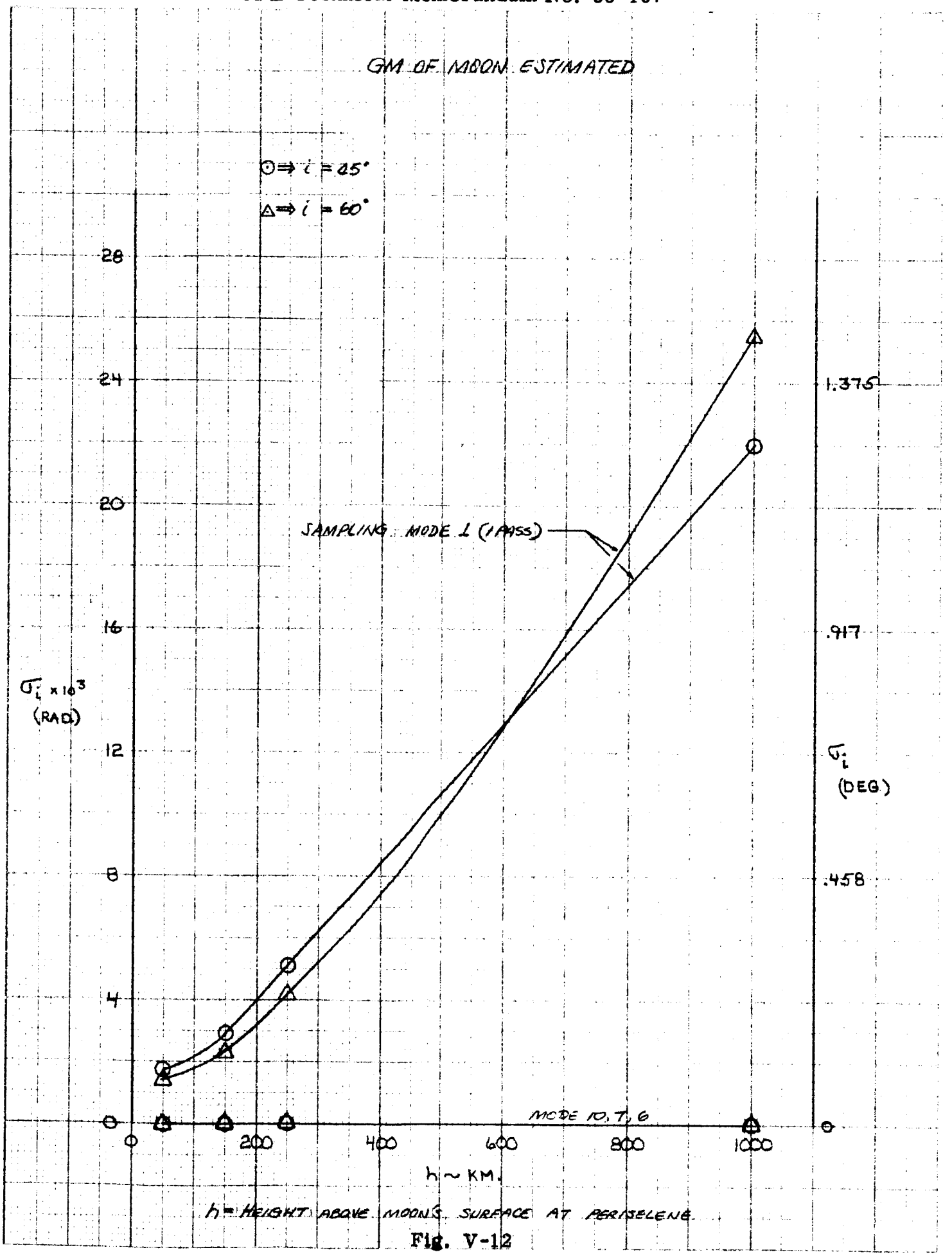
GM OF MOON ESTIMATED
⊙ ⇒ i = 45°
△ ⇒ i = 60°
SAMPLING MODE 1 (1 PASS)
MODE 10, 7, 6
σi × 10³ (RAD)
σi (DEG)
28
24
20
16
12
8
4
0
1.375
.917
.458
0
200
400
600
800
1000
h ~ KM.
h = HEIGHT ABOVE MOON'S SURFACE AT PERISELENE

Fig. V-12

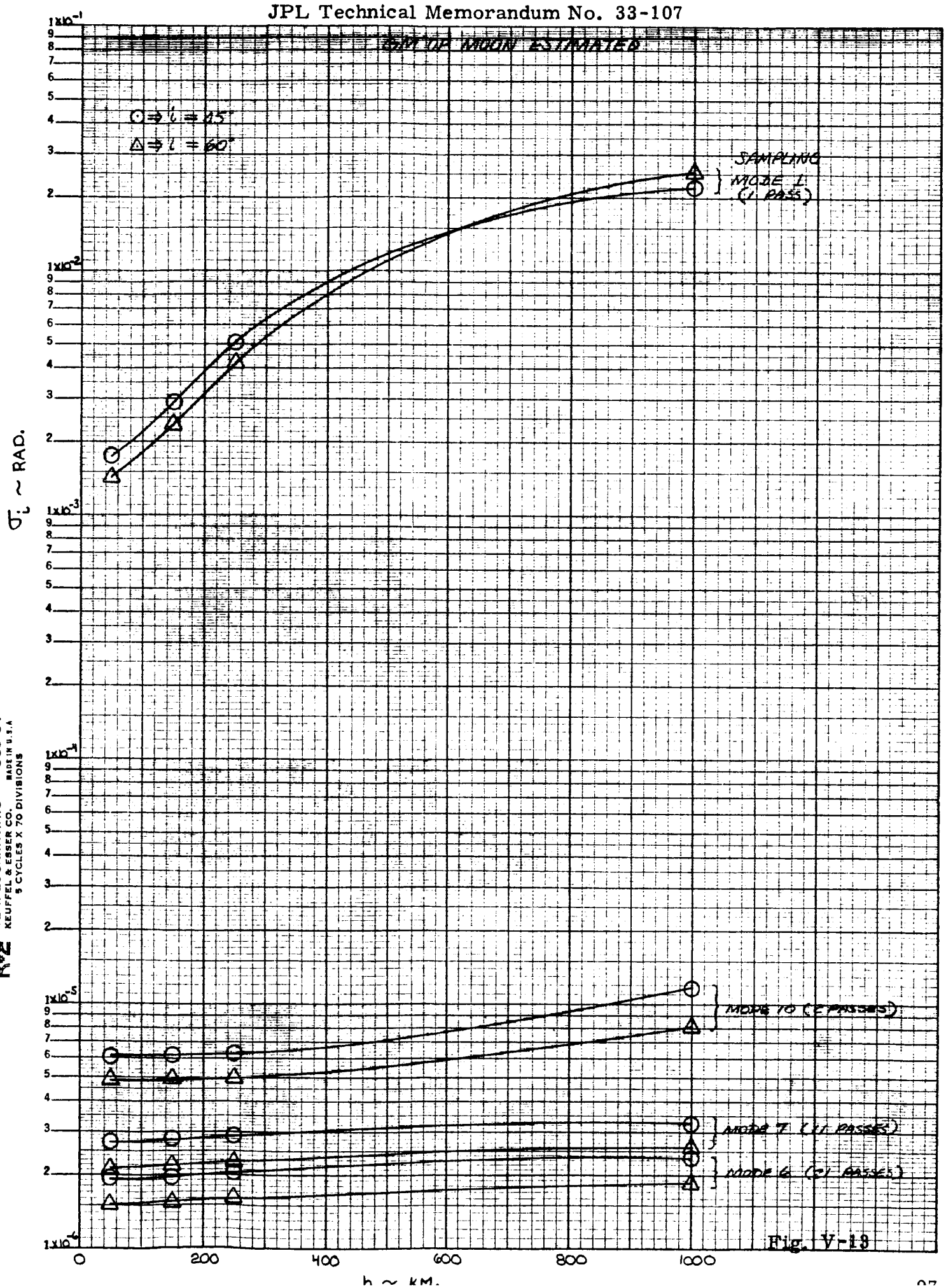
BOTTOM OF MOON ESTIMATED
⊙ ⇒ i = 45°
△ ⇒ i = 60°
SAMPLING MODE L (1 PASS)
MODE 10 (2 PASSES)
MODE 7 (11 PASSES)
MODE 6 (21 PASSES)
σi ~ RAD.
h ~ KM.
0
200
400
600
800
1000
1x10⁻¹
1x10⁻²
1x10⁻³
1x10⁻⁴
1x10⁻⁵
1x10⁻⁶
K+E SEMI-LOGARITHMIC 359-91
KEUFFEL & ESSER CO. MADE IN U.S.A.
5 CYCLES X 70 DIVISIONS

Fig. V-13

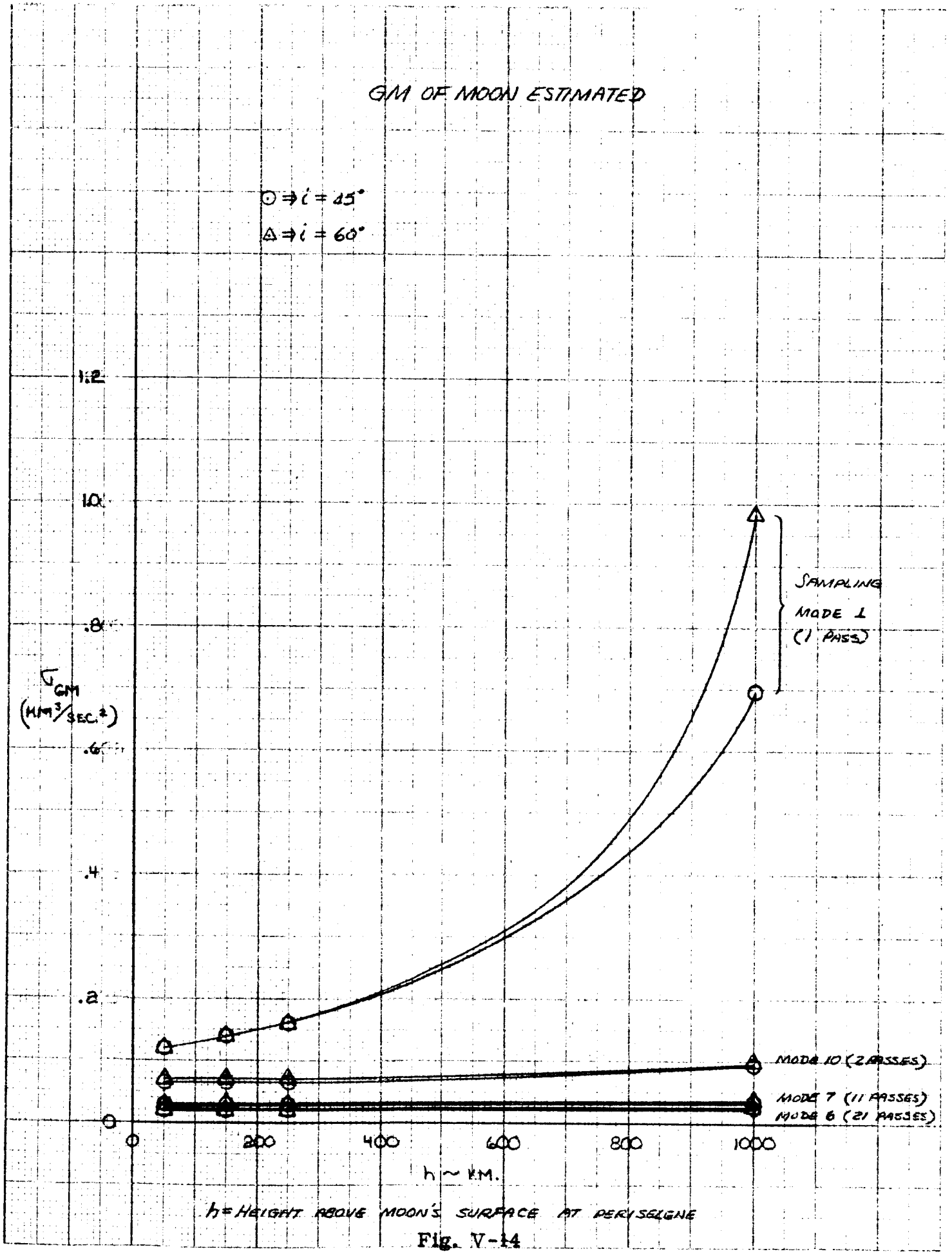
GM OF MOON ESTIMATED
⊙ ⇒ i = 45°
△ ⇒ i = 60°
1.2
1.0
.8
.6
.4
.2
0
σ_GM (KM³/SEC.²)
SAMPLING MODE 1 (1 PASS)
MODE 10 (2 PASSES)
MODE 7 (11 PASSES)
MODE 6 (21 PASSES)
0
200
400
600
800
1000
h ~ KM.
h = HEIGHT ABOVE MOON'S SURFACE AT PERISELENE

Fig. V-14

Table V-5. Variances of Cartesian Coordinates ($i = 45°$)[a]
(mass of the Moon not estimated)

$\Omega = 0$, $t_0 = 100$ sec, $\omega = 45°$, $t = 0$
x, y, z are coordinates in rotating Cartesian system
$\bar{x}$, $\bar{y}$, $\bar{z}$ are coordinates in fixed Cartesian system

	h = 50 km	150 km	250 km	1000 km
Information from 20 points (~ 1 orbit), sampling mode 1				
σ_x	3.429×10^{-3}	3.698×10^{-3}	4.004×10^{-3}	1.1103×10^{-2}
σ_y	3.053×10^{-2}	3.214×10^{-2}	3.437×10^{-2}	1.8973×10^{-1}
σ_z	2.618	3.805	6.486	3.780×10
$\sigma_{\bar{x}}$	1.7749×10^{-2}	1.8556×10^{-2}	1.9255×10^{-2}	1.0562×10^{-1}
$\sigma_{\bar{y}}$	1.8573	2.699	4.599	2.684×10
$\sigma_{\bar{z}}$	1.8459	2.681	4.574	2.662×10
Information from 40 points (~ 2 orbits), sampling mode 10				
σ_x	2.453×10^{-3}	2.821×10^{-3}	3.031×10^{-3}	6.015×10^{-3}
σ_y	2.244×10^{-2}	2.480×10^{-2}	2.692×10^{-2}	4.257×10^{-2}
σ_z	1.1557×10^{-2}	1.1947×10^{-2}	1.2898×10^{-2}	2.345×10^{-2}
$\sigma_{\bar{x}}$	1.3593×10^{-2}	1.4763×10^{-2}	1.5772×10^{-2}	2.362×10^{-2}
$\sigma_{\bar{y}}$	1.4524×10^{-2}	1.5979×10^{-2}	1.7173×10^{-2}	3.230×10^{-2}
$\sigma_{\bar{z}}$	1.8093×10^{-2}	1.9733×10^{-2}	2.176×10^{-2}	3.488×10^{-2}
Information from 220 points (~ 11 orbits), sampling mode 7				
σ_x	1.0022×10^{-3}	1.0901×10^{-3}	1.1846×10^{-3}	1.9470×10^{-3}
σ_y	9.462×10^{-3}	1.0433×10^{-2}	1.1407×10^{-2}	1.7779×10^{-2}
σ_z	5.085×10^{-3}	5.518×10^{-3}	5.990×10^{-3}	9.421×10^{-3}
$\sigma_{\bar{x}}$	5.702×10^{-3}	6.222×10^{-3}	6.752×10^{-3}	1.0716×10^{-2}
$\sigma_{\bar{y}}$	6.314×10^{-3}	6.915×10^{-3}	7.531×10^{-3}	1.1634×10^{-2}
$\sigma_{\bar{z}}$	7.637×10^{-3}	8.423×10^{-3}	9.252×10^{-3}	1.4491×10^{-2}
Information from 420 points (~ 21 orbits), sampling mode 6				
σ_x	7.360×10^{-4}	7.887×10^{-4}	8.419×10^{-4}	1.3129×10^{-3}
σ_y	6.883×10^{-3}	7.609×10^{-3}	8.278×10^{-3}	1.2980×10^{-2}
σ_z	3.620×10^{-3}	3.904×10^{-3}	4.259×10^{-3}	6.725×10^{-3}
$\sigma_{\bar{x}}$	4.133×10^{-3}	4.584×10^{-3}	4.879×10^{-3}	7.820×10^{-3}
$\sigma_{\bar{y}}$	4.571×10^{-3}	4.972×10^{-3}	5.431×10^{-3}	8.461×10^{-3}
$\sigma_{\bar{z}}$	5.556×10^{-3}	6.070×10^{-3}	6.572×10^{-3}	1.0459×10^{-2}

[a]Data plotted in Fig. V-15 through V-20.

Table V-6. Variances of Cartesian Coordinates ($i = 60°$)[a]
(mass of the Moon not estimated)

$\mathcal{A} = 0$, $t_0 = 100$ sec, $\Omega = 45°$, $\hat{t} = 0$
x, y, z are coordinates in rotating Cartesian system
$\bar{x}$, $\bar{y}$, $\bar{z}$ are coordinates in fixed Cartesian system

	h = 50 km	150 km	250 km	1000 km
Information from 20 points (~ 1 orbit), sampling mode 1				
σ_x	3.427×10^{-3}	3.696×10^{-3}	4.001×10^{-3}	1.1333×10^{-2}
σ_y	3.054×10^{-2}	3.216×10^{-2}	3.440×10^{-2}	1.9603×10^{-1}
σ_z	2.142	3.111	5.300	3.196×10
$\sigma_{\bar{x}}$	1.7747×10^{-2}	1.8552×10^{-2}	1.9248×10^{-2}	1.0914×10^{-1}
$\sigma_{\bar{y}}$	1.8594	2.700	4.599	2.775×10
$\sigma_{\bar{z}}$	1.0643	1.5444	2.635	1.5839×10
Information from 40 points (~ 2 orbits), sampling mode 10				
σ_x	2.708×10^{-3}	3.1311×10^{-3}	3.388×10^{-3}	6.093×10^{-3}
σ_y	2.526×10^{-2}	2.731×10^{-2}	2.911×10^{-2}	4.395×10^{-2}
σ_z	8.951×10^{-3}	9.135×10^{-3}	9.751×10^{-3}	1.7725×10^{-2}
$\sigma_{\bar{x}}$	1.5179×10^{-2}	1.6253×10^{-2}	1.7156×10^{-2}	2.478×10^{-2}
$\sigma_{\bar{y}}$	1.2427×10^{-2}	1.3291×10^{-2}	1.4073×10^{-2}	2.550×10^{-2}
$\sigma_{\bar{z}}$	2.089×10^{-2}	2.259×10^{-2}	2.437×10^{-2}	3.832×10^{-2}
Information from 220 points (~ 11 orbits), sampling mode 7				
σ_x	1.0905×10^{-3}	1.1857×10^{-3}	1.3018×10^{-3}	2.021×10^{-3}
σ_y	1.0526×10^{-2}	1.1576×10^{-2}	1.2723×10^{-2}	1.9808×10^{-2}
σ_z	3.950×10^{-3}	4.273×10^{-3}	4.644×10^{-3}	7.323×10^{-3}
$\sigma_{\bar{x}}$	6.295×10^{-3}	6.882×10^{-3}	7.464×10^{-3}	1.1776×10^{-2}
$\sigma_{\bar{y}}$	5.376×10^{-3}	5.836×10^{-3}	6.402×10^{-3}	9.843×10^{-3}
$\sigma_{\bar{z}}$	4.357×10^{-3}	9.592×10^{-3}	1.0624×10^{-2}	1.6624×10^{-2}
Information from 420 points (~ 21 orbits), sampling mode 6				
σ_x	8.067×10^{-4}	8.615×10^{-4}	9.254×10^{-4}	1.4397×10^{-3}
σ_y	7.688×10^{-3}	8.463×10^{-3}	9.183×10^{-3}	1.4473×10^{-2}
σ_z	2.799×10^{-3}	3.011×10^{-3}	3.287×10^{-3}	5.200×10^{-3}
$\sigma_{\bar{x}}$	4.576×10^{-3}	5.079×10^{-3}	5.418×10^{-3}	8.623×10^{-3}
$\sigma_{\bar{y}}$	3.892×10^{-3}	4.197×10^{-3}	4.617×10^{-3}	7.209×10^{-3}
$\sigma_{\bar{z}}$	6.392×10^{-3}	6.957×10^{-3}	7.612×10^{-3}	1.2017×10^{-2}

[a]Data plotted in Fig. V-15 through V-20.

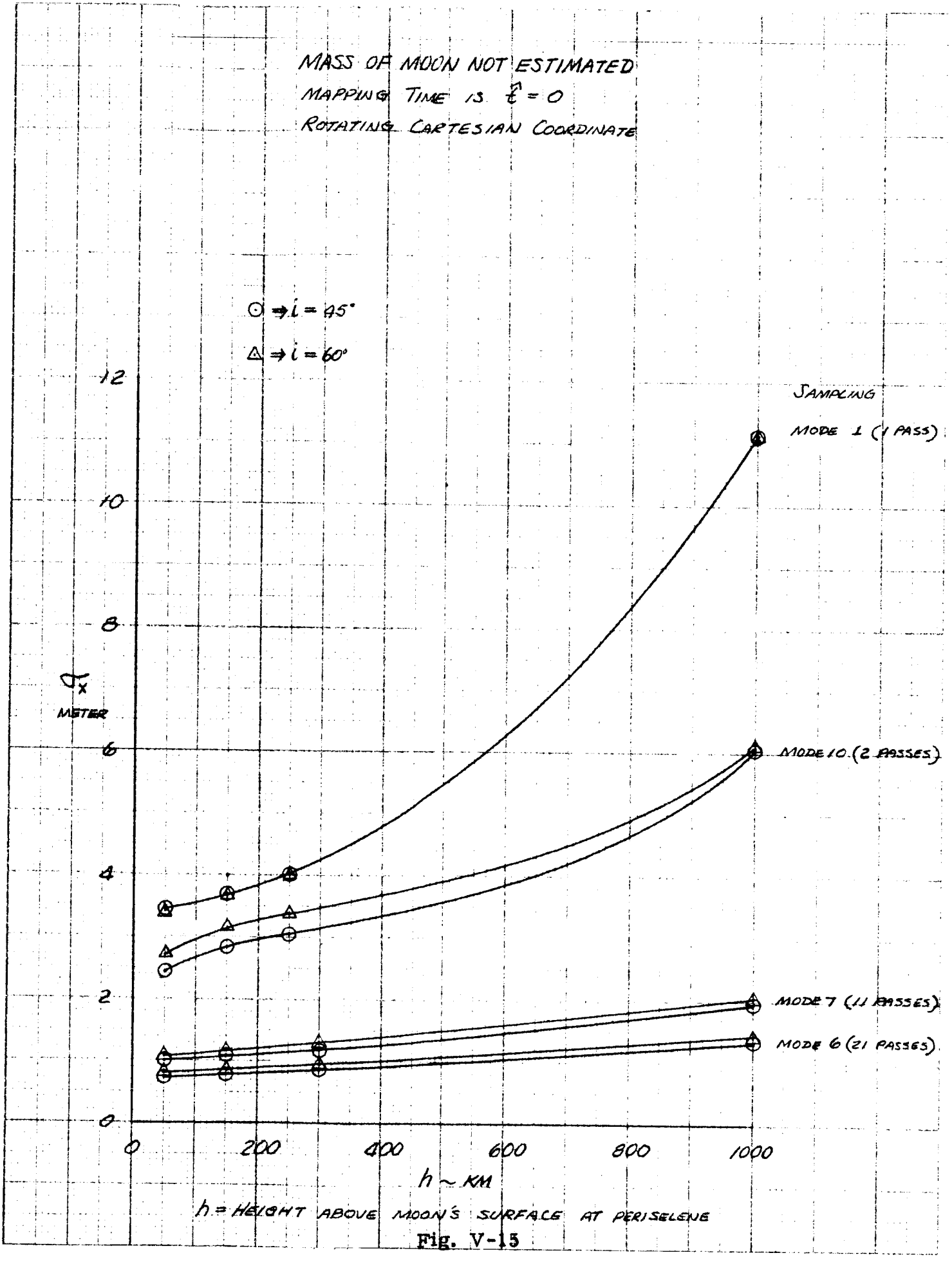
MASS OF MOON NOT ESTIMATED
MAPPING TIME IS $\hat{t} = 0$
ROTATING CARTESIAN COORDINATE
⊙ ⇒ $i = 45°$
△ ⇒ $i = 60°$
SAMPLING
MODE 1 (1 PASS)
MODE 10 (2 PASSES)
MODE 7 (11 PASSES)
MODE 6 (21 PASSES)
σ_x
METER
0
2
4
6
8
10
12
0
200
400
600
800
1000
$h \sim$ KM
h = HEIGHT ABOVE MOON'S SURFACE AT PERISELENE

Fig. V-15

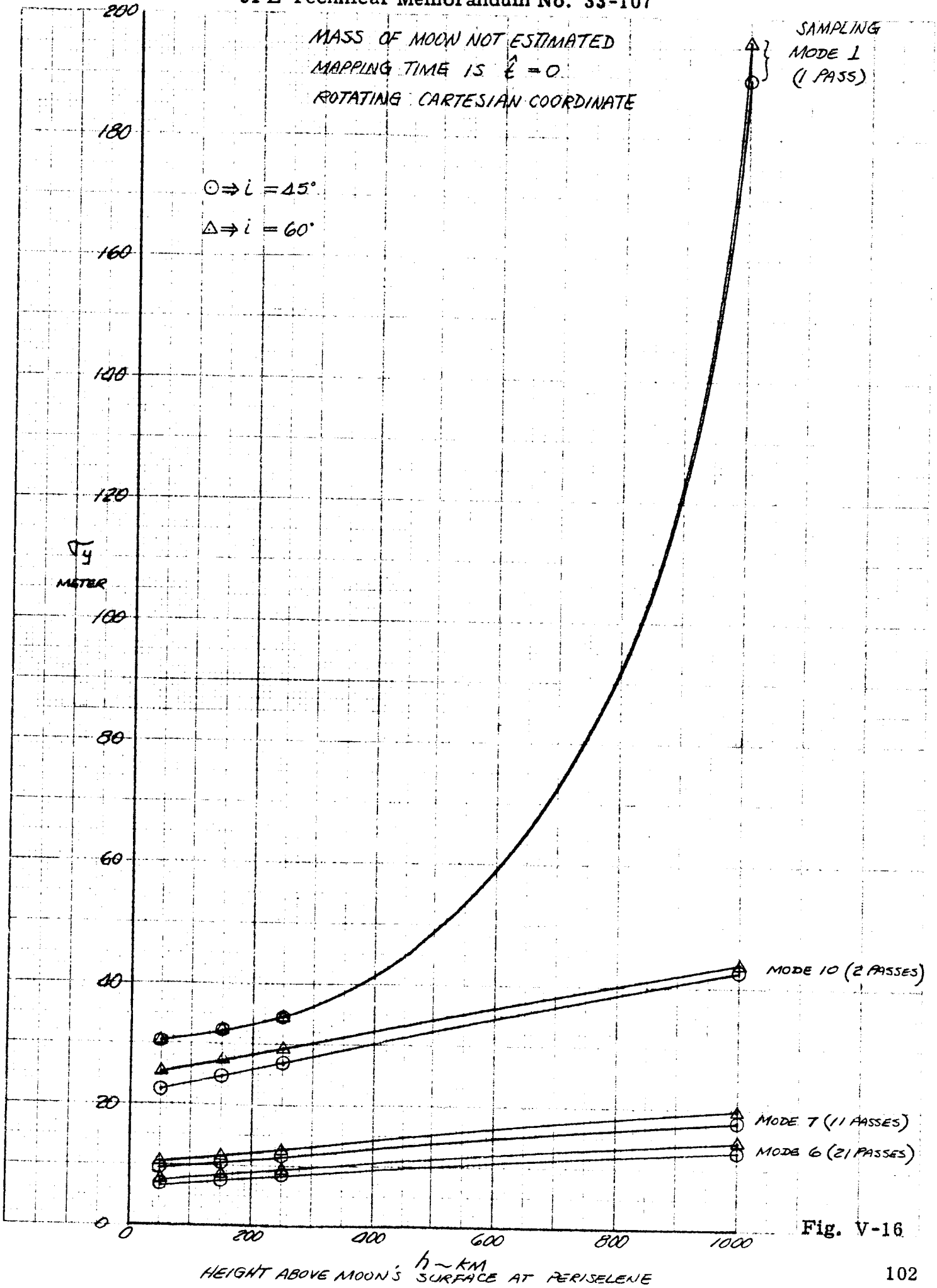
MASS OF MOON NOT ESTIMATED
MAPPING TIME IS $\hat{t} = 0$
ROTATING CARTESIAN COORDINATE
⊙ ⇒ $i = 45°$
△ ⇒ $i = 60°$
SAMPLING MODE 1 (1 PASS)
MODE 10 (2 PASSES)
MODE 7 (11 PASSES)
MODE 6 (21 PASSES)
σ_y METER
0
20
40
60
80
100
120
140
160
180
200
0
200
400
600
800
1000
$h \sim$ KM
HEIGHT ABOVE MOON'S SURFACE AT PERISELENE

Fig. V-16

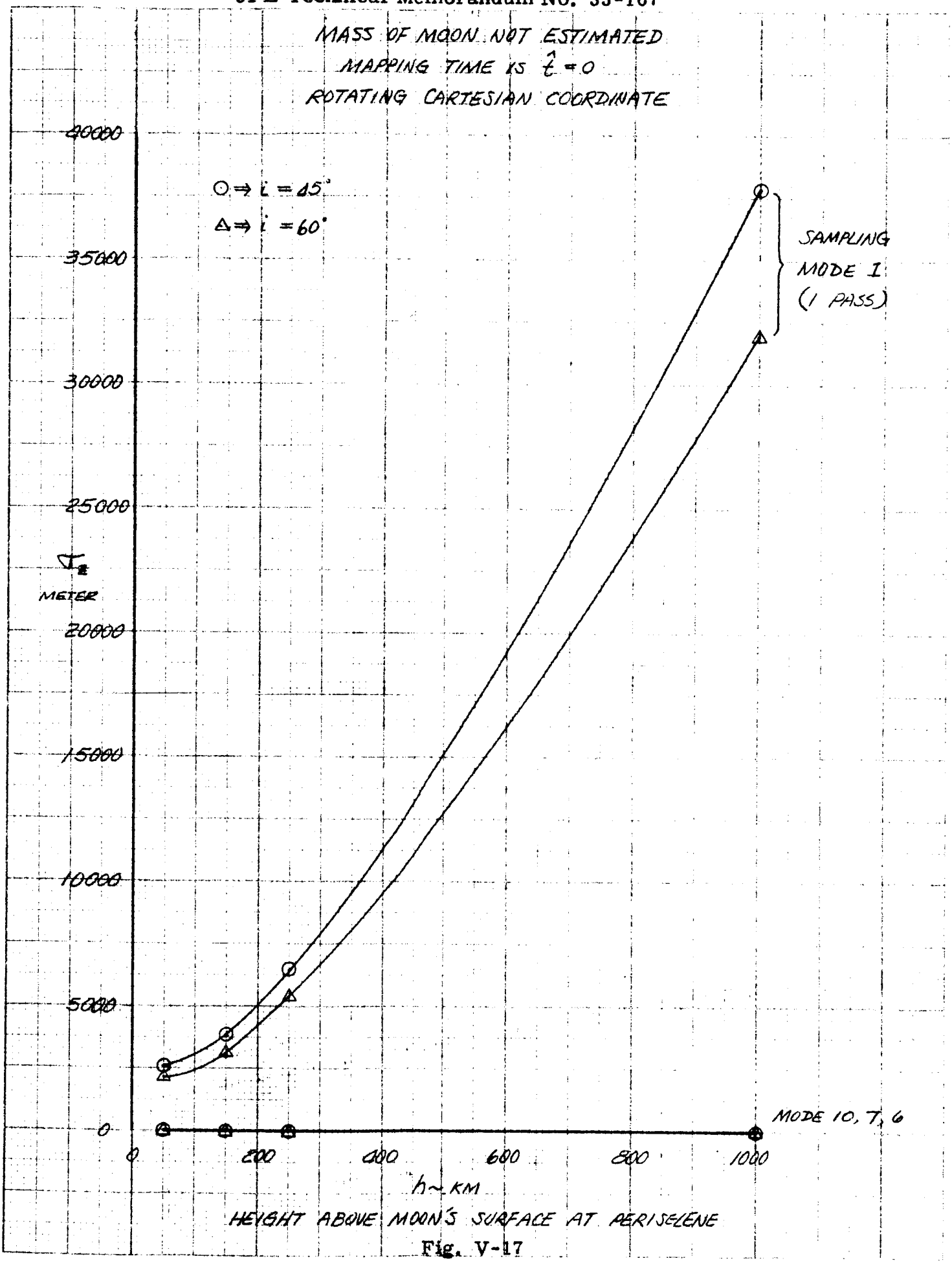
MASS OF MOON NOT ESTIMATED
MAPPING TIME IS $\hat{t} = 0$
ROTATING CARTESIAN COORDINATE
⊙ ⇒ $i = 45°$
△ ⇒ $i = 60°$
SAMPLING MODE I (1 PASS)
MODE 10, 7, 6
σ_z METER
40000
35000
30000
25000
20000
15000
10000
5000
0
0
200
400
600
800
1000
h ~ KM
HEIGHT ABOVE MOON'S SURFACE AT PERISELENE

Fig. V-17

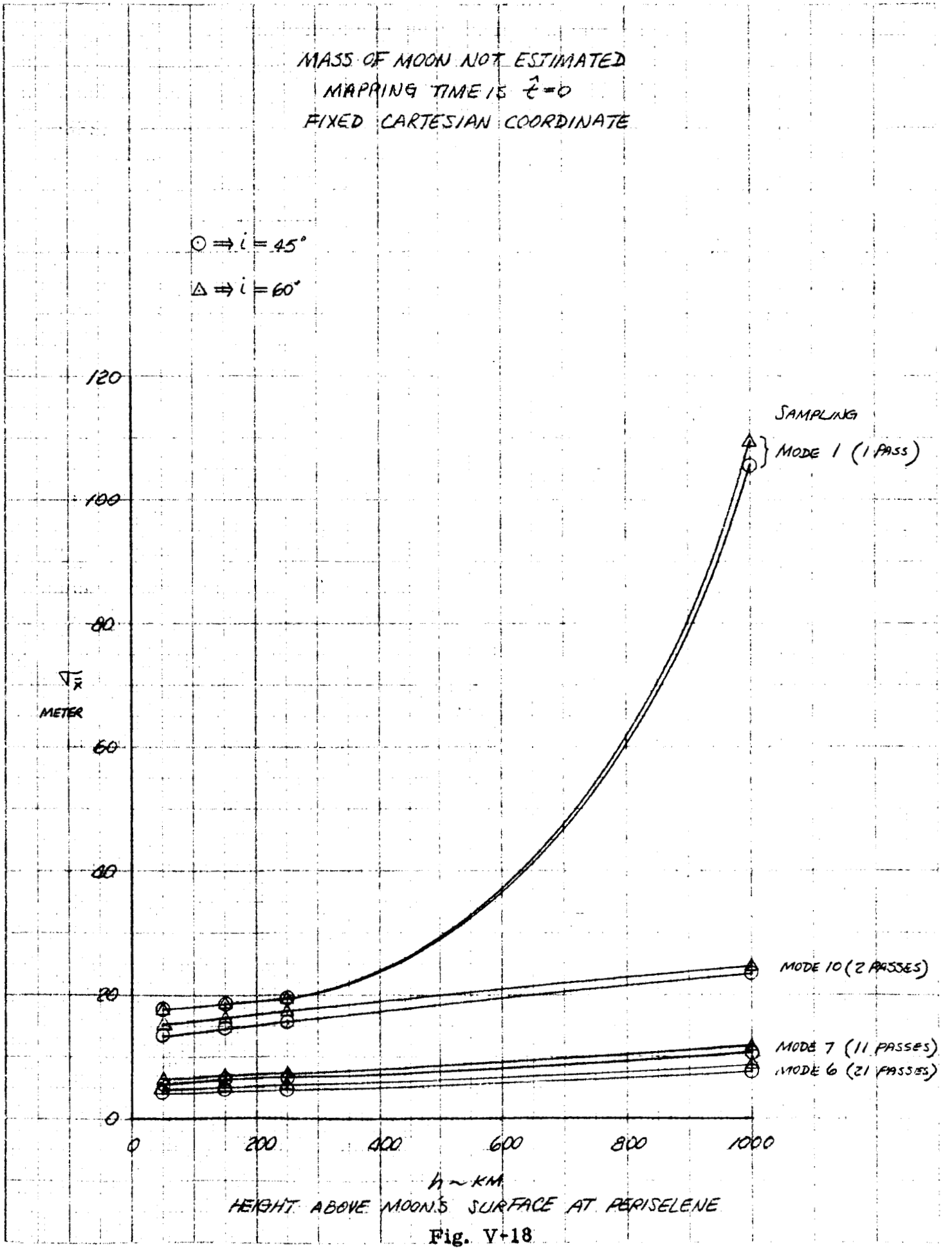
MASS OF MOON NOT ESTIMATED
MAPPING TIME IS $\hat{t}=0$
FIXED CARTESIAN COORDINATE
⊙ ⇒ $i = 45°$
△ ⇒ $i = 60°$
120
100
80
60
40
20
0
$\sqrt{\bar{x}}$
METER
SAMPLING
MODE 1 (1 PASS)
MODE 10 (2 PASSES)
MODE 7 (11 PASSES)
MODE 6 (21 PASSES)
0
200
400
600
800
1000
$h \sim$ KM
HEIGHT ABOVE MOON'S SURFACE AT PERISELENE

Fig. V-18

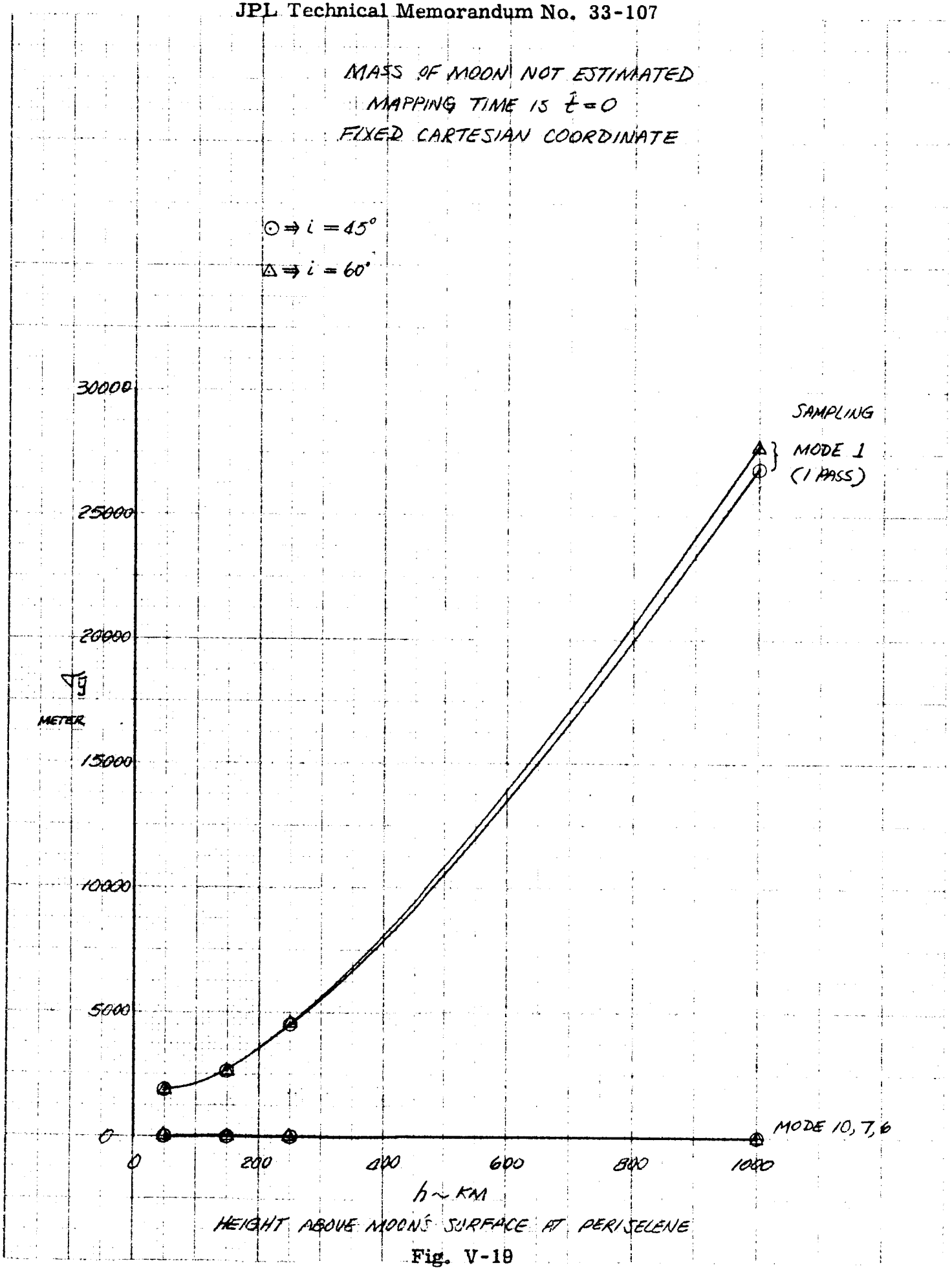
MASS OF MOON NOT ESTIMATED
MAPPING TIME IS $\hat{t}=0$
FIXED CARTESIAN COORDINATE
⊙ ⇒ $i = 45°$
△ ⇒ $i = 60°$
30000
25000
20000
15000
10000
5000
0
METER
SAMPLING
MODE 1
(1 PASS)
MODE 10, 7, 6
0
200
400
600
800
1000
h ~ KM
HEIGHT ABOVE MOON'S SURFACE AT PERISELENE

Fig. V-19

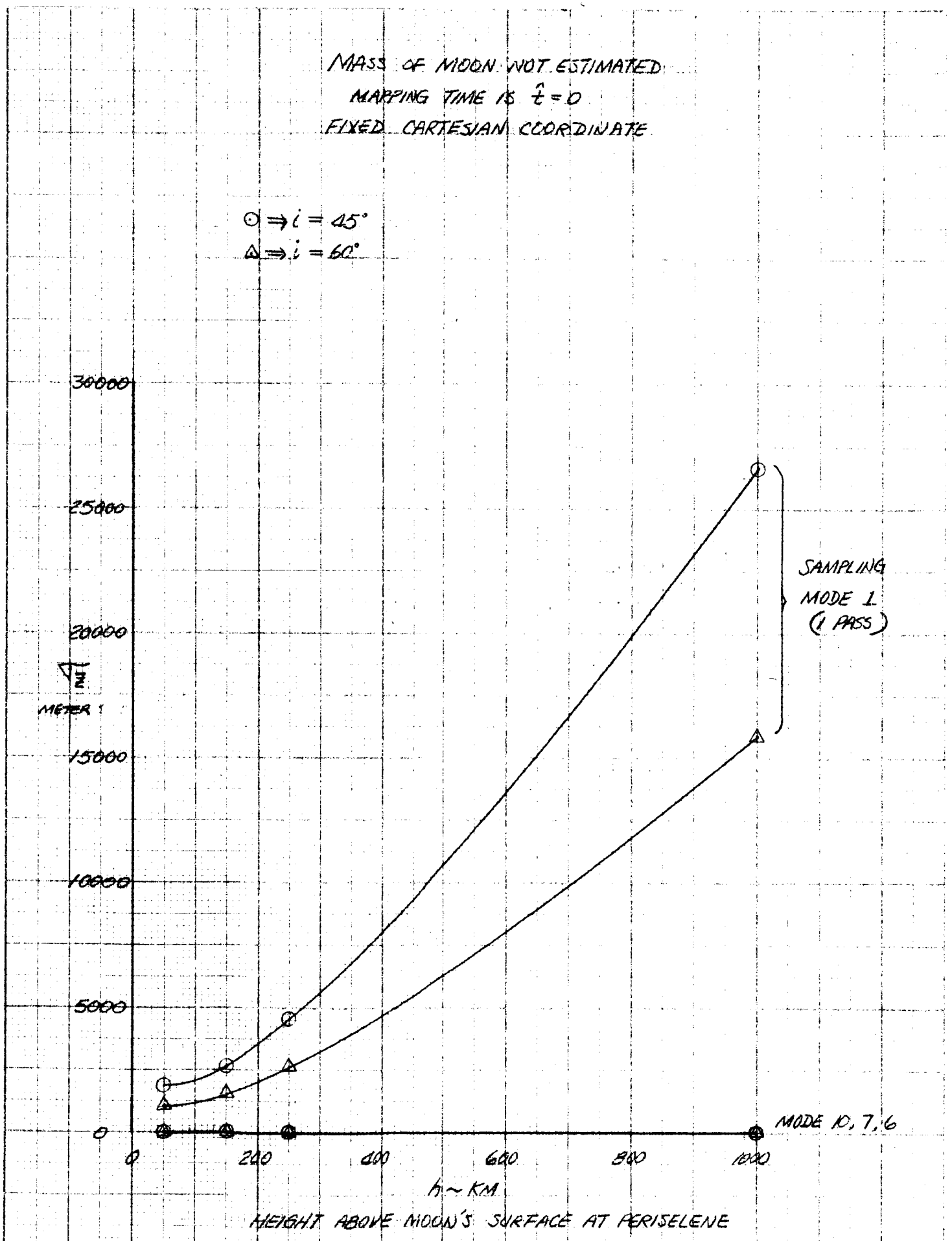
MASS OF MOON NOT ESTIMATED
MAPPING TIME IS $\hat{t} = 0$
FIXED CARTESIAN COORDINATE
⊙ ⇒ $i = 45°$
△ ⇒ $i = 60°$
30000
25000
20000
15000
10000
5000
0
$\sqrt{N}$
METER
SAMPLING MODE 1 (1 PASS)
MODE 10, 7, 6
0
200
400
600
800
1000
h ~ KM
HEIGHT ABOVE MOON'S SURFACE AT PERISELENE

Fig. V-20

Table V-7. Variances of Cartesian Coordinates (i = 45°)[a]
(mass of the Moon estimated)

$\Omega = 0$, $t_0 = 100$ sec, $\omega = 45°$, $t = 0$
x, y, z are coordinates in rotating Cartesian system
$\bar{x}$, $\bar{y}$, $\bar{z}$ are coordinates in fixed Cartesian system

	h = 50 km	150 km	250 km	1000 km
Information from 20 points (~ 1 orbit), sampling mode 1				
σ_x	1.7688×10^{-2}	2.199×10^{-2}	2.676×10^{-2}	1.2508×10^{-1}
σ_y	4.922×10^{-2}	6.026×10^{-2}	7.452×10^{-2}	3.283×10^{-1}
σ_z	2.627	4.142	8.256	7.752×10
$\sigma_{\bar{x}}$	2.039×10^{-2}	2.135×10^{-2}	2.281×10^{-2}	3.378×10^{-1}
$\sigma_{\bar{y}}$	1.8613	2.955	5.883	5.491×10
$\sigma_{\bar{z}}$	1.8550	2.904	5.793	5.473×10
Information from 40 points (~ 2 orbits), sampling mode 10				
σ_x	8.698×10^{-3}	9.438×10^{-3}	1.0115×10^{-2}	2.168×10^{-2}
σ_y	2.518×10^{-2}	2.850×10^{-2}	3.155×10^{-2}	6.352×10^{-2}
σ_z	1.1846×10^{-2}	1.2395×10^{-2}	1.3464×10^{-2}	2.866×10^{-2}
$\sigma_{\bar{x}}$	1.3738×10^{-2}	1.5073×10^{-2}	1.6259×10^{-2}	2.619×10^{-2}
$\sigma_{\bar{y}}$	1.6587×10^{-2}	1.8619×10^{-2}	2.036×10^{-2}	4.453×10^{-2}
$\sigma_{\bar{z}}$	2.154×10^{-2}	2.433×10^{-2}	2.725×10^{-2}	6.427×10^{-2}
Information from 220 points (~ 11 orbits), sampling mode 7				
σ_x	3.667×10^{-3}	3.906×10^{-3}	4.162×10^{-3}	6.614×10^{-3}
σ_y	1.0492×10^{-2}	1.1221×10^{-2}	1.2007×10^{-2}	1.8806×10^{-2}
σ_z	5.187×10^{-3}	5.605×10^{-3}	6.061×10^{-3}	9.462×10^{-3}
$\sigma_{\bar{x}}$	5.739×10^{-3}	6.227×10^{-3}	6.755×10^{-3}	1.0737×10^{-2}
$\sigma_{\bar{y}}$	7.149×10^{-3}	7.640×10^{-3}	8.157×10^{-3}	1.3078×10^{-2}
$\sigma_{\bar{z}}$	9.020×10^{-3}	9.617×10^{-3}	1.0344×10^{-2}	1.6181×10^{-2}
Information from 420 points (~ 21 orbits), sampling mode 6				
σ_x	2.642×10^{-3}	2.911×10^{-3}	3.080×10^{-3}	4.910×10^{-3}
σ_y	7.557×10^{-3}	8.413×10^{-3}	8.839×10^{-3}	1.3983×10^{-2}
σ_z	3.695×10^{-3}	3.979×10^{-3}	4.345×10^{-3}	6.792×10^{-3}
$\sigma_{\bar{x}}$	4.152×10^{-3}	4.613×10^{-3}	4.883×10^{-3}	7.800×10^{-3}
$\sigma_{\bar{y}}$	5.127×10^{-3}	5.476×10^{-3}	5.987×10^{-3}	9.577×10^{-3}
$\sigma_{\bar{z}}$	6.496×10^{-3}	7.144×10^{-3}	7.578×10^{-3}	1.1973×10^{-2}

[a] Data plotted in Fig. V-1 through V-27.

Table V-8. Variances of Cartesian Coordinates (i = 60°)[a]
(mass of the Moon estimated)

$\Omega = 0$, $t_0 = 100$ sec, $\omega = 45°$, $t = 0$
x, y, z are coordinates in rotating Cartesian system
$\bar{x}$, $\bar{y}$, $\bar{z}$ are coordinates in fixed Cartesian system

	h = 50 km	150 km	250 km	1000 km
Information from 20 points (~ 1 orbit), sampling mode 1				
σ_x	1.7683×10^{-2}	2.197×10^{-2}	2.672×10^{-2}	1.7414×10^{-1}
σ_y	4.919×10^{-2}	6.021×10^{-2}	7.445×10^{-2}	4.704×10^{-1}
σ_z	2.150	3.382	6.740	9.204×10
$\sigma_{\bar{x}}$	2.038×10^{-2}	2.135×10^{-2}	2.223×10^{-2}	4.929×10^{-1}
$\sigma_{\bar{y}}$	1.8643	2.948	5.869	7.980×10
$\sigma_{\bar{z}}$	1.0722	1.6610	3.315	4.588×10
Information from 40 points (~ 2 orbits), sampling mode 10				
σ_x	1.0030×10^{-2}	1.0809×10^{-2}	1.1451×10^{-2}	2.260×10^{-2}
σ_y	2.931×10^{-2}	3.266×10^{-2}	3.517×10^{-2}	7.051×10^{-2}
σ_z	9.145×10^{-3}	9.396×10^{-3}	1.0046×10^{-2}	2.024×10^{-2}
$\sigma_{\bar{x}}$	1.5594×10^{-2}	1.6823×10^{-2}	1.7871×10^{-2}	2.813×10^{-2}
$\sigma_{\bar{y}}$	1.4586×10^{-2}	1.5827×10^{-2}	1.6904×10^{-2}	3.492×10^{-2}
$\sigma_{\bar{z}}$	2.691×10^{-2}	2.970×10^{-2}	3.220×10^{-2}	7.193×10^{-2}
Information from 220 points (~ 11 orbits), sampling mode 7				
σ_x	4.155×10^{-3}	4.358×10^{-3}	4.585×10^{-3}	7.303×10^{-3}
σ_y	1.2203×10^{-2}	1.2828×10^{-2}	1.3634×10^{-2}	2.139×10^{-2}
σ_z	4.012×10^{-3}	4.326×10^{-3}	4.697×10^{-3}	7.351×10^{-3}
$\sigma_{\bar{x}}$	6.419×10^{-3}	6.924×10^{-3}	7.465×10^{-3}	1.1778×10^{-2}
$\sigma_{\bar{y}}$	6.218×10^{-3}	6.538×10^{-3}	6.982×10^{-3}	1.1153×10^{-2}
$\sigma_{\bar{z}}$	1.1069×10^{-2}	1.1560×10^{-2}	1.2316×10^{-2}	1.9599×10^{-2}
Information from 420 points (~ 21 orbits), sampling mode 6				
σ_x	2.995×10^{-3}	3.297×10^{-3}	3.440×10^{-3}	5.290×10^{-3}
σ_y	8.791×10^{-3}	9.739×10^{-3}	1.0151×10^{-2}	1.6000×10^{-2}
σ_z	2.845×10^{-3}	3.058×10^{-3}	3.339×10^{-3}	5.244×10^{-3}
$\sigma_{\bar{x}}$	4.645×10^{-3}	5.172×10^{-3}	5.447×10^{-3}	8.639×10^{-3}
$\sigma_{\bar{y}}$	4.457×10^{-3}	4.861×10^{-3}	5.147×10^{-3}	8.232×10^{-3}
$\sigma_{\bar{z}}$	7.935×10^{-3}	8.763×10^{-3}	9.170×10^{-3}	1.4573×10^{-2}

[a]Data plotted in Fig. V-21 through V-27.

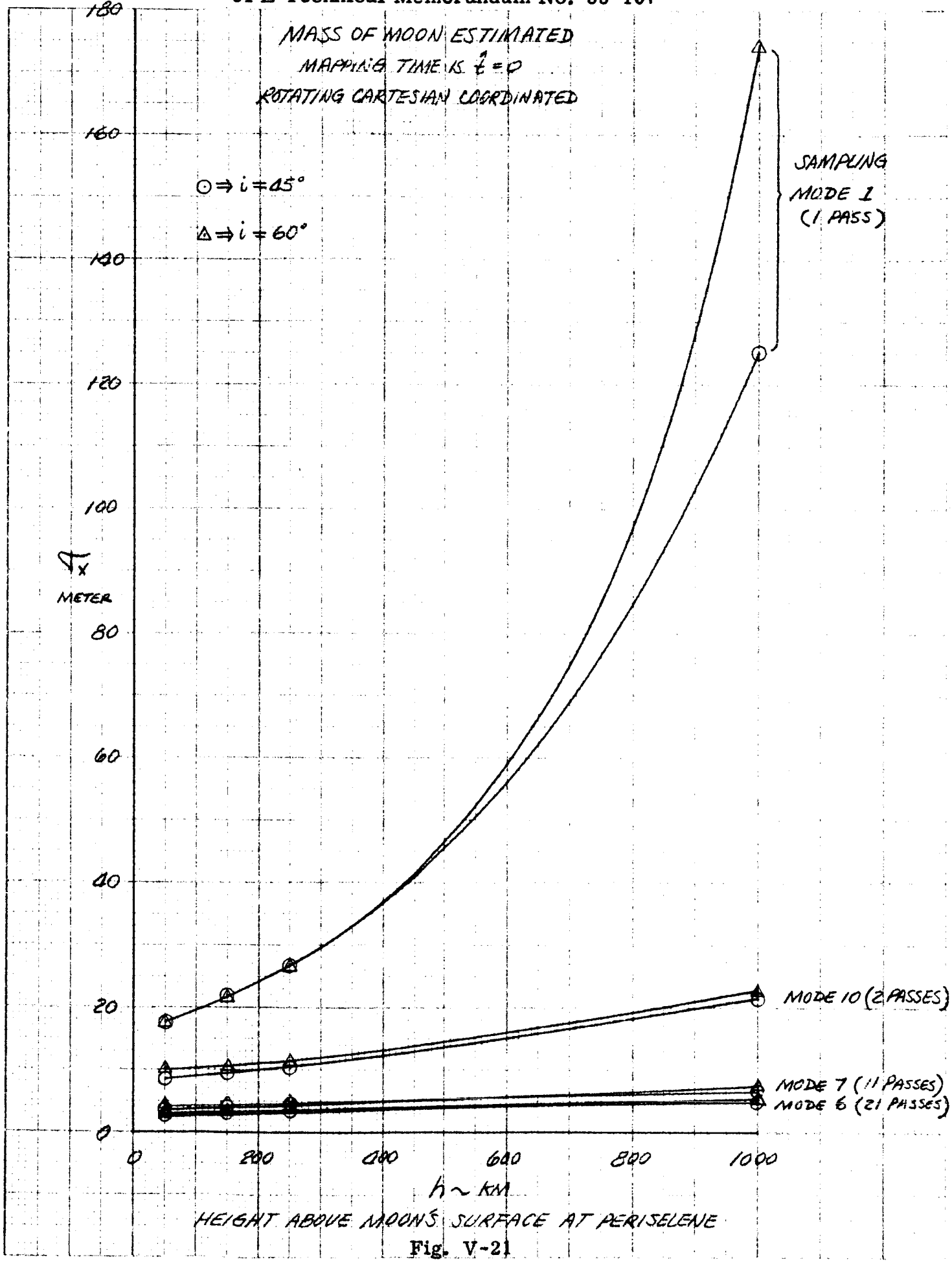
MASS OF MOON ESTIMATED
MAPPING TIME IS $\hat{t}=0$
ROTATING CARTESIAN COORDINATED
⊙ ⇒ i = 45°
△ ⇒ i = 60°
SAMPLING MODE 1 (1 PASS)
MODE 10 (2 PASSES)
MODE 7 (11 PASSES)
MODE 6 (21 PASSES)
σ_x METER
0
20
40
60
80
100
120
140
160
180
0
200
400
600
800
1000
h ~ KM
HEIGHT ABOVE MOON'S SURFACE AT PERISELENE

Fig. V-21

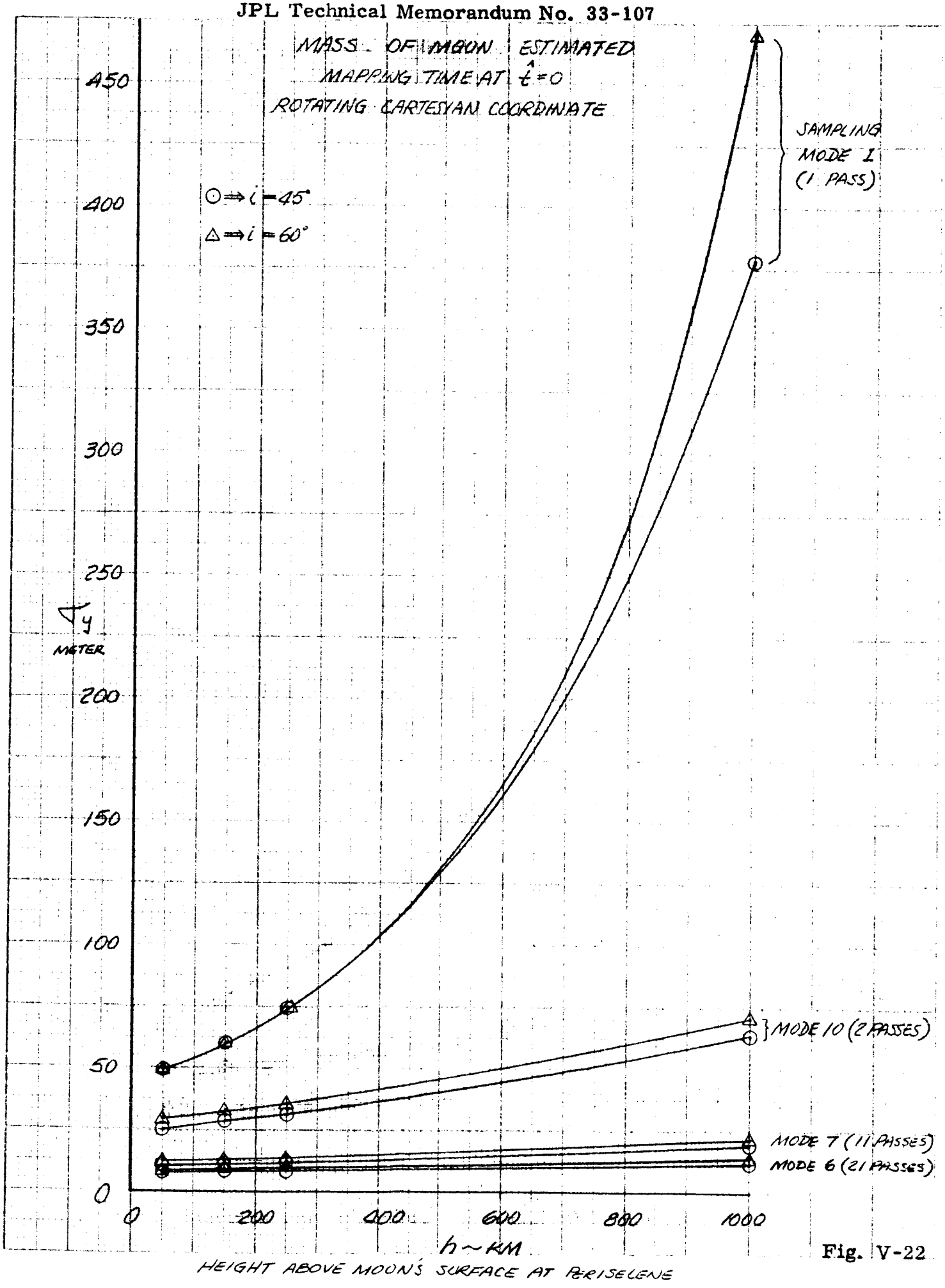
MASS OF MOON ESTIMATED
MAPPING TIME AT $\hat{t}=0$
ROTATING CARTESIAN COORDINATE
⊙ ⇒ $i=45°$
△ ⇒ $i=60°$
SAMPLING MODE I (1 PASS)
MODE 10 (2 PASSES)
MODE 7 (11 PASSES)
MODE 6 (21 PASSES)
σ_y METER
0
50
100
150
200
250
300
350
400
450
0
200
400
600
800
1000
$h \sim$ KM
HEIGHT ABOVE MOON'S SURFACE AT PERISELENE

Fig. V-22

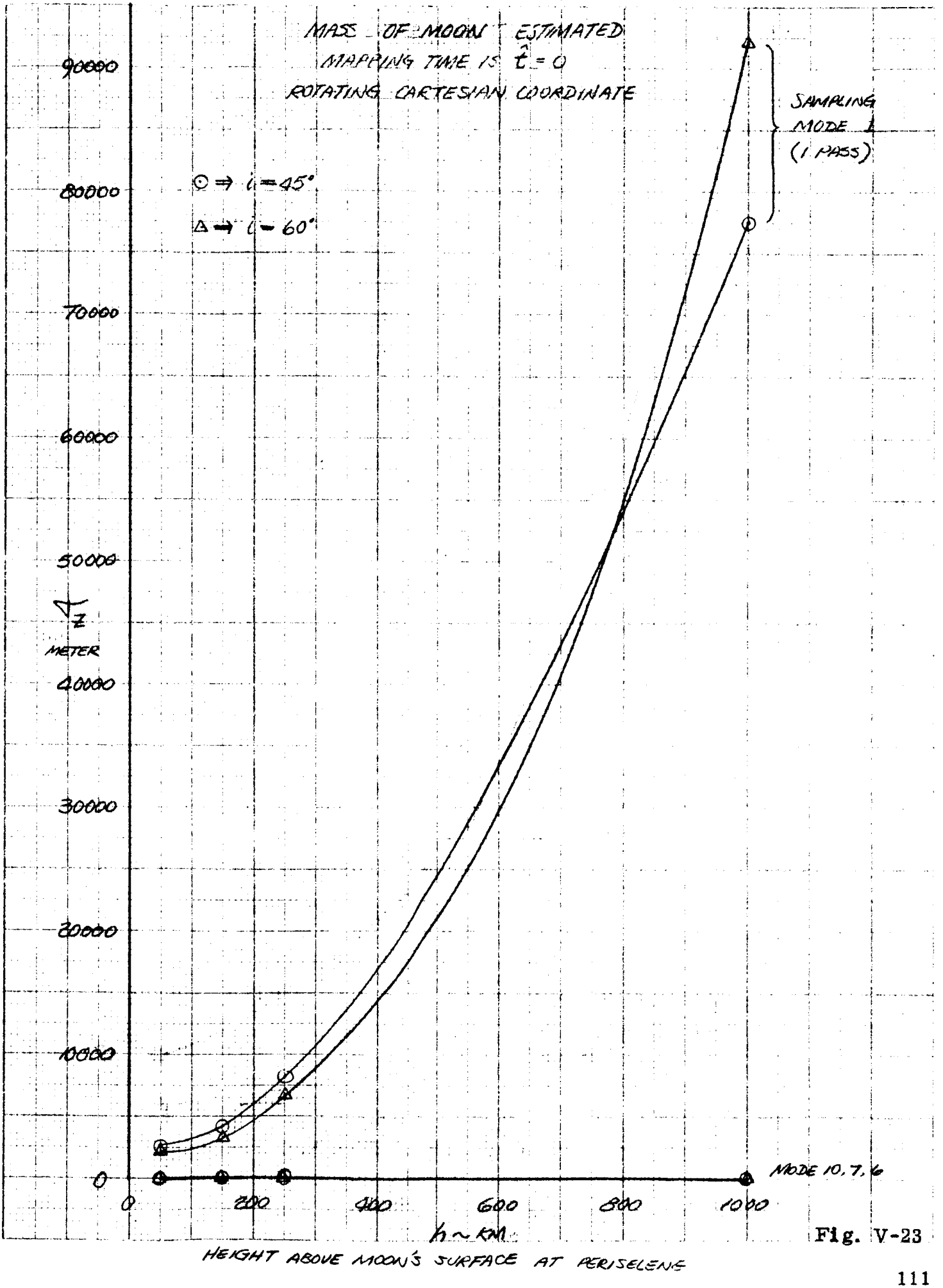
MASS OF MOON ESTIMATED
MAPPING TIME IS $\hat{t} = 0$
ROTATING CARTESIAN COORDINATE
⊙ ⇒ $i = 45°$
△ ⇒ $i = 60°$
SAMPLING MODE 1 (1 PASS)
MODE 10, 7, 6
90000
80000
70000
60000
50000
40000
30000
20000
10000
0
∇_z
METER
0
200
400
600
800
1000
$h \sim$ KM
HEIGHT ABOVE MOON'S SURFACE AT PERISELENE

Fig. V-23

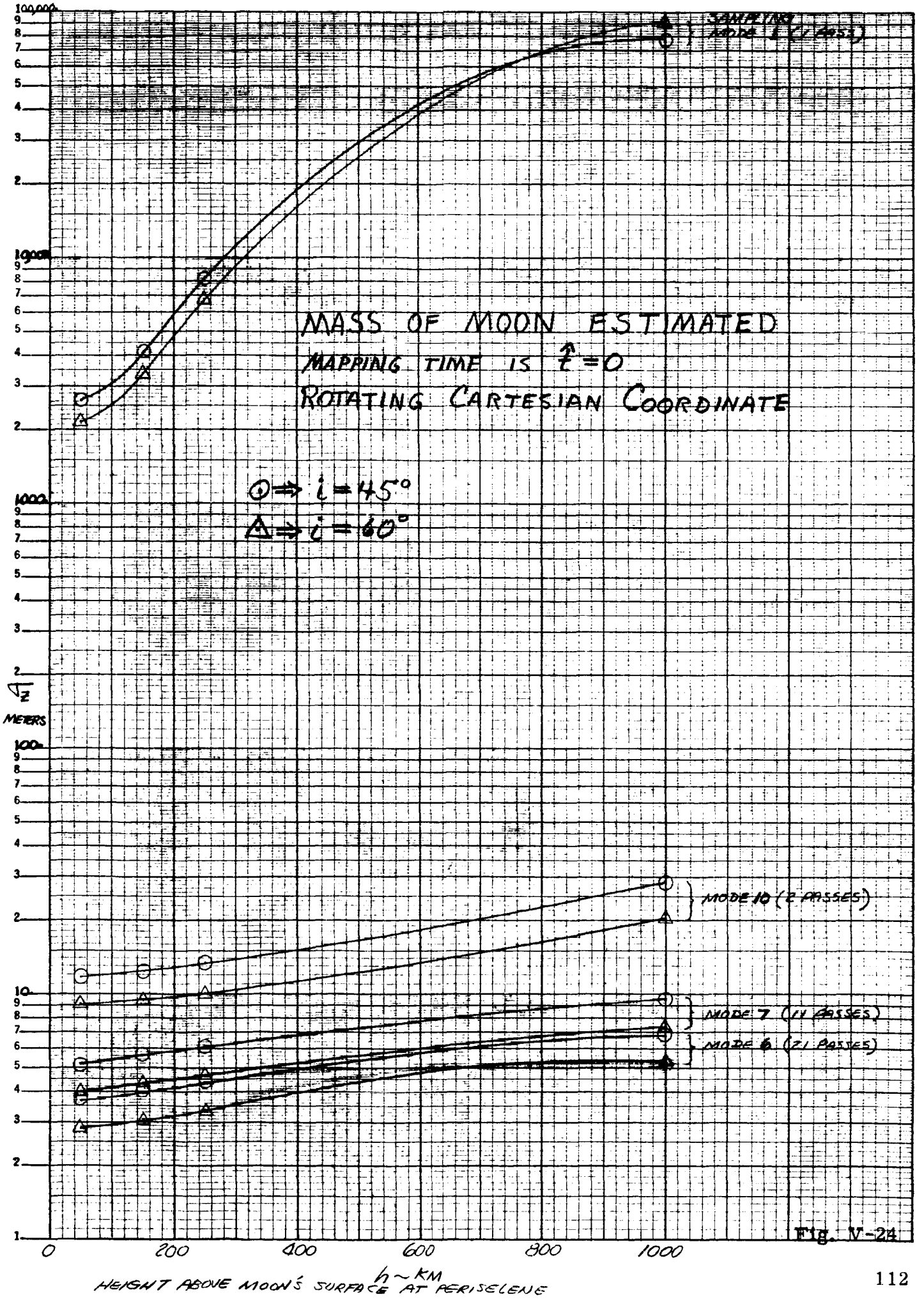
SAMPLING MODE 1 (1 PASS)
MASS OF MOON ESTIMATED
MAPPING TIME IS $\hat{t}=0$
ROTATING CARTESIAN COORDINATE
⊙ ⇒ $i=45°$
△ ⇒ $i=60°$
MODE 10 (2 PASSES)
MODE 7 (11 PASSES)
MODE 6 (21 PASSES)
$\sqrt{N}$
METERS
100,000
10,000
1000
100
10
1
0
200
400
600
800
1000
$h \sim$ KM
HEIGHT ABOVE MOON'S SURFACE AT PERISELENE

Fig. V-24

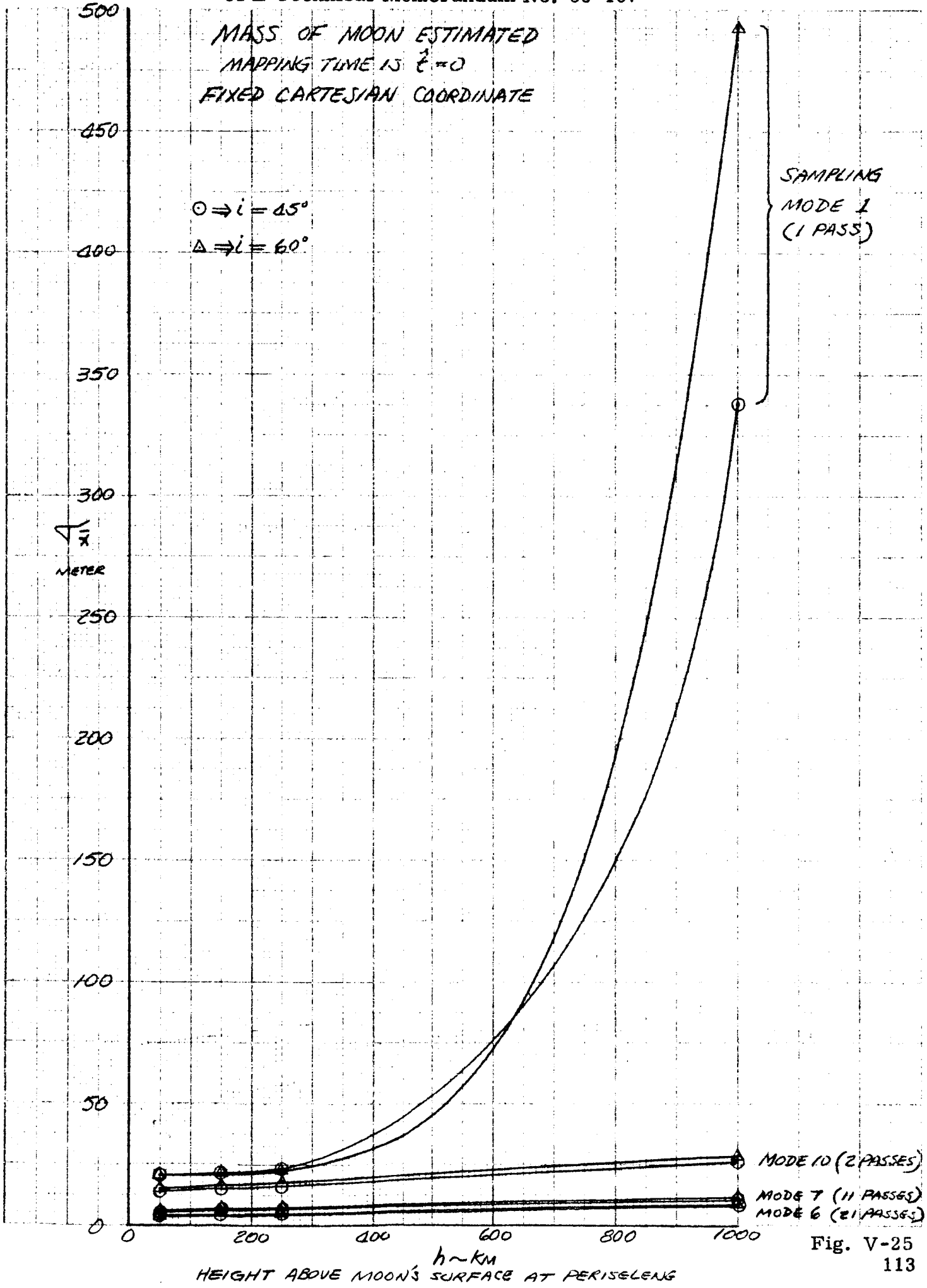
MASS OF MOON ESTIMATED
MAPPING TIME IS $\dot{t}=0$
FIXED CARTESIAN COORDINATE
⊙ ⇒ $i = 45°$
△ ⇒ $i = 60°$
SAMPLING MODE 1 (1 PASS)
MODE 10 (2 PASSES)
MODE 7 (11 PASSES)
MODE 6 (21 PASSES)
$\sqrt{\bar{x}}$ METER
500
450
400
350
300
250
200
150
100
50
0
0
200
400
600
800
1000
h ~ KM
HEIGHT ABOVE MOON'S SURFACE AT PERISELENE

Fig. V-25

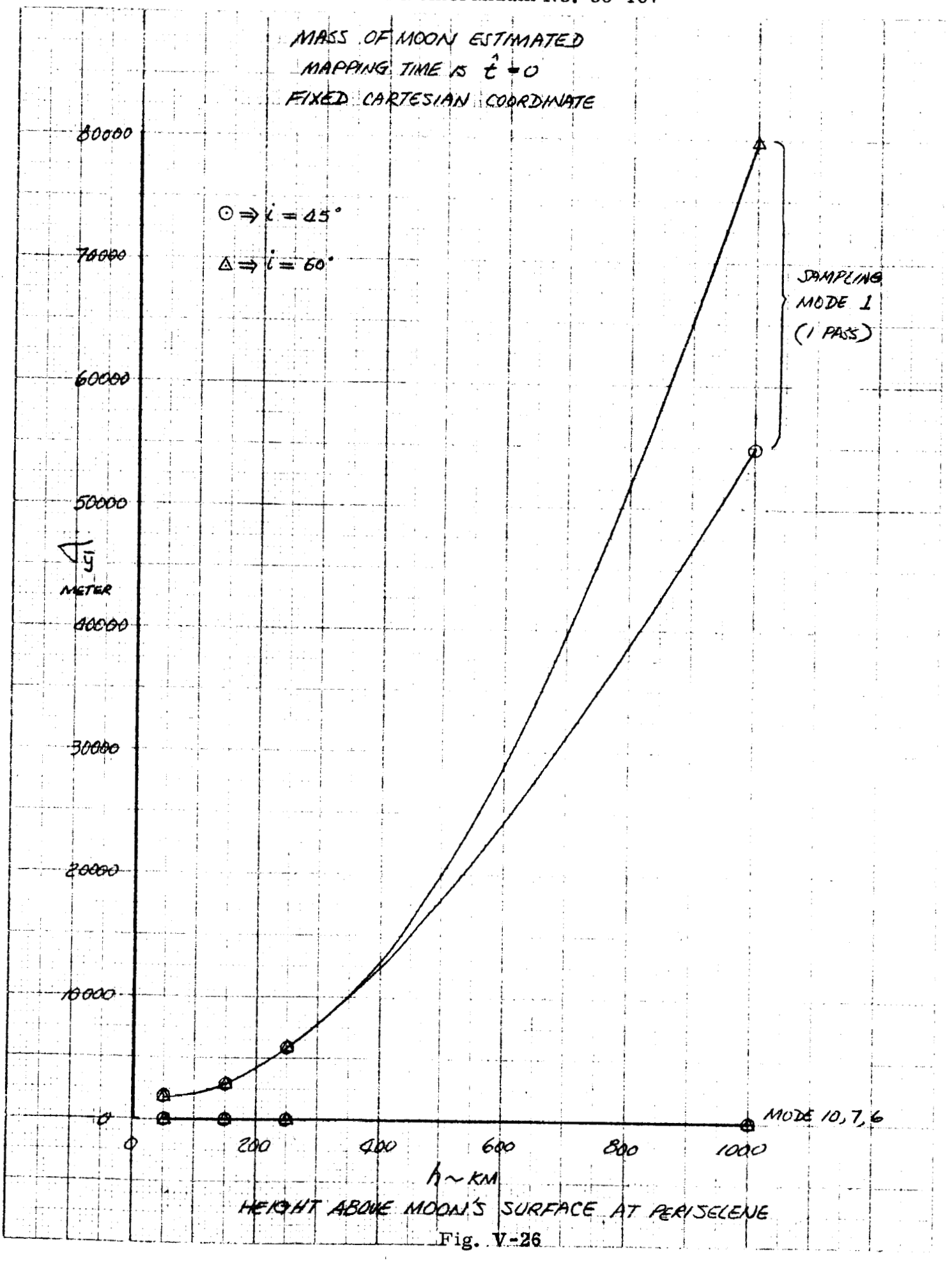
MASS OF MOON ESTIMATED
MAPPING TIME IS $\hat{t} = 0$
FIXED CARTESIAN COORDINATE
⊙ ⇒ $i = 45°$
△ ⇒ $i = 60°$
80000
70000
60000
50000
40000
30000
20000
10000
0
σ_r
METER
SAMPLING MODE 1 (1 PASS)
MODE 10, 7, 6
0
200
400
600
800
1000
$h \sim$ KM
HEIGHT ABOVE MOON'S SURFACE AT PERISELENE

Fig. V-26

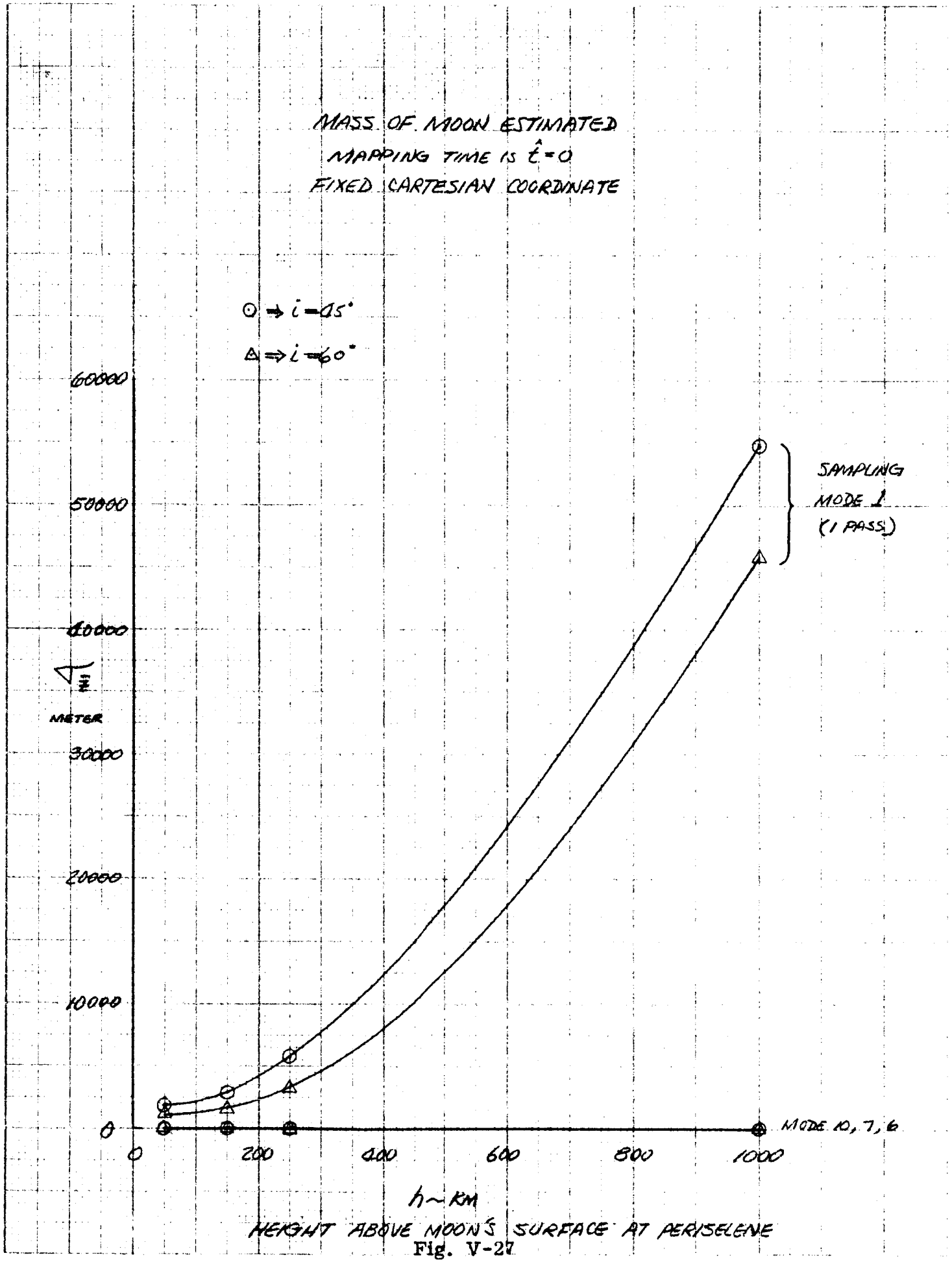
MASS OF MOON ESTIMATED
MAPPING TIME IS $\hat{t}=0$
FIXED CARTESIAN COORDINATE
⊙ ⇒ $i=45°$
△ ⇒ $i=60°$
60000
50000
40000
30000
20000
10000
0
$\sqrt{\frac{m}{r}}$
METER
SAMPLING
MODE 1
(1 PASS)
MODE 10, 7, 6
0
200
400
600
800
1000
$h \sim$ KM
HEIGHT ABOVE MOON'S SURFACE AT PERISELENE

Fig. V-27

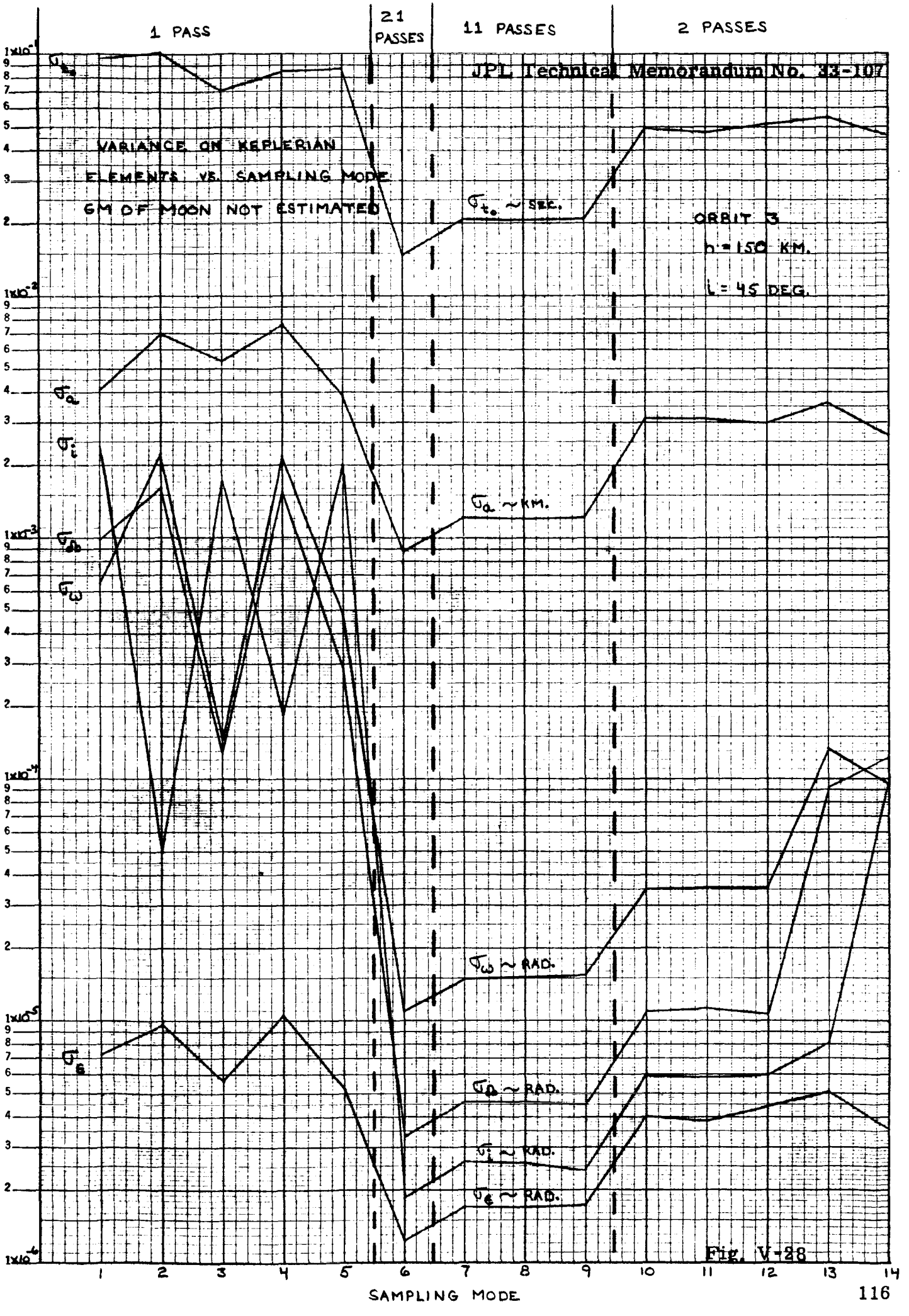

Fig. V-28

K+E SEMI-LOGARITHMIC 359-91 KEUFFEL & ESSER CO. MADE IN U.S.A. 5 CYCLES X 70 DIVISIONS

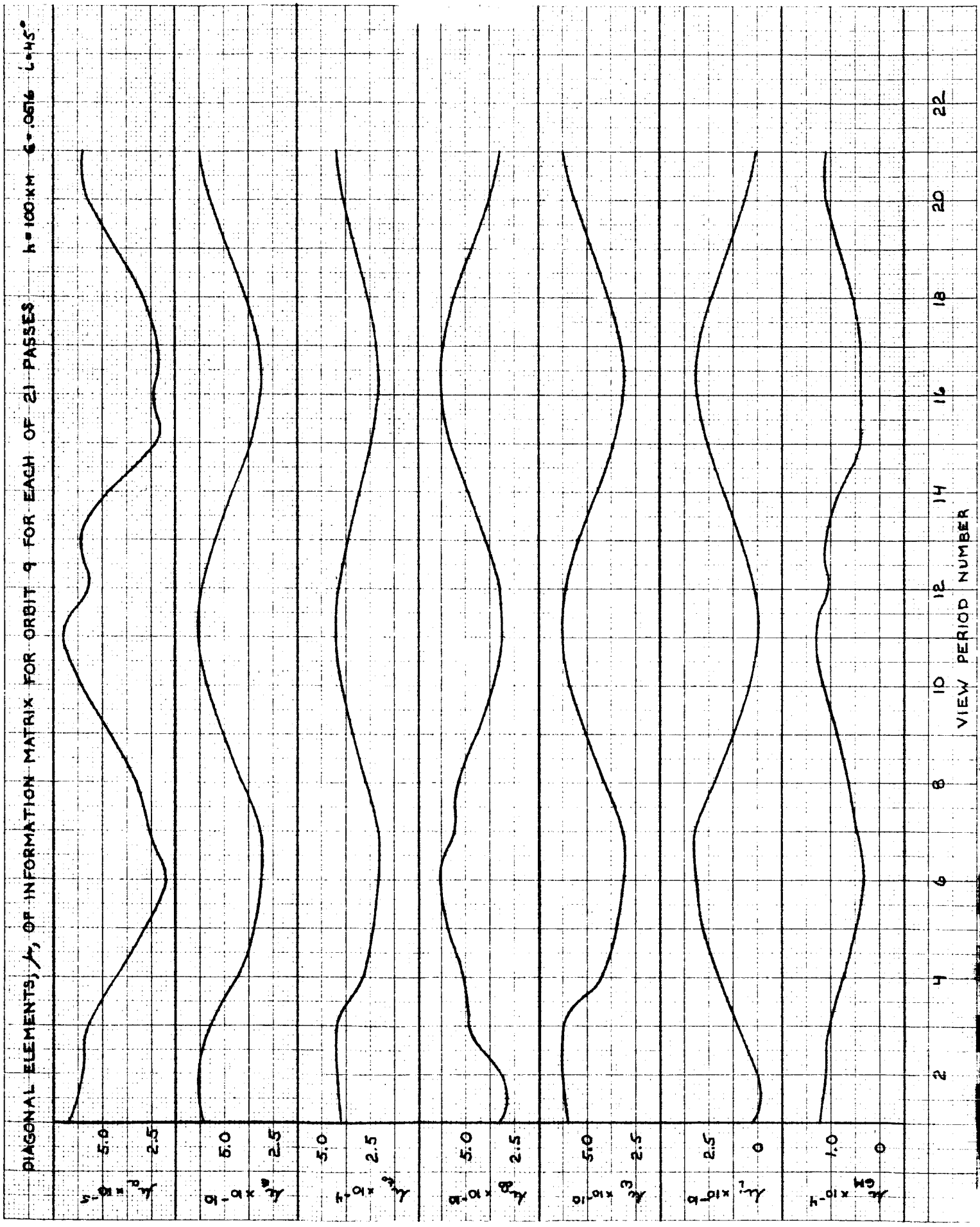

Fig. V-29

CLEARPRINT PAPER CO. NO. 239X MILLIMETERS 200 BY 250 DIVISIONS PRINTED IN U.S.A. ON CLEARPRINT TECHNICAL PAPER NO. 1015

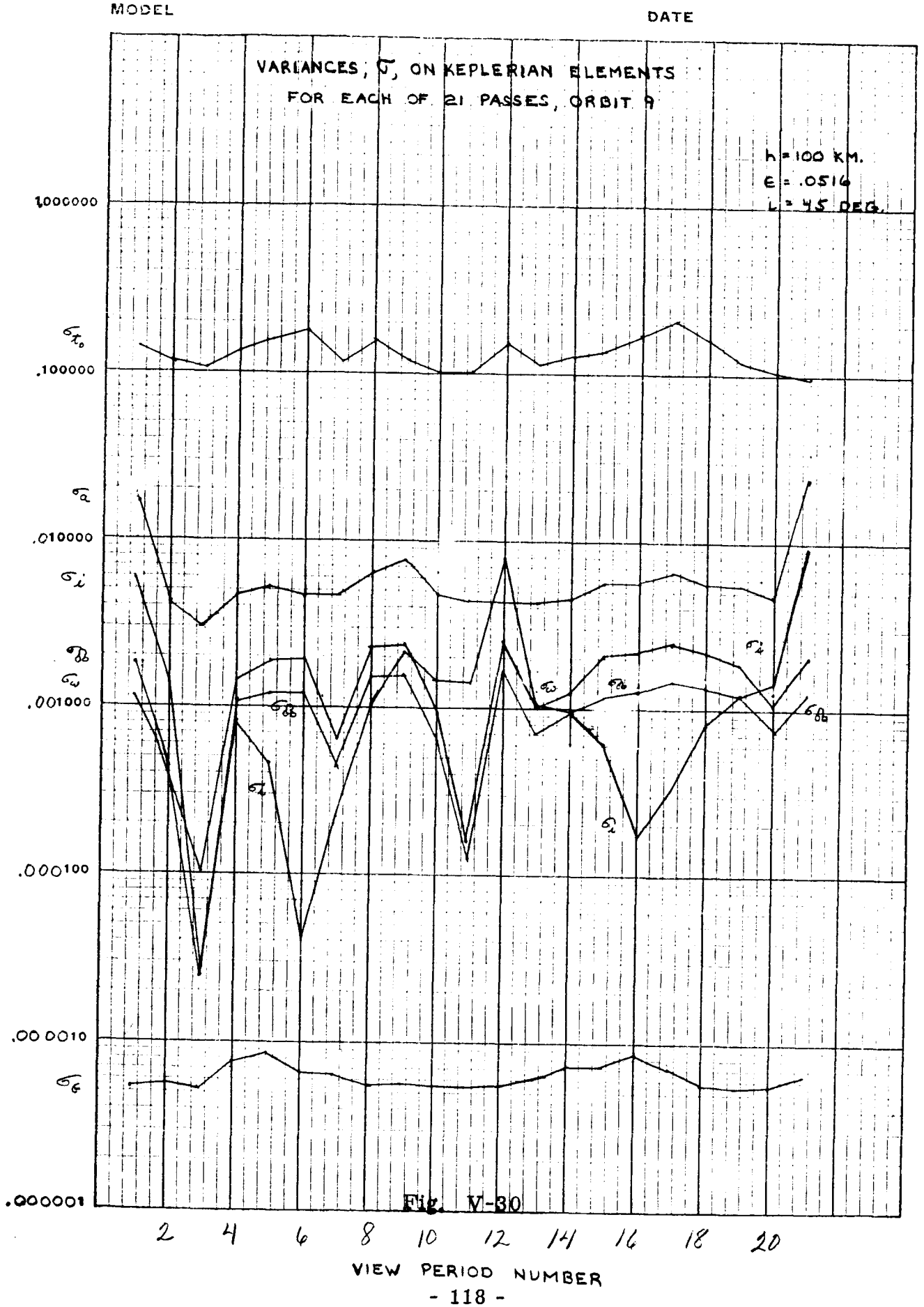

Fig. V-30

K+E SEMI-LOGARITHMIC 359-96
KEUFFEL & ESSER CO. MADE IN U.S.A.
7 CYCLES X 60 DIVISIONS

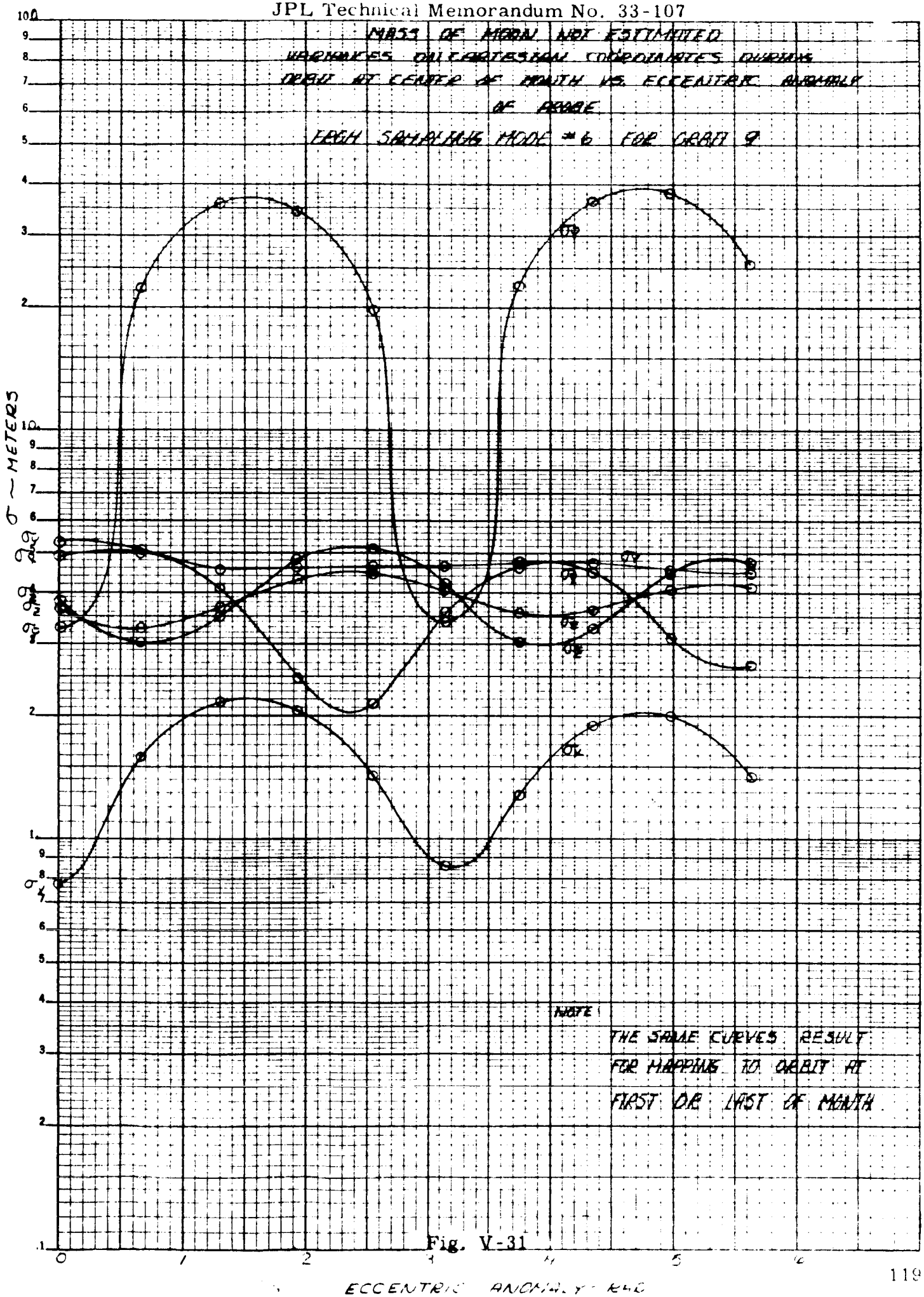
MASS OF MOON NOT ESTIMATED
HARMONICS ON CARTESIAN COORDINATES DURING
ORBIT AT CENTER OF MONTH VS. ECCENTRIC ANOMALY
OF ORBIT
FROM SATURNUS MODE #6 FOR ORBIT 9
σ ~ METERS
NOTE
THE SAME CURVES RESULT
FOR MAPPING TO ORBIT AT
FIRST OR LAST OF MONTH
ECCENTRIC ANOMALY - RAD

Fig. V-31

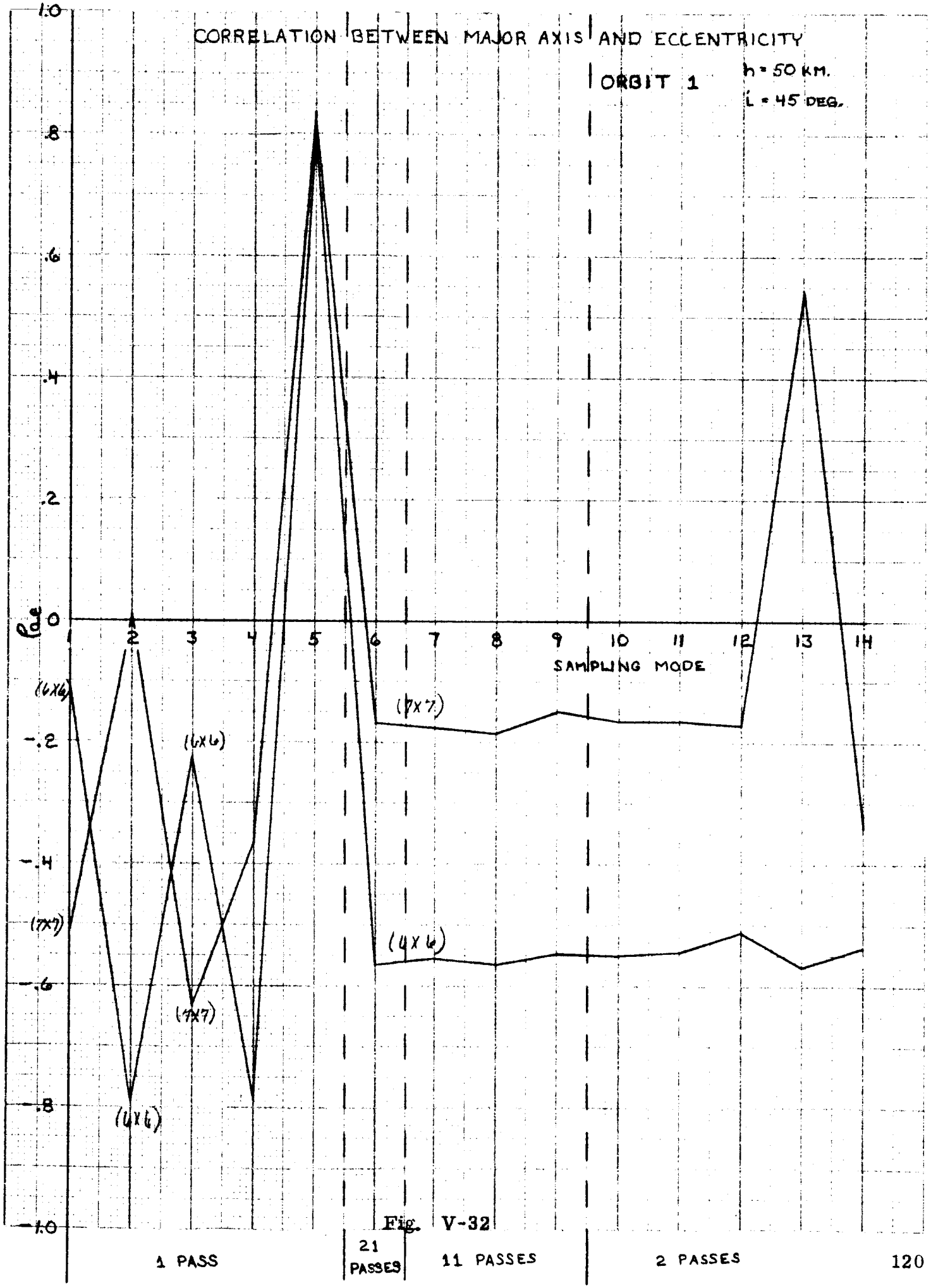
CORRELATION BETWEEN MAJOR AXIS AND ECCENTRICITY
ORBIT 1
h = 50 KM.
i = 45 DEG.
1.0
.8
.6
.4
.2
0
-.2
-.4
-.6
-.8
-1.0
ρae
1
2
3
4
5
6
7
8
9
10
11
12
13
14
SAMPLING MODE
(6X6)
(7X7)
(6X6)
(7X7)
(6X6)
(7X7)
(6X6)
1 PASS
21 PASSES
11 PASSES
2 PASSES

Fig. V-32

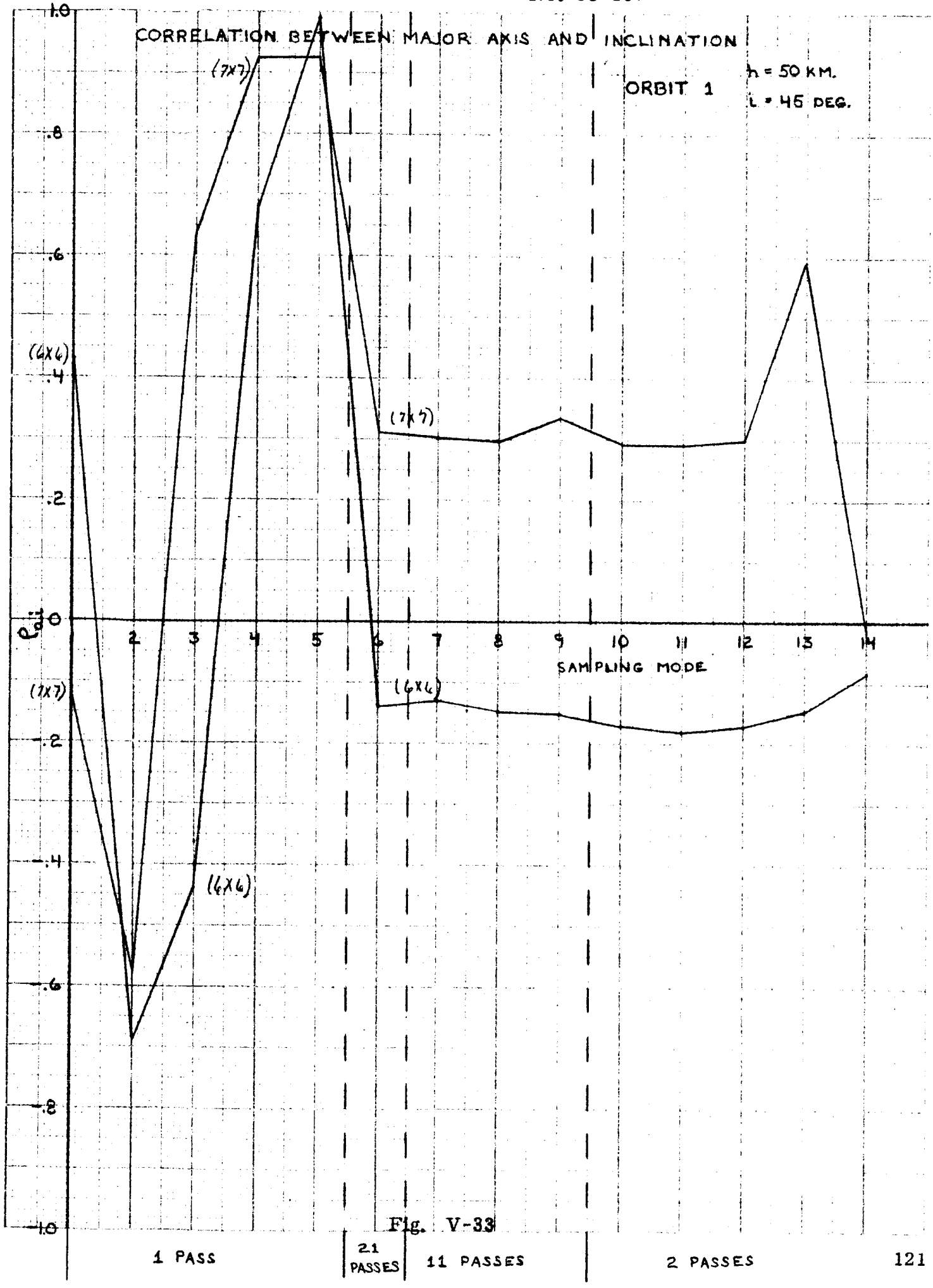
CORRELATION BETWEEN MAJOR AXIS AND INCLINATION
ORBIT 1
h = 50 KM.
L = 45 DEG.
(7X7)
(6X6)
(7X7)
(6X6)
(7X7)
(6X6)
1.0
.8
.6
.4
.2
0
-.2
-.4
-.6
-.8
-1.0
2
3
4
5
6
7
8
9
10
11
12
13
14
SAMPLING MODE
1 PASS
21 PASSES
11 PASSES
2 PASSES

Fig. V-33

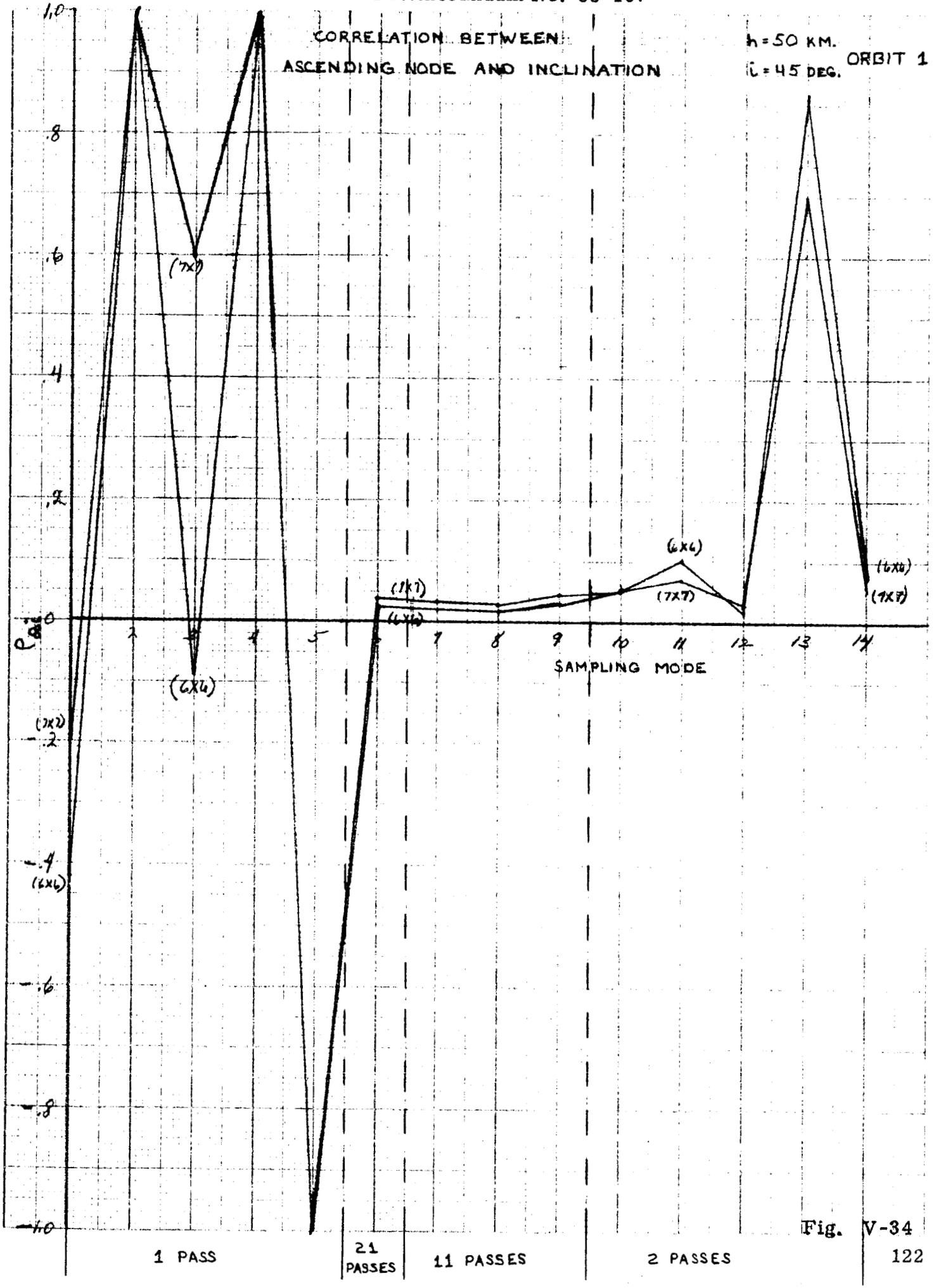
CORRELATION BETWEEN
ASCENDING NODE AND INCLINATION
h = 50 KM.
i = 45 DEG.
ORBIT 1
1.0
.8
.6
.4
.2
0
-.2
-.4
-.6
-.8
-1.0
(7X7)
(6X6)
(7X7)
(6X6)
(7X7)
(6X6)
(6X6)
(7X7)
(7X7)
(6X6)
1
2
3
4
5
6
7
8
9
10
11
12
13
14
SAMPLING MODE
1 PASS
21 PASSES
11 PASSES
2 PASSES

Fig. V-34

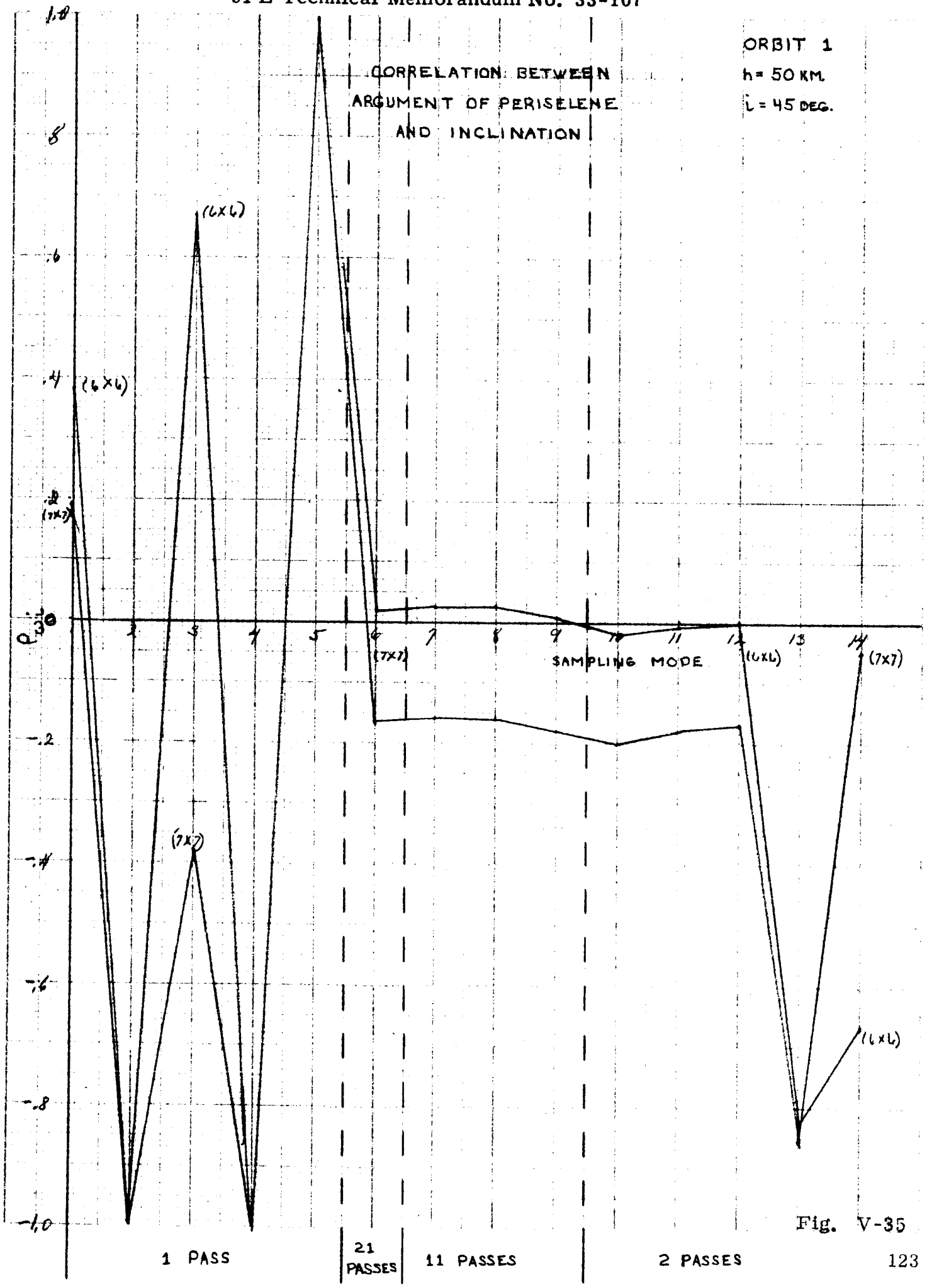
CORRELATION BETWEEN
ARGUMENT OF PERISELENE
AND INCLINATION
ORBIT 1
h = 50 KM
i = 45 DEG.
1.0
.8
.6
.4
.2
0
-.2
-.4
-.6
-.8
-1.0
(6x6)
(7x7)
(6x6)
(7x7)
(7x7)
(6x6)
(6x6)
(7x7)
SAMPLING MODE
1 PASS
21 PASSES
11 PASSES
2 PASSES

Fig. V-35

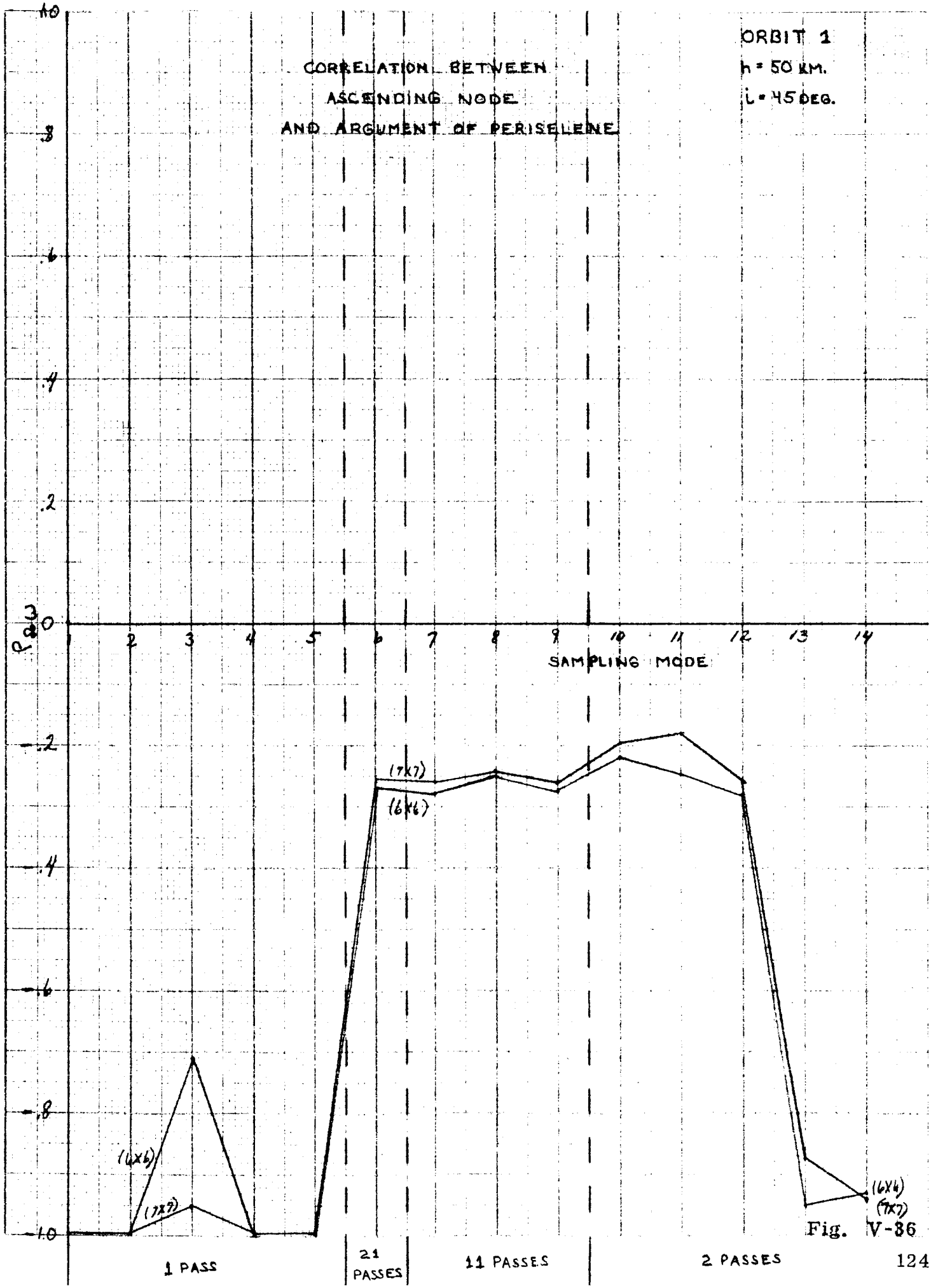
CORRELATION BETWEEN
ASCENDING NODE
AND ARGUMENT OF PERISELENE
ORBIT 1
h = 50 KM.
i = 45 DEG.
ρ
SAMPLING MODE
(7X7)
(6X6)
(4X6)
(7X7)
(6X6)
(7X7)
1 PASS
21 PASSES
11 PASSES
2 PASSES

Fig. V-36